



# LIBRARIES

UNIVERSITY OF WISCONSIN-MADISON

## **Mechanical controls on fracture development in carbonate aquifers: implications for groundwater flow systems: final report to the Wisconsin Department of Natural Resources. [DNR-142] 2001**

Muldoon, Maureen A. et al.

[Wisconsin]: [publisher not identified], 2001

<https://digital.library.wisc.edu/1711.dl/VLTL6DLFCS4QF8I>

<http://rightsstatements.org/vocab/InC/1.0/>

For information on re-use see:

<http://digital.library.wisc.edu/1711.dl/Copyright>

The libraries provide public access to a wide range of material, including online exhibits, digitized collections, archival finding aids, our catalog, online articles, and a growing range of materials in many media.

When possible, we provide rights information in catalog records, finding aids, and other metadata that accompanies collections or items. However, it is always the user's obligation to evaluate copyright and rights issues in light of their own use.

051402

**Mechanical Controls on Fracture  
Development in Carbonate Aquifers:  
Implications for Groundwater Flow Systems:  
Final Report to the WI Dept. of Natural Resources**

**by Maureen A. Muldoon (et al.)**

**Water Resources Library**  
University of Wisconsin  
1975 Willow Dr., 2<sup>nd</sup> Floor  
Madison, WI 53706-1177  
(608)262-3069



**MECHANICAL CONTROLS ON FRACTURE DEVELOPMENT IN CARBONATE  
AQUIFERS: IMPLICATIONS FOR GROUNDWATER FLOW SYSTEMS**

*Final Report to the Wisconsin Department of Natural Resources*

by

Maureen A. Muldoon  
Dept. Of Geology, UW-Oshkosh

Chad Underwood  
Montgomery Watson Hazra, Madison, WI

Michele Cooke  
Geosciences Department, Univ. Of Massachusetts, Amherst

Juan Antonio (Toni) Simo  
Dept. Of Geology and Geophysics, UW-Madison

RECEIVED-DNR  
AUG 14 2001  
DRINKING WATER &  
GROUNDWATER

July, 2001

## CONTENTS

INTRODUCTION	1
Background	1
Purpose and Scope	2
SETTING	4
Lithostratigraphy	4
Hydrogeology	9
Regional Fractures	11
STRATIGRAPHIC CONTROLS ON VERTICAL FRACTURE PATTERNS	15
Introduction	15
Mechanical Controls on Fracture Formation	17
Methods	19
Mapping Vertical Fractures in Quarry Walls	19
Measurement of Dolomite Stiffness	21
Identification of Mechanical Interfaces	25
Results	28
Mechanical Stratigraphy	28
Stiffness Variations Among Facies	29
Identification of Mechanical Interfaces	30
Classification of Mechanical Interfaces	32
Mechanical Stratigraphy Prediction	34
Discussion	38
STATISTICAL CHARACTERIZATION OF FRACTURE PROPERTIES	42
Methods	42
Measurements of Fracture Density	43
Scanline Surveys	44
Fracture Density	45
Summary of Fracture Density Data Collected Previously	45
Observed Fracture Density	48
Scanlines across vertical quarry faces	48
Analysis of Vertical Core Data	52
Horizontal Core	54
Predicting Fracture Density	57
Fracture Orientation	57
Predicting Fracture Orientation	61
Fracture Length Distribution	62
Predicting Length Distributions	63
Fracture Aperture	68

SIMULATION OF FRACTURE FORMATION	69
Introduction	69
Previous work on fracture termination	69
New fracture initiation along bedding contacts	70
Numerical Modeling	72
Model Set-up	73
Model Results	77
Sliding-only Interface Models	80
Opening-only Interface Models	80
Sliding and Opening Interface Models	82
Discussion	85
Expected types of fracture intersection with bed contacts	85
Conclusions	89
SIMULATION OF FLUID FLOW	91
Background	91
Summary of Existing Codes	92
REFERENCES	94
APPENDICES	101

## FIGURES

1.	Location map of Door County and summary of bedrock geology	5
2.	Summary of Silurian stratigraphy for the Door Peninsula.	6
3.	Photograph of the lithologic variations typical of cycle contacts in the inner shelf facies association.	8
4.	Photographs illustrating the lithologic characteristics of the inner-middle shelf facies association.	8
5.	Photographs illustrating the lithologic characteristics of the middle shelf facies association.	10
6.	Simplified water-table map of Door County showing regional flow system.	12
7.	Water-level data from the Jarmen Road research site.	13
8.	Photo of regional fracture traces in an alfalfa field.	13
9.	Locations of where fracture data were collected.	16
10.	Stratigraphic controls on fracture patterns.	18
11.	Stratigraphic position of locations where fracture data were collected.	20
12.	Stratigraphy, mechanical stratigraphy, and fracture map for the lower wall of Big Quarry	22
13.	Stratigraphy, mechanical stratigraphy, and fracture map for the upper wall of Big Quarry	23
14.	Stratigraphy and fracture map at Mathey Road Quarry.	24
15.	Interval sampling method used to statistically identify mechanical interfaces	27
16.	Quantitative criteria used to determine which stratigraphic horizons have enough fracture tips to be considered mechanical interface.	27
17.	Mechanical interfaces at Big Quarry as identified by quantitative criteria, comparison of visually mapped interfaces with those identified by quantitative criteria.	31
18.	Comparison of observed mechanical interface distribution with all stratigraphic horizons for Big Quarry.	35
19.	Probability of a stratigraphic horizon acting as a mechanical interface.	37
20.	Percent error for Monte Carlo simulation.	37
21.	Comparison between one realization of the predicted mechanical stratigraphy and the observed mechanical interface distribution for Big Quarry.	39
22.	Average fracture densities for various facies associations of the Silurian dolomite.	49
23.	Fracture density versus mechanical unit thickness for units in the Byron/Hendricks Formations.	50
24.	Fracture density based on observations of vertical fractures in the core collected from the Jarmen Road research site.	53
25.	Fracture density in lower Big Quarry as determined from A) horizontal core and B) two scanline surveys.	55
26.	Predicted fracture density for the units exposed in Big Quarry.	58

27.	Rose diagrams of fracture orientations from scanline surveys.	59
28.	Rose diagrams of fracture orientations for the three facies associations within the Silurian dolomite.	62
29.	Histograms of fracture lengths for the three facies associations in the Silurian dolomite.	64
30.	Histograms of "uncensored" fracture lengths from Big Quarry which serve to illustrate the problem of "censored" data.	66
31.	Histograms of fracture lengths for the three facies associations in the Silurian dolomite shown with the "best-fit" line for a negative exponential distribution.	67
32.	Postulated mechanisms for fracture propagation through and termination at bedding contacts.	71
33.	Conceptualization of the interface constitutive properties in shear-normal (t-s) stress space.	74
34.	Model used to examine fracture termination at weak mechanical interfaces.	75
35.	Maximum tension (principal stress) around the tip of a 1m vertical fracture under 5 MPa remote isotropic tension and maximum tensile stress along a bonded interface.	79
36.	Model results for the bonded and sliding-only interface models.	81
37.	Slip distribution along the moderate-strength sliding-only interface.	82
38.	Model results for very weak and moderate-strength opening-only interfaces.	83
39.	Distribution of maximum tension along very weak and moderate-strength interfaces that deform under combination of sliding and opening.	84
40.	Inferred variations in geometry of fracture-bed contact intersection for bedding contacts with different strengths.	86
41.		

### Tables

1.	Summary of location, orientation, and length of scanlines.	46
2.	Observed fracture densities for the Inner Shelf Facies Association exposed within the Byron Formation (Big Quarry).	56
3.	Statistics for rose diagrams of fracture orientation from each scanline site.	60
4.	Strength properties of mechanical interfaces.	77

### Appendices

A.	Data from scanline surveys collected from fracture pavements	
B.	Log of fracture locations from horizontal core collected from the lower exposure in Big Quarry	

# INTRODUCTION

## Background

Carbonate aquifers form important regional sources of drinking water in eastern and southern Wisconsin. Previous work in Door County suggests that vertical fractures as well as horizontal partings and dissolution zones provide the primary pathways for groundwater flow in the Silurian aquifer (Sherrill, 1978; Bradbury and Muldoon, 1992). Stratigraphic, geophysical, and hydrogeologic data were used to identify laterally continuous high-permeability zones within the Silurian dolomite in the vicinity of Sturgeon Bay (Muldoon and others, in review). While these features appear to correlate with stratigraphy, it is not clear why certain stratigraphic discontinuities (fractures) develop into regionally important high-permeability features while others do not. It is our hypothesis that the distribution of vertical fractures and the mechanical properties of the various stratigraphic units contribute to the development of these bedding-parallel high-permeability zones.

Detailed hydrogeologic characterization in the northern Door Peninsula has documented the presence of distinct shallow and deep flow systems within the Silurian dolomite aquifer (Bradbury and Muldoon, 1992). Stratigraphic characterization indicates that there are no low-permeability layers such as shale or clay to impede the vertical movement of groundwater and cause the "perching" of the shallow flow system above the deeper potentiometric surface. We postulate that the occurrence of the shallow flow system may be controlled by variations in vertical fracture pattern due to the heterogeneous Silurian lithology.

The accuracy of predictions of groundwater movement and contaminant transport in fractured-rock aquifers is often limited by how well the fracture network has been characterized. The three-dimensional distribution of fractures in the subsurface is difficult to characterize with limited outcrop and sparse borehole data and yet those are the data typically available in most groundwater investigations. In this study, we integrate lithostratigraphic and hydrogeologic data

with a detailed characterization of the mechanical stratigraphy of the Silurian dolomite in order to better predict the distribution of fractures in the subsurface. By integrating methodologies and approaches from fracture mechanics and hydrogeology we can assess whether fracture network geometry can help explain the development of horizontal high-permeability features and the existence of two discrete flow systems in the Silurian dolomite.

### **Purpose and Scope**

The purpose of this study was to gain a better understanding of the development of vertical fractures and horizontal partings in order to constrain how fractures contribute to the development of two flow systems and the development of horizontal high-permeability zones.

This study addresses the problems of 1) mechanical controls on fracture development and 2) fracture controls on flow system configuration and bedding-parallel high-permeability zones in carbonate strata. The objectives of this study are to 1) evaluate the role of lithologic variations on fracture development, and 2) determine whether fracture distribution can help explain the development of horizontal high-permeability features and the existence of two discrete flow systems in the Silurian dolomite.

We used a combination of field mapping, laboratory experiments, and numerical experiments in order to assess the role of lithology on the development of the fracture network. The methods used to reach the above objectives include the following:

1. *Characterization of the fracture network:* Vertical fractures were mapped on quarry walls in order to assess fracture patterns and fracture densities within specific lithostratigraphic facies of the Silurian dolomite. Mapped fracture patterns were used to assess the mechanical stratigraphy of the Silurian strata in Door County. The mechanical stiffness of the dolomite was also measured along quarry faces. Scanline mapping of fractures exposed on quarry floors and natural dolomite pavement surfaces provided additional information on fracture densities as well

as data on fracture orientation, length, and termination characteristics within specific lithostratigraphic facies.

2. *Numerical modeling of fracture terminations:* The role of lithologic variations on fracture development were analyzed using FRIC2D, a code developed by Cooke (1996). This code examines the mechanical deformation of strata using Boundary Element Method (BEM).

3. *Numerical simulation of fracture network:* Initially we had planned on using numerical flow models that couple discrete fracture flow with reactive transport to simulate the evolution of the flow system in Door County and then to compare the flow system that evolves from the integrated mechanical-hydrologic models with the observed flow system in Door County. We have been unable to acquire a suitable code, however, we have compiled both the mechanical data and the statistics on fracture properties that allow us to simulate realistic 3-dimensional fracture networks.

## SETTING

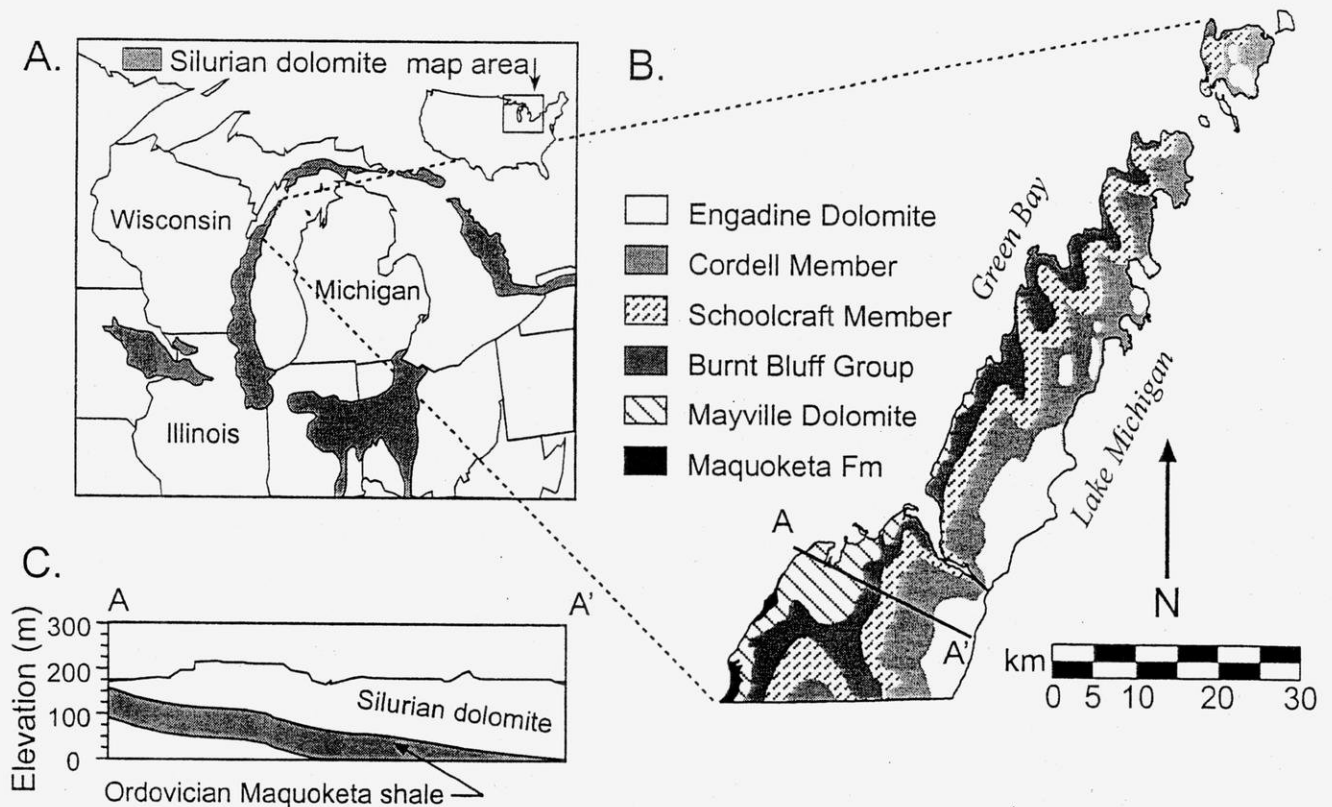
Door County, Wisconsin occupies much of the peninsula that lies between Lake Michigan and Green Bay in northeast Wisconsin (Figure 1). It is underlain by approximately 160 meters of Lower Silurian (Llandoverly; Watkins and Kuglitsch, 1997) dolomite (Hegrenes, 1996). The Silurian strata were deposited in the western margin of the Michigan Basin, a relatively undeformed cratonic structural basin (Sleep and Sloss, 1978; Howell and van der Pluijm, 1990 and 1999).

### **Lithostratigraphy**

Chamberlin (1877) first mapped and subdivided the Silurian strata of the Door Peninsula into stratigraphic units. Over a century later, Waldhuetter (1994), Harris and Waldhuetter (1996), Hegrenes (1996), Watkins and Kuglitsch (1997), and Simo and others (1998) provided a sedimentological and sequence stratigraphic characterization of the Silurian section exposed in outcrop and in the subsurface.

Silurian lithologies studied can be grouped into one of three following facies associations: inner shelf, inner-middle shelf, and middle shelf facies associations as illustrated in Figure 2 (Simo and others, 1998). As a first approximation, the facies associations correspond to Chamberlain's stratigraphic units. The Mayville Dolomite, Manistique Formation and Engadine Dolomite mostly contain middle shelf association. The Byron Dolomite is characterized by inner shelf facies associations, and the Hendricks Dolomite corresponds to inner-middle shelf facies association. Overall, the stratigraphic succession shows a shallowing from the Mayville to the Byron followed by a deepening through the Engadine (Figure 2).

The inner facies association is interpreted as deposited in shallow (<10 m), restricted-marine, low energy, and tidal flat environment and commonly contains surfaces with evidence of subaerial exposure, some with decimeter-scale depositional relief. The inner shelf facies association is



**Engadine Dolomite:** The Engadine Dolomite (~11 m thick) is a light-gray, thickly-bedded dolostone with poorly preserved fauna, no chert nodules, and vuggy porosity.

**Manistique Formation:** The Manistique Formation (27 m thick) consists of subtidal facies, and represent a transgressive package over the uppermost restricted-marine facies of the Hendricks Dolomite. The Manistique Formation is subdivided into two members, with the upper Cordell Member richer in chert that the lower Schoolcraft Member.

The *Burnt Bluff Group* consists of the Byron and Hendricks Dolomite

**Hendricks Dolomite:** Similar to the upper Byron, the Hendricks Dolomite records a cyclic succession of subtidal and supratidal facies, with cycles of 1-3 m thickness, and a total thickness up to 28 m.

**Byron Dolomite:** The Mayville-Byron contact records a change from the coral-brachiopod-rich rocks (Mayville Dolomite) to a laminated, mud-cracked mudstone (Byron Dolomite). Most of the Byron Dolomite consists of restricted shallow-subtidal to supratidal facies, and is 23-25 m thick. In Door County, the Byron Dolomite culminates in an argillaceous, bluish-gray, mudstone.

**Mayville Dolomite:** The Mayville Dolomite (approximately 62 m) consists of deep- to shallow-subtidal facies arranged into two shallowing-upward successions interpreted as deposited in moderate- to high-energy, subtidal, open-shelf environment. Bedding is typically massive or wavy, and occasionally is rippled; thickness varies from thin to medium beds. Chert is very abundant in the lower part of the section.

**Maquoketa Formation:** In Door County, the Maquoketa is a poorly exposed shale succession that is thinly laminated and greenish-gray in color.

**Figure 1.** Location of Door County and summary of bedrock geology. **A)** map of generalized Silurian subcrop shown as shaded area (modified from Shaver et al., 1978), **B)** geologic map of Door County (digitized from Chamberlin (1878) by Roffers (1996)) and **C)** a simplified cross section of southern Door County.

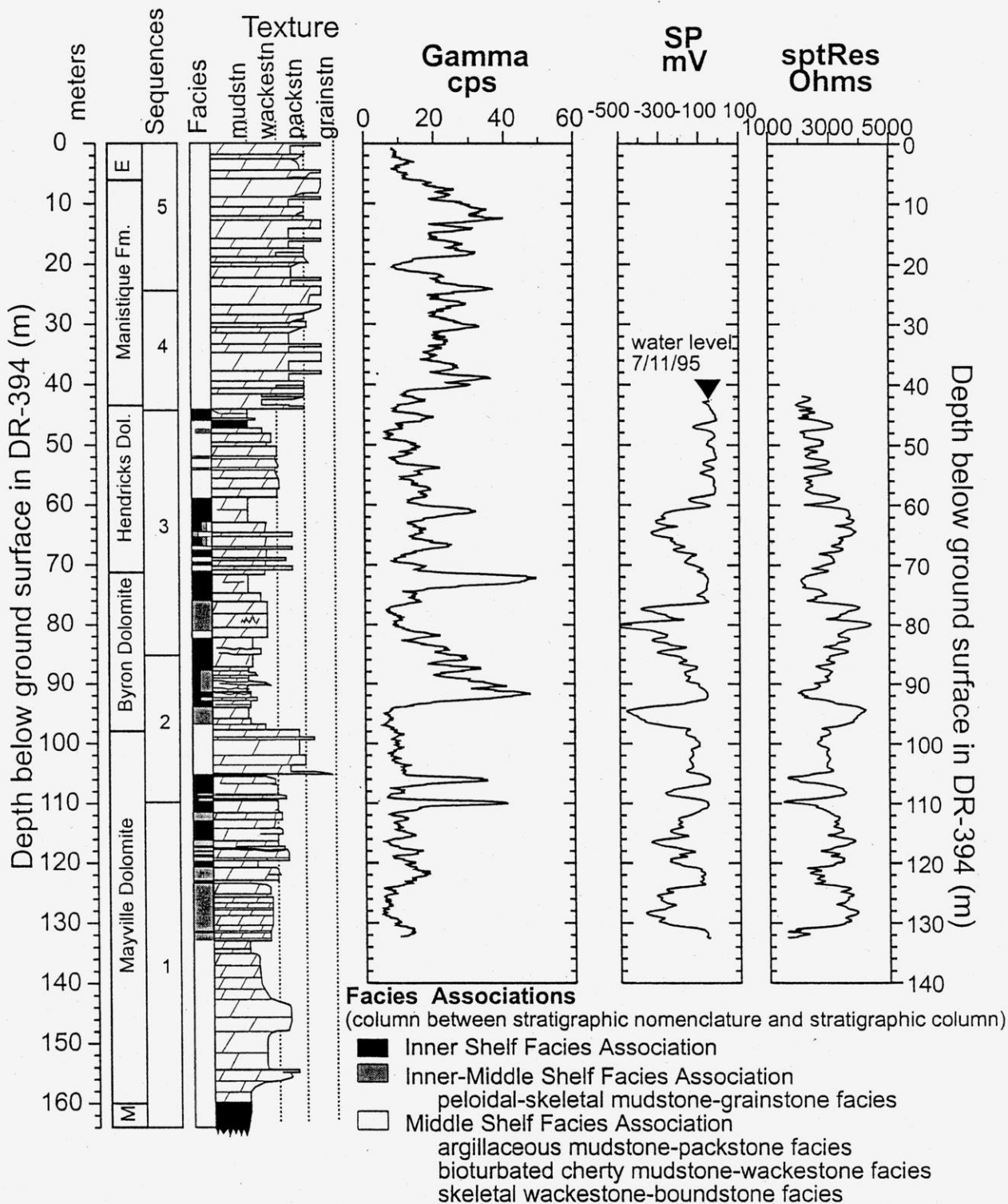


**Figure 2.** Summary of Silurian stratigraphy for the Door Peninsula. From left to right the figure includes the following: depth scale (meters); stratigraphic nomenclature (after Steiglitz 1989); sequences (after Harris and others, 1998); facies associations (color-coded white to black, legend is included at bottom of figure); stratigraphic column showing depositional texture (after Dunham 1962) brick pattern is dolomite, black is shale; the natural gamma; spontaneous potential (SP); and single-point resistivity (sptRes) logs from corehole DR-394.

characterized by meter-scale (~0.3-0.9 m) depositional cycles. Complete cycles contain a lower part with fenestral mudstone-packstone, and an upper part characterized by algal lamination; a diagenetic cap tops most of the cycles. The basal fenestral mudstone-packstone may be bioturbated, and often contains intraclasts. Occasionally, cycle bases contain a 2-5 cm-thick white mudstone, which is laterally continuous across outcrop exposure. The upper part of a typical cycle consists of mat-laminated facies, which may contain modal stromatolite at the base, and peloidal-ostracod mudstone-packstone. Mudcracked, thin and crinkly laminites characterize the cycle top. The laminated lithologies are typically very well cemented and the top affected by cemented sheet- and vertical-cracks are very and micro-karst. The diagenetic cap varies in thickness and occasionally is truncated by the overlying surface. Cycle boundaries separate the very well cemented laminite/diagenetic cap and the overlying less cemented fenestral mudstone-packstone. At these contacts, thin and discontinuous organic-rich mudstones may occur. Cycle boundaries are the most obvious bedding breaks in quarries and outcrops, and are laterally extensive for the length of the exposure. All the lithologies in the inner shelf facies association are dolomitized by fine-crystalline, mimetic dolomite. Figure 3 illustrates the lithologic variations at the contact between cycles in the inner shelf facies association.

The inner-middle shelf facies association represents slightly deeper depositional conditions and is a transition between inner and middle shelf deposition. This facies association predominantly consists of fine-crystalline, peloidal-skeletal mudstone-grainstones with continuous thin bedding, minor cross bedding and abundant stylolites, and mat- and fenestral-laminated mudstone-packstones. Fragments of stromatoporids, coral and brachiopods are common in the peloidal-skeletal mudstone-grainstones. These two lithologies alternate and define medium bedded depositional cycles. Laminated mudstone cycle caps, if present, are generally thinner than in the inner shelf facies association and rarely include a diagenetic cap. Organic-rich laminae within this association are less common than in the inner shelf facies association. Laterally continuous bedding planes commonly occur at the cycle boundary, but other less continuous bedding planes may occur within the cycle. Figure 4 illustrates the lithologic characteristics of the inner-middle shelf facies association.

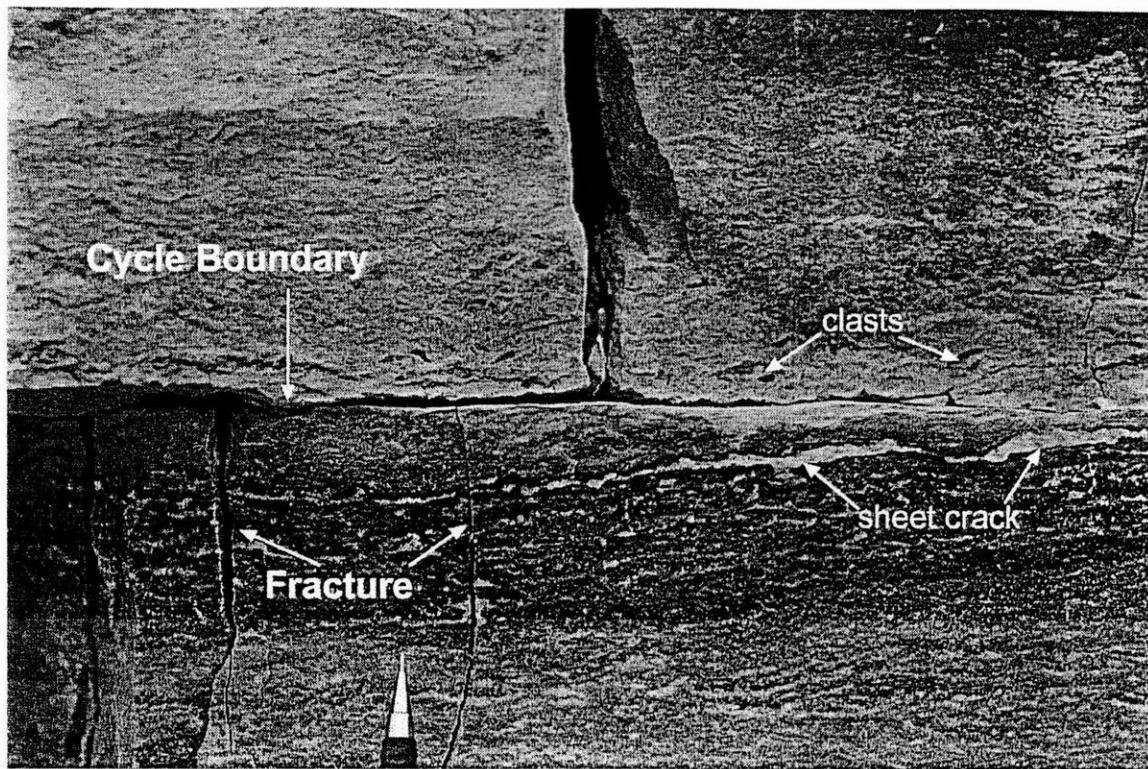


**Figure 3.** Fracture termination at the top of a shallowing upward cycle boundary in the inner shelf facies association. Sheet cracks below the cycle boundary are indicative of a supratidal setting. The intraclastic conglomerate above the cycle boundary was deposited in a deeper environment.

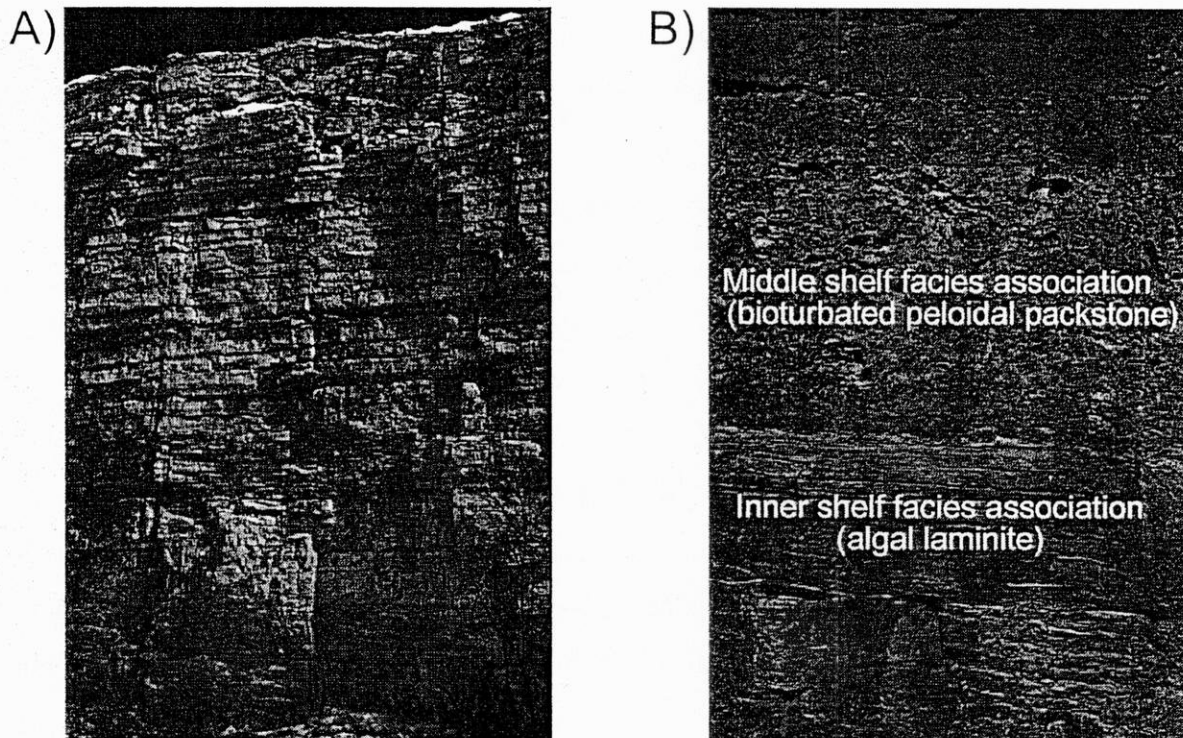


**Figure 4.** Photographs illustrating the lithologic characteristics of the inner-middle shelf facies association typical of the Hendricks Fm. **A)** Typical outcrop of the Hendricks Fm., upper level Big Quarry. Note the alternating light and dark layers. **B)** Close up illustrating the fine-grained laminites of the inner shelf facies association and the coarser-grained packstone of the middle shelf facies association (above); pocket knife for scale.

The middle shelf facies association consists of coarse crystalline, bioturbated and massive skeletal (brachiopods, corals and stromatoporids) wackestone-boundstones (with some chert nodules), and bioturbated cherty mudstone-wackestones. Bedding planes are discontinuous and organic-rich laminae are not present. Depositional cycles are thickly bedded and defined by an upward decrease in mud and an increase in grain size (Hegrenes, 1996). Bedding planes are few and not laterally extensive. Figure 5 illustrates the lithologic characteristics of the middle shelf facies association.

### **Hydrogeology**

In the Door Peninsula, the Silurian aquifer is a self-contained unconfined aquifer system, bounded on three sides by surface water and beneath by the Ordovician Maquoketa Shale. The dolomite is the primary aquifer for the Door Peninsula, providing over 99% of all water used for agriculture, industry, and drinking-water supply (Ellefson and others, 1987). The area receives about 76.5 cm/yr of precipitation, including both rain and snow. Due to the thin soils and permeable bedrock, runoff is negligible over much of the study area and approximately 24 cm/yr recharges the groundwater (Bradbury, 1989). Groundwater recharge does not occur uniformly throughout the year; the primary recharge period is during spring snowmelt and additional recharge usually occurs in the fall of the year when vegetation has gone quiescent (Bradbury and others, 2000).

The dolomite is densely fractured and secondary dissolution has enlarged both fracture apertures and primary porosity. Groundwater flow is characterized by recharge through vertical fractures and rapid lateral movement along horizontal high-permeability zones (Sherrill, 1978; Bradbury and Muldoon, 1992) that appear to be laterally continuous on the scale of kilometers (Muldoon and others, in review). Silurian stratigraphy plays an important role in the distribution of hydraulic conductivity of the aquifer throughout eastern Wisconsin. By combining stratigraphic, geophysical, and hydrogeologic data, Muldoon and others (in review) were able to correlate fourteen high-permeability zones within the Silurian aquifer. Several of these zones are regional

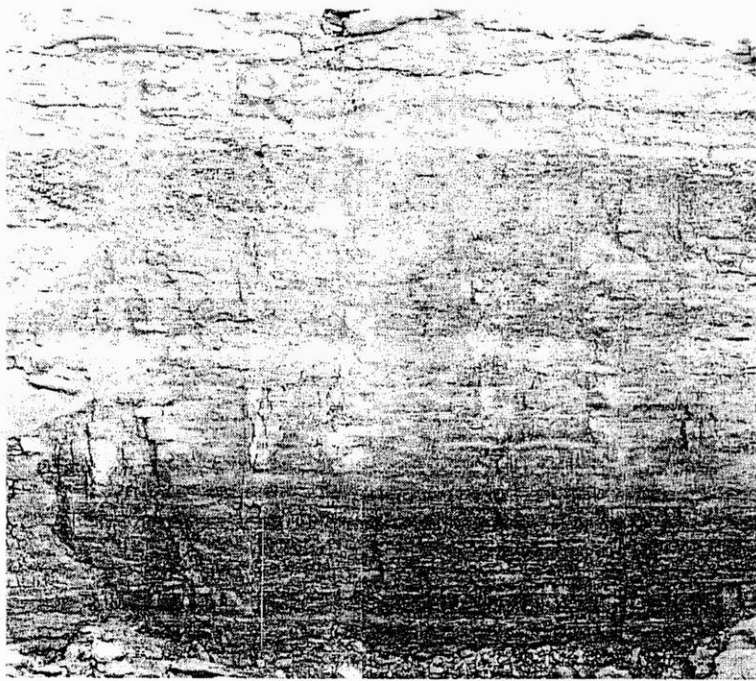


**Figure 5.** Photographs illustrating the lithologic characteristics of the middle shelf facies association. **A)** Typical outcrop of the Manistique and Engadine Fm., Mathey Road Quarry. Note that the overall massive appearance. **B)** Close up illustrating the stromatoporoid fossils that have been replaced by chert; lens cap for scale.

in extent and can be correlated in wells more than 10 miles apart. These zones parallel bedding and appear most pronounced within the inner shelf facies association and at contacts between facies associations.

Water table and potentiometric-surface maps for Door County (Sherrill, 1978; Bradbury and others, 1991; Bradbury and others, 1998) indicate potentiometric highs in the center of the peninsula both north and south of Sturgeon Bay. A simplified version of Sherrill's map, shown in Figure 6, indicates that regional flow is primarily away from these potentiometric highs towards Lake Michigan to the east and Green Bay to the west. There are two flow systems in the fractured dolomite aquifer (Bradbury and Muldoon, 1992). The majority of the wells within the county are completed in the deeper aquifer and Sherrill's map is representative of the deeper flow system. Figure 7 shows long-term water level data collected from wells and piezometers at the Jarmen Road site. Well MW1 and piezometer MW2A represent the deep flow system, while piezometers MW2D, MW6A and well MW3 represent the shallow system. These wells and piezometers continually contained water, while the intermediate piezometer, MW7C, was frequently dry.

Accounts of contaminant releases suggest that groundwater flow rates can be very rapid in the dolomite aquifer. Bradbury and Muldoon (1992) reported groundwater velocities of 64 and 116 m/day based on elevated nitrate levels in two domestic wells after a nitrate release during manure pit construction. Groundwater velocities measured in a series of natural-gradient tracer tests conducted at Bissen Quarry ranged from 0.47 to 118.2 m/day with a mean velocity of 12.7 m/day and a median velocity of 5.9 m/day (Muldoon, 1999). These values are believed to represent a mix of fracture and matrix groundwater velocities. The values greater than 20 m/day are believed to be representative of velocities within the fracture network.

### **Regional Fractures**

Previous work in Door County suggests that vertical fractures as well as horizontal bedding planes and dissolution zones provide the primary pathways for groundwater flow in the Silurian

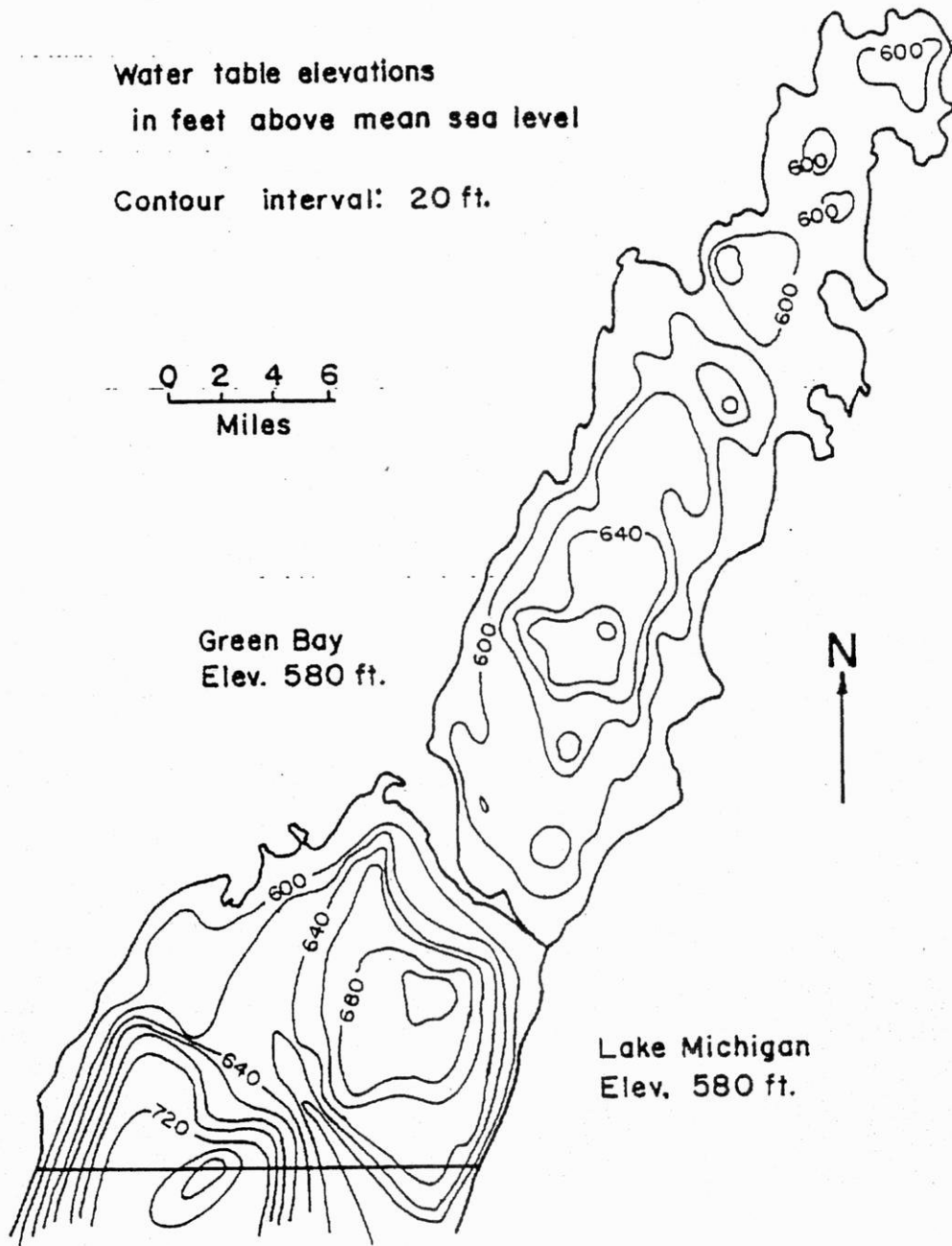


**Figure 6.** Simplified version of Sherrill's (1978) water-table map of Door County (from Nauta, 1987).

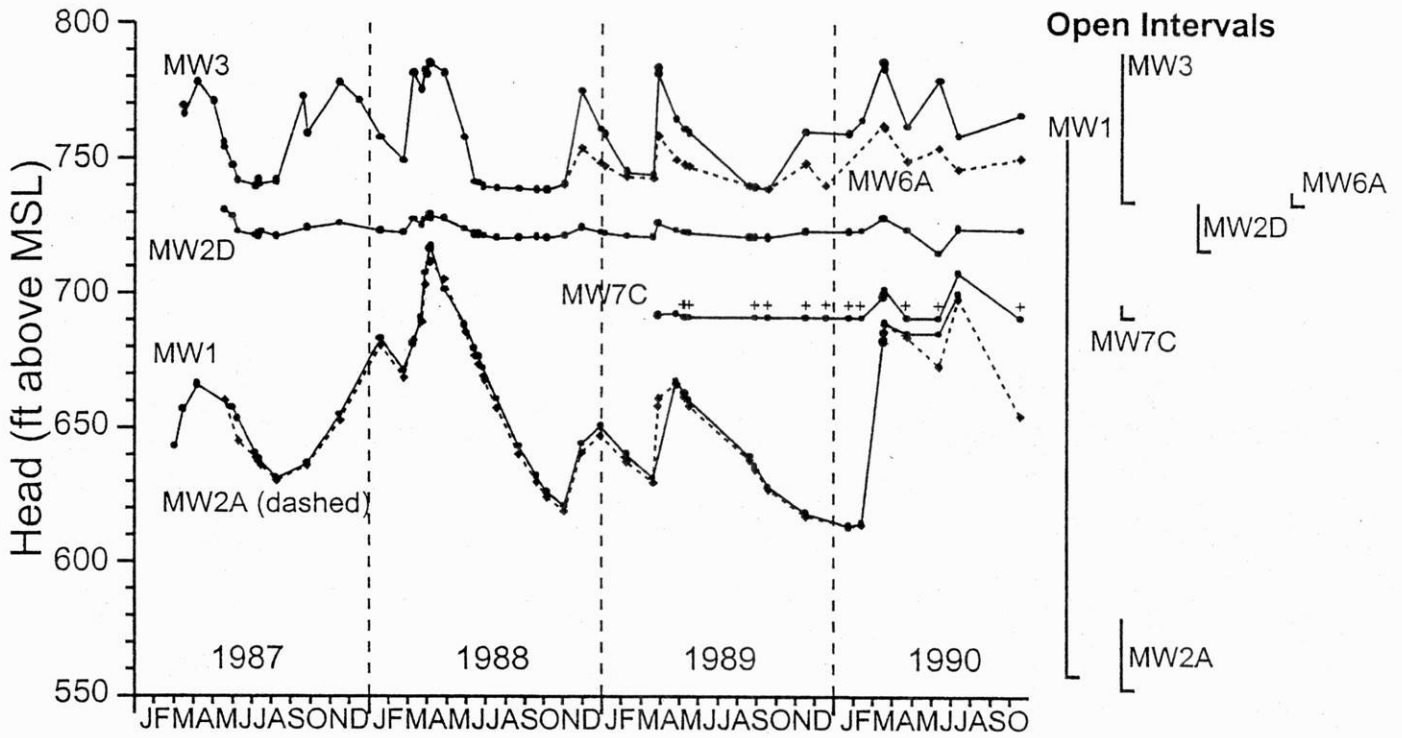


**Figure 7.** Hydraulic head of wells and piezometers at the Jarmen Road site. Lines on the right side of the figure indicate the open interval of the well or piezometer; small x's (MW7C) indicate that the well was dry (from Bradbury and Muldoon, 1992).

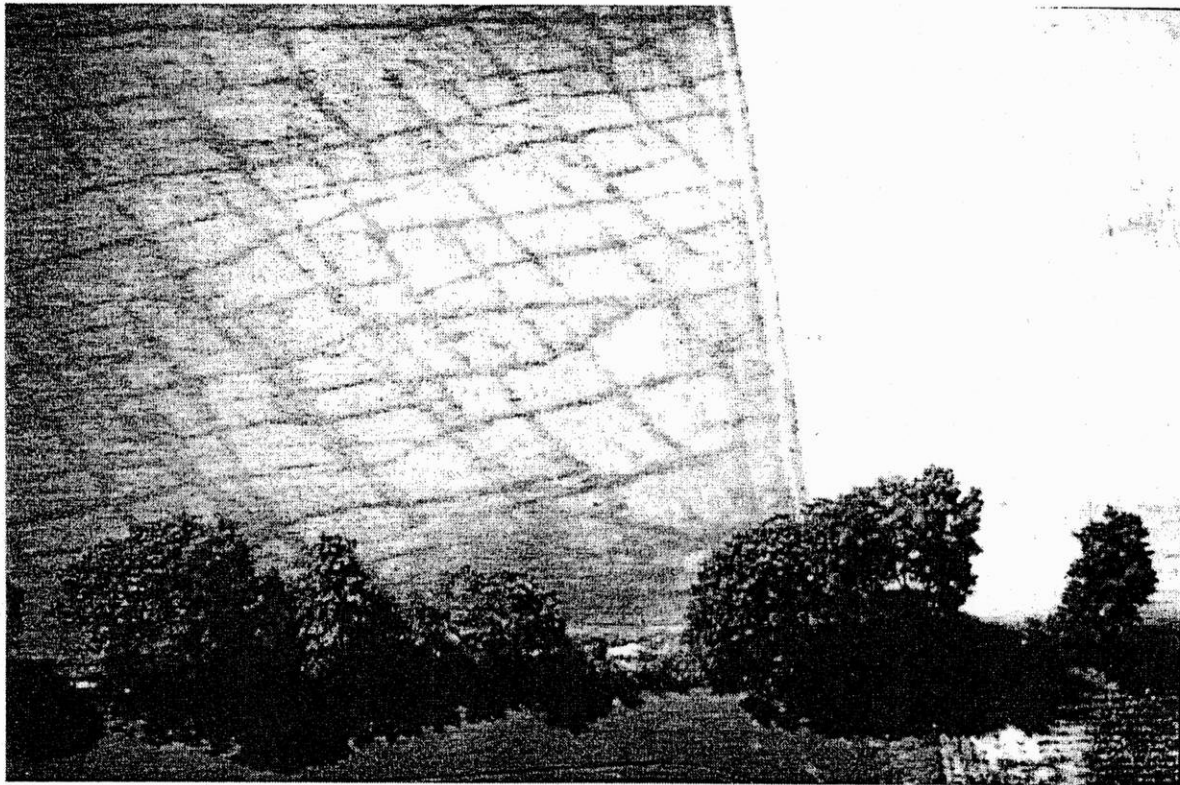


**Figure 8.** Oblique airphoto of fracture traces in an alfalfa field in north-central Door County (photo by Bradbury).

dolomite (Sherrill, 1978; Bradbury and Muldoon, 1992). Figure 8 shows two predominant joint sets in an alfalfa field in northern Door County; fractures are spaced approximately 10 to 20 ft apart. Fracture orientations in the Door Peninsula (Roffers, 1996) resemble those in other parts of the Michigan Basin (Holst and Foote, 1981; Holst, 1982; LaPointe and Hudson, 1985). Roffers' (1996) multi-scale analysis identified four major fracture sets ( $069^{\circ}$ ,  $152^{\circ}$ ,  $046^{\circ}$ ,  $135^{\circ}$ ) and four minor fracture sets ( $088^{\circ}$ ,  $165^{\circ}$ ,  $030^{\circ}$ ,  $118^{\circ}$ ) in Door County. These fracture orientations are consistent at different scales (from outcrop to lineament scale) and in different facies (Roffers, 1996). Aside from early Paleozoic subsidence in the Michigan Basin, the mid-continent region has been relatively free of tectonic activity since the Precambrian (Howell and van der Pluijm, 1990). Consequently, fractures are one of the few structural features present in this part of the continent. Relatively undeformed sedimentary rocks (i.e. neither faulted nor folded) may develop opening-mode fractures due to regional extension associated with uplift and erosion (e.g. Price, 1966; Voight and St. Pierre, 1974; Lajtai, 1977; Narr and Currie, 1982) and/or increased pore fluid pressure at depth (e.g. Secor, 1965; Ladiera and Price, 1981; Magara, 1981; Engelder, 1985; Lorenz and others, 1991). Fracture orientations over much of the Michigan Basin are likely controlled by the present day stress field ( $\sim 50$ ; Haimson, 1978) or past stress fields associated with the Appalachian and Ouachita Orogenies (134 and 1, respectively; Cradock and Van der Pluijm, 1989).

## STRATIGRAPHIC CONTROLS ON VERTICAL FRACTURE PATTERNS

### Introduction

Previous work on fracture distribution in Door County has focused on mapping features visible at the land surface and summarizing fracture characteristics based on these exposures; to date, no work has characterized the density and truncation patterns of fractures within the various stratigraphic units. As part of this study, Underwood (1999) mapped vertical fractures on quarry walls at two sites and recorded field observations at seven additional sites (Figure 9) in order to assess the stratigraphic controls on fracture patterns in the Silurian dolomite of northeastern Wisconsin. Locations of scanline surveys (discussed in the next section) are also shown in Figure 9.

The stratigraphic features that control fracture patterns in sedimentary rock can be evaluated in terms of mechanical stratigraphy (i.e. the thickness and the material properties of mechanical units and the material properties of mechanical interfaces). Stratigraphic horizons (such as cycle boundaries, bedding planes, ...) that resist fracture propagation act as mechanical interfaces that bound mechanical units since fractures abut these horizons. Thus, mapping of fracture patterns delineates mechanical units. In order to assess any bias incurred from visual delineation of mechanical interfaces, we developed a quantitative method to identify mechanical interfaces from fracture pattern using both fracture termination percentage and the number of fractures that terminate at each stratigraphic horizon. Below, we use data obtained from fracture maps of vertical quarry walls to develop empirical relationships between sedimentary stratigraphy and mechanical stratigraphy. These relations allow us to predict mechanical stratigraphy and subsequent fracture patterns at depth where only stratigraphic data is available (i.e. from core observations). Comparing stochastically predicted mechanical stratigraphy to observed mechanical stratigraphy tests this methodology.

● Locations of detailed fracture maps of vertical quarry walls

▲ Fracture observation sites

1. Wequiock Falls Co. Park
2. Bayshore Co. Park
3. Bissen Quarry
4. Big Quarry
5. Walker Road Quarry
6. Mathey Rd. Quarry
7. Jarmen Rd. Research Site
8. Hwy 42 Roadcut
9. Peninsula Players Rd. Quarry

Sites 1 & 2 (▲) are located in Brown County.

● Locations of scanline surveys

Gibson Lane Quarry is located in Kewaunee County.



**Figure 9.** Locations where fracture data were collected as part of this study. Underwood's (1999) fracture mapping locations (black circles) and fracture observation locations (black triangles) are numbered 1 to 9. Locations of scanline surveys are shown with gray circles.

### *Mechanical Controls on Fracturing*

In relatively undeformed sedimentary rocks, opening-mode fracture patterns (joint patterns) are typically controlled by stratigraphy rather than faulting or folding (e.g. Becker and Gross, 1996; Hanks and others, 1997); fractures tend to terminate at specific stratigraphic horizons (e.g. Gross and others, 1995). Under these conditions, fracture density typically depends on material properties and bed thickness of stratigraphic units (e.g. Huang and Angelier, 1989). The properties of a stratigraphic section that control fracture patterns may be described in terms of mechanical stratigraphy composed of mechanical units and mechanical interfaces (e.g. Corbett and others, 1987; Gross and others, 1995; Hanks and others, 1997). A mechanical unit represents one or more lithostratigraphic units with fractures typically spanning the thickness of the unit and abutting the bounding stratigraphic horizons. The stratigraphic horizons along which many fractures abut are termed mechanical interfaces (Figure 10).

The stratigraphic characteristics that comprise the mechanical stratigraphy of a sedimentary succession are those that control fracture initiation and termination in rock strata. Vertical opening-mode fractures (joints) typically initiate from flaws somewhere within a mechanical unit and terminate at mechanical interfaces (Gross, 1993). In layered formations consisting of interbedded brittle/ductile rocks, fractures typically initiate in the brittle layer and terminate at the contact with ductile layers (e.g. Cook and Erdogan, 1972; Erdogan and Biricikoglu, 1973; Helgeson and Aydin, 1991; Rijken and Cooke, in review). Within layered formations that are dominated by one lithology, such as the Silurian dolomite of Door County, fractures terminate at mechanical interfaces due to interface slip (e.g. Teufel and Clark, 1984; Renshaw and Pollard, 1995) and/or local debonding along interfaces that are weak in tension (Underwood, 1999, Cooke and Underwood, 2001).

While the properties of the mechanical interfaces control fracture termination, mechanical unit thickness controls fracture density and length (e.g., Gross, 1993); thicker mechanical units will have longer and more widely spaced fractures than thinner units. Understanding fracture density relationships therefore requires knowledge of the distribution of mechanical interfaces, which

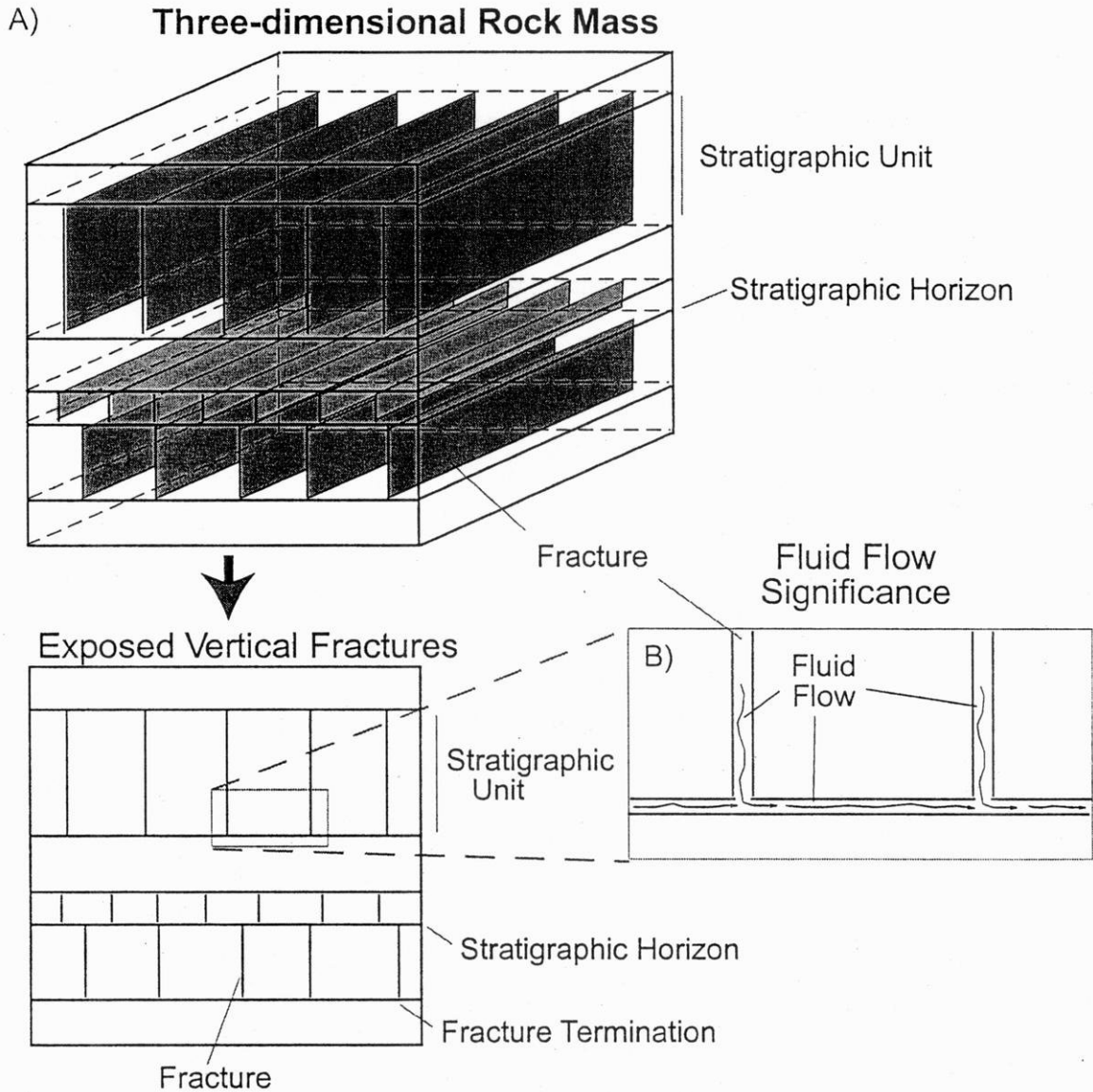


**Figure 10.** A) Stratigraphic controls on fracture patterns. Fractures develop within stratigraphic units and abut against stratigraphic horizons (modified from Gross et al., 1995). Decreases in mechanical unit thickness increase fracture density. B) Termination of vertical fractures can redirect vertical component of flow to horizontal fractures.

control fracture initiation and propagation. Field investigations indicate that the product of fracture density and bed thickness is approximately 1.0 (Price, 1966; Hobbs, 1967; McQuillan, 1973; Huang and Angelier, 1989; Narr and Suppe, 1991; Gross, 1993; Gross and others, 1995; Wu and Pollard, 1995; Becker and Gross, 1996; Bai and Pollard, 2000). One explanation for this relationship relies on the concept of a stress shadow (Lachenbruch, 1961; Nur, 1982; Pollard and Segall, 1987; Gross and others, 1995); new fracture growth is inhibited within a zone of decreased stress adjacent to an open fracture (Pollard and Segall, 1987). The size of the stress shadow is directly proportional to the height of the fracture, so that thicker mechanical units will have longer and more widely spaced fractures than thinner units (Pollard and Segall, 1987; Gross, 1993).

## **Methods**

The mechanical stratigraphy of the Silurian dolomite and the effectiveness of different types of stratigraphic horizons (e.g. cycle boundaries) on terminating vertical opening-mode fractures was investigated through four steps: 1) mapping fractures and measuring dolomite stiffness on vertical quarry walls at two locations and observing fracture patterns at seven additional locations, 2) correlation of previously characterized stratigraphic horizons with mechanical interfaces that arrest fracture propagation, 3) development of empirical relationships between sedimentary strata and vertical fracture pattern, and 4) comparison of fracture pattern predicted from these empirical relations to the observed fracture pattern. Sites for mapping quarry walls (Figure 9), which were chosen to represent the three facies associations of the Silurian dolomite, include Big Quarry (inner shelf and inner-middle shelf facies associations) and Mathey Road Quarry (middle shelf facies association).

### ***Mapping Vertical Fractures in Quarry Walls***

Vertical fractures were mapped along quarry walls which exposed different portions and facies associations of the Silurian succession. Figure 11 illustrates the location of fracture mapping and observation sites in relation to the stratigraphic section. Underwood (1999) mapped a horizontal pavement surface as well as vertical quarry walls in both the lower (Figure 12c) and upper quarry

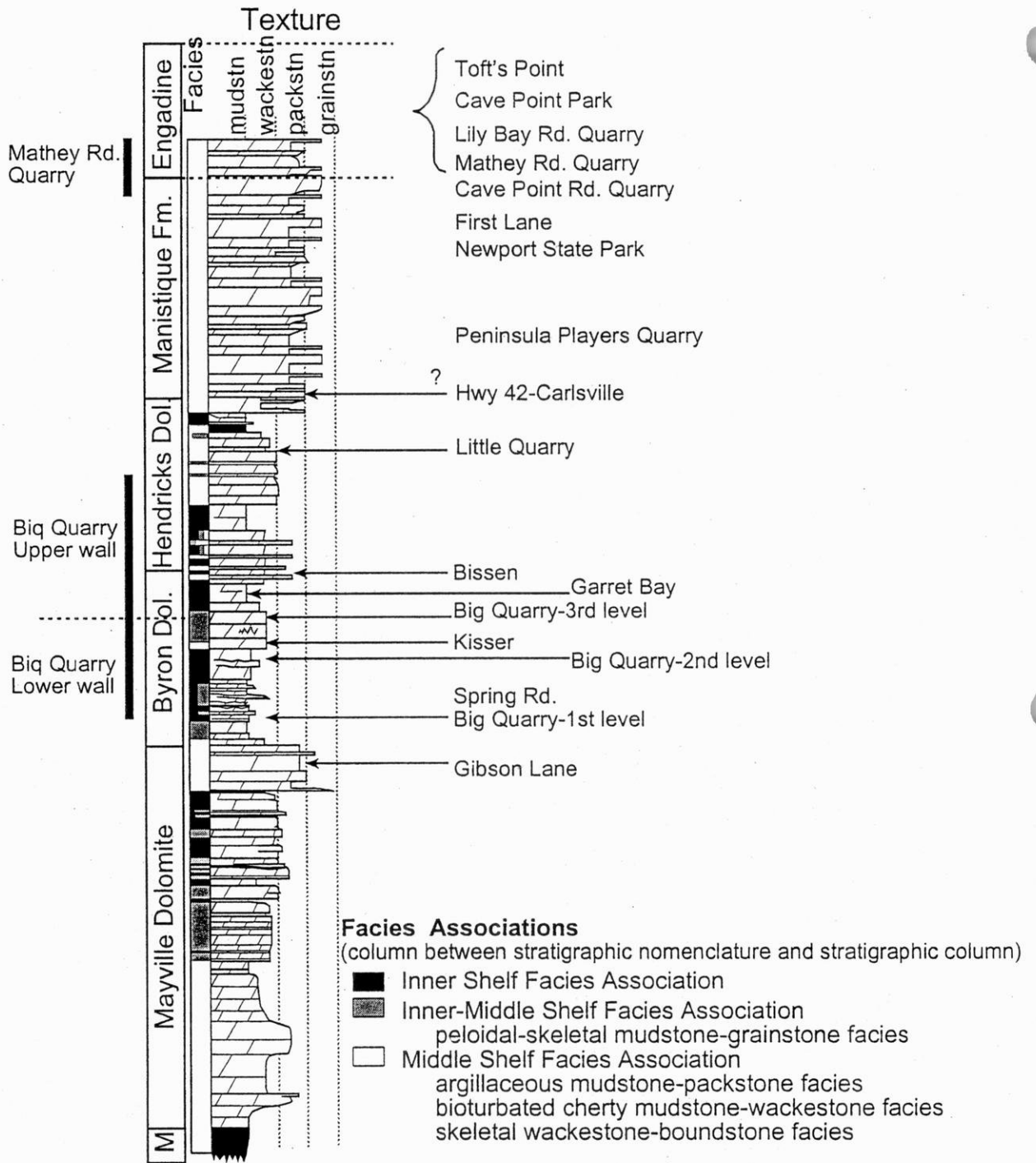


**Figure 11.** Stratigraphic position of locations where fracture data were collected as part of this study. Locations of scan line surveys are shown to the right of the stratigraphic column. Vertical lines to the left of the stratigraphic column indicate the stratigraphic position of vertical quarry walls where fracture patterns were mapped in detail by Underwood (1999).

(Figure 13c). The Big Quarry section exposes the entire Byron Formation and the majority of the Hendricks Formation. The two primary sets of vertical fractures occur at  $\sim 40^\circ$  and  $\sim 170^\circ$  in Big Quarry and the orientation of the quarry walls are controlled by the dominant fracture sets so that walls formed along one fracture set expose the other set of fractures. Comparison of fractures on differently orientated walls within Big Quarry reveal very little difference in fracture pattern between the two observed fracture sets (Underwood, 1999). Along both of these quarry walls, vertical fractures about the same stratigraphic horizons, and variations in fracture density among stratigraphic units correlate between each wall (Underwood, 1999). The similarity of fracture patterns at different orientations suggests that all fracture sets develop similarly within a given stratigraphic unit.

The middle shelf facies association exposed in the Mathey Road Quarry belongs to the Cordell Member of the Manistique Formation and the Engadine Dolomite (Figure 11). Underwood (1999) was only able to map vertical fractures along one quarry wall (Figure 14).

The fracture maps from Big Quarry and Mathey Road Quarry as well as observations of fracture patterns in the seven additional quarries provided valuable, but qualitative, understanding of how lithostratigraphic variations affect the distribution of vertical fractures throughout the Silurian sequence. Measurements of dolomite stiffness and the identification of mechanical interfaces, both described below, helped us develop a more quantitative characterization.

### ***Measurement of Dolomite Stiffness***

Variations in rock stiffness may produce variations in fracture density (e.g. Gross and others, 1985); otherwise, fracture density is expected to correlate with thickness of mechanical units (e.g. Huang and Angelier, 1989). The *in situ* stiffness of stratigraphic units was determined using a Schmidt Hammer, a portable device that measures the rebound of a hammer impacting the rock (e.g. Poole and Farmer, 1980). The error in the stiffness values obtained from the Schmidt Hammer can be evaluated from the range in multiple readings at the same locality (Poole and Farmer, 1980). For the purpose of this study, the Schmidt Hammer results are not



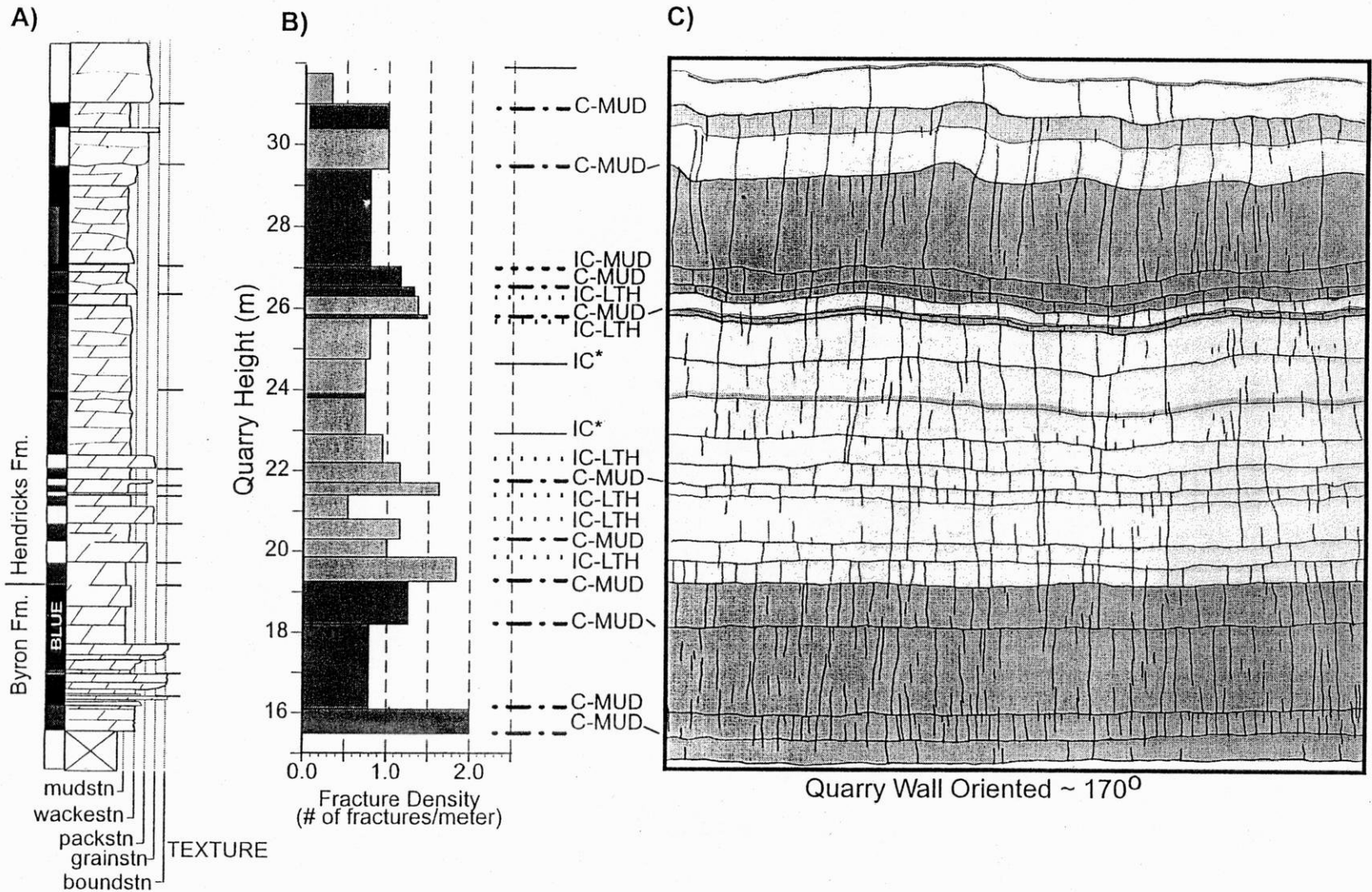


**Figure 13.** a) Lithostratigraphy; facies associations are color coded the same as figure 2: black= inner shelf, gray=inner-middle, white=middle shelf), b) mechanical stratigraphy, and c) fracture map for the upper Byron and lower Hendricks Formations. In the mechanical stratigraphy and fracture maps the inner-middle and middle shelf facies associations have been grouped; dark gray layers represent inner shelf facies, while lighter gray layers represent inner-middle/middle shelf facies. The abbreviations for mechanical interfaces are as follows: C=cycle boundaries, IC=intracycle boundaries, ORG = organic horizons, MUD = mud horizons, \* = no stratigraphic equivalent. Dashed lines indicate a major scour surface; irregular circles are weathered stromatopoids.

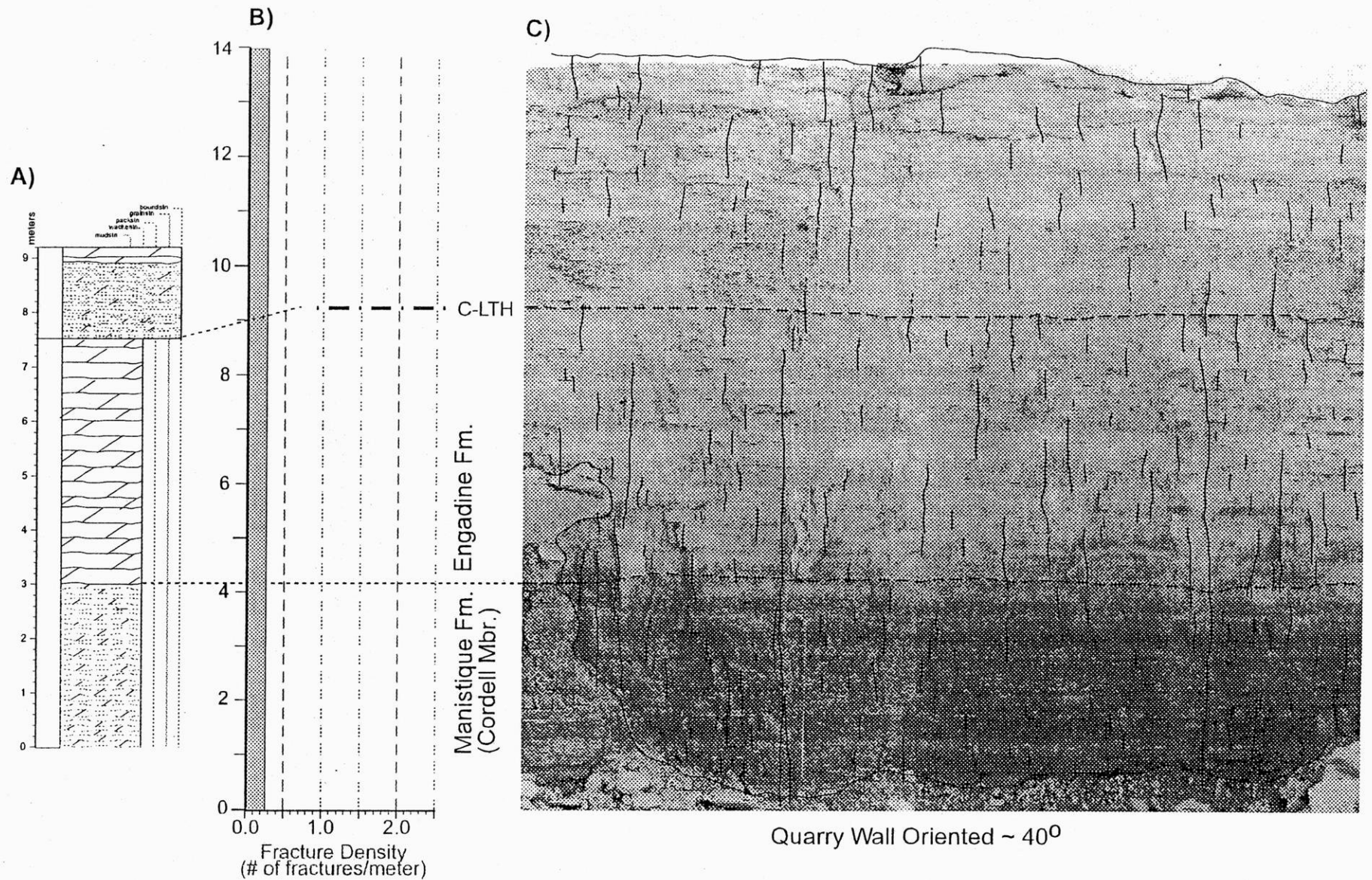


**Figure 14.** a) Lithostratigraphy; facies associations are color coded the same as figure 2: black= inner shelf, gray=inner-middle, white=middle shelf), b) mechanical stratigraphy, and c) fracture map for Mathey Rd. Quarry. In the mechanical stratigraphy and fracture maps the inner-middle and middle shelf facies associations have been grouped; dark gray layers represent inner shelf facies, while lighter gray layers represent inner-middle/middle shelf facies. The abbreviation for mechanical interfaces are as follows: C=cycle boundaries, IC=intracycle boundaries, ORG = organic horizons, MUD = mud horizons, \* = no stratigraphic equivalent.

intended to indicate absolute stiffness values; rather we use the results to determine the relative stiffness of each facies association within the Silurian dolomite.

### *Identification of Mechanical Interfaces*

We use two methods to determine the location of mechanical interfaces. The first field method employs visual identification of mechanical interfaces where numerous vertical fractures abut distinct stratigraphic horizons (Figures 12c & 13c). This method, however, may involve visual bias since the mapper's eye may be drawn to visually distinct horizons such as color contrasts or highly weathered horizons. Such visual bias may over-emphasize visually distinct horizons or neglect indistinct but significant horizons.

To assess visual bias we have developed a second, more quantitative method to identify mechanical interfaces that examines both the percentage of fracture terminations and the number of fractures that terminate at successive stratigraphic horizons. With this method, a stratigraphic horizon is considered to act as a mechanical interface only if both a small percentage of fractures propagate through the horizon and a sufficient number of fractures terminate at the horizon. Comparing the quantitatively determined interface distribution with qualitatively mapped interfaces can assess the visual bias involved in mapping interfaces in the field. To our knowledge, this is the first study to assess visual bias in characterizing mechanical stratigraphy and the first to propose an objective methodology for evaluating mechanical stratigraphy from fracture patterns.

To quantitatively determine the locations of mechanical interfaces within the stratigraphic sequence, we examine the occurrence of fracture tips within successive sampling intervals specified in the analysis. This assessment of fracture pattern is sensitive to the thickness of the sampling interval (Figure 15). In the presence of undulating stratigraphic horizons, a thin sampling interval may result in fracture tips along one horizon counted within two adjacent intervals; this yields two interfaces where only one exists. In contrast, a thick sampling interval may group more than one horizon into a single interval; this yields one interface where more than

one exists. Within the Silurian section, the minimum distance between two stratigraphic horizons is about 10 cm, while typical surface undulations are less than 10 cm. Consequently, a sampling interval thickness of 10 cm prevents the grouping of two adjacent interfaces and generally prevents the splitting of a single undulating interface. Unusually high undulating surfaces require additional consideration in this analysis.

In order for a stratigraphic interval to contain a mechanical interface, we require that the majority of the fractures that intersect the interval terminate within the interval rather than propagate through the interval. This is expressed as:

$$\% \text{ Terminations} = \frac{\text{No. of Terminations}}{\text{No. of Terminations} + \text{No. of Crossings}} \times 100\%$$

However, the majority criterion, on its own, is not robust unless we observe a significant number of fracture terminations. Let us consider one of the Big Quarry exposures which is 13 m in length. If only 3 fractures intersect a horizon along 13 m of exposure and 2 of the 3 fractures terminate at the horizon, the resulting percent termination is 66%. However, this is likely not a significant horizon because of the low number of fractures that actually intersect the horizon. We determine the critical number of fracture tips required for a sample interval to contain a mechanical interface by examining the frequency of the number of fracture tips counted within each 10 cm sampling interval (Figure 16).

The nearly horizontal portion of the data trend in Figure 16 suggests relatively infrequent stratigraphic horizons that contain many fracture tips, whereas the linearly sloping data trend suggests frequent horizons that contain fewer fracture tips. We interpret the horizontal data trend (Figure 16) to represent fracture termination at mechanical interfaces, whereas the sloping data trend represents relatively random termination of fractures within mechanical units (i.e. fracture termination is not constrained by stratigraphy). It follows that the cutoff between these two data trends is the critical number of fractures within the Big Quarry outcrop required for an interval to

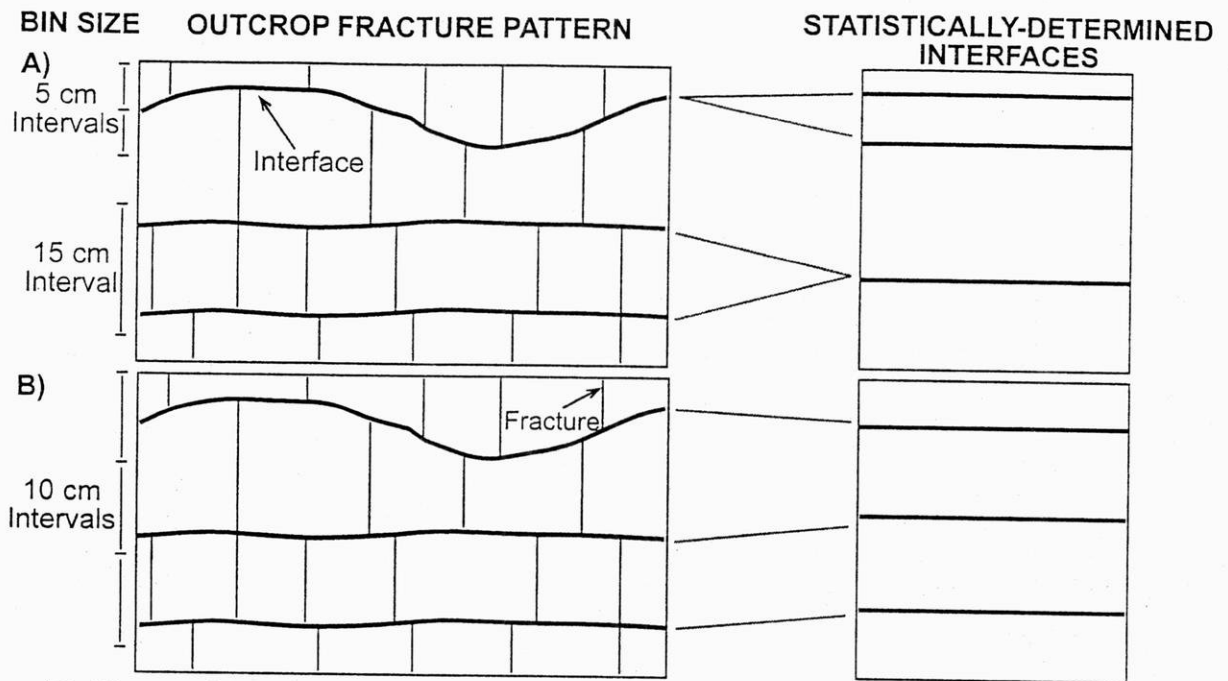


**Figure 15.** The stratigraphic interval sampling method used to statistically identify mechanical interfaces counts the number of fracture tips within each stratigraphic interval. **A)** If a sample interval is too thin, the method may split one interface into two. Likewise, a thick interval may group two interfaces into one. **B)** The optimum interval size will correctly sample the number of fracture terminations at an interface.

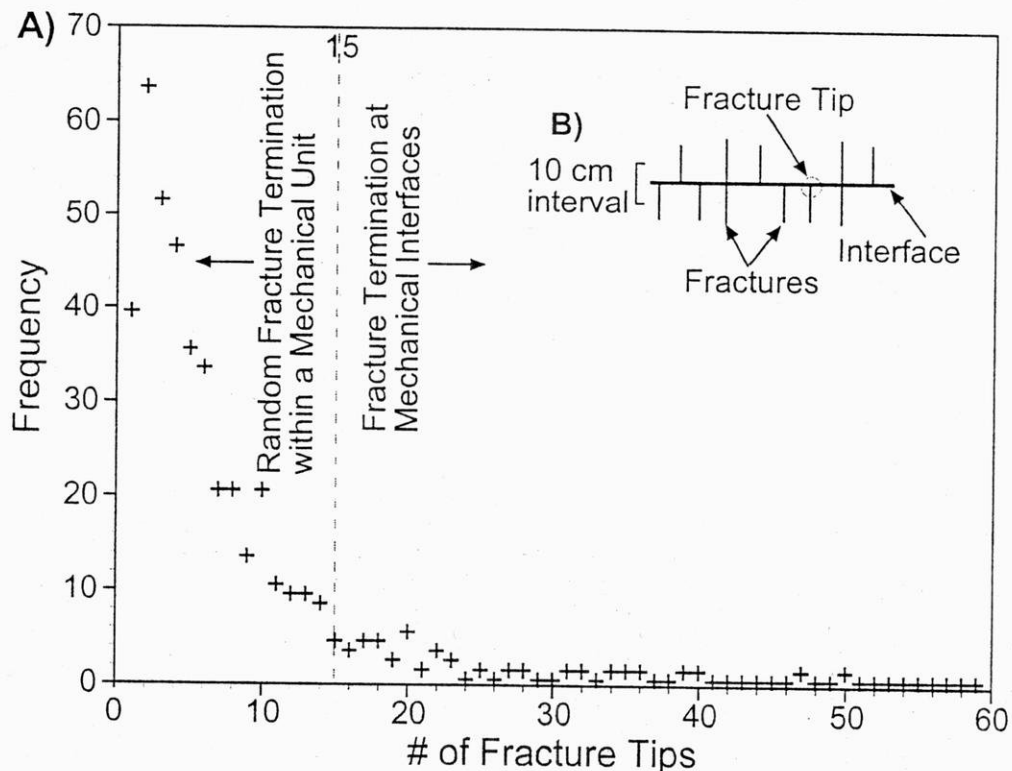


**Figure 16.** **A)** The frequency of fracture tips within sampling intervals provides a method to determine which stratigraphic horizons have enough fracture tips to be considered mechanical interfaces. Many sample intervals contain < 15 fracture tips suggesting that fracture termination within these intervals is sparse due to relatively random fracture termination. When fracture termination is stratigraphically controlled, the number of fracture tips within one interval should be > 15. **B)** Determination of the number of fracture terminations at a stratigraphic horizon.

contain a mechanical interface. We qualitatively assess this cutoff at 15 fracture terminations within a 10 cm stratigraphic interval.

The placement of the frequency curve in Figure 16, and consequently the cutoff between stratigraphy controlled and random fracture terminations, will vary with length of the mapped interval because longer exposures will have more numerous fractures than shorter exposures. Therefore, the cutoff that we determine, 15, is relevant for the 13 m of available exposure mapped out of Big Quarry. Since the fracture density of most mapped layers in this study is approximately 1.5 fractures/meter, an average layer exposes about 20 fractures, an adequate population size for assessing the percentage of fracture termination. This also suggests that the termination of 15 fractures within an average interval (of ~20 fractures) reflects the influence of stratigraphy on fracture termination.

If the cutoff value is too high (e.g. 20 fractures), this method may underestimate the number of mechanical interfaces. Similarly, a low cutoff (e.g. 10 fractures) may overestimate the number of mechanical interfaces. A low cutoff is more conservative and should be used since potential interfaces must also pass the majority termination criterion. Among the horizons that terminate more than 15 fractures, only four do not pass the majority test for fracture intersection (Figure 17). In some respects, this evaluation is stochastic because the number of fracture tips that fall within each sample interval may vary with position of the initial interval. Decreasing sample interval thickness minimizes this variation. A 10 cm thick sample interval could misallocate interfaces by up to 5 cm; however, this relatively small error does not greatly influence the distribution of mechanical interfaces.

## **Results**

### ***Mechanical Stratigraphy***

Several generalizations can be drawn from fracture maps in quarries walls representative of different portions of the Silurian dolomite. Fractures in the thinly-bedded inner shelf facies association (Figure 12c) are generally evenly distributed, densely spaced, and frequently abut

against depositional cycle boundaries, and in some cases, fractures abut against horizons within a depositional cycle. Organic horizons, always found at cycle boundaries, appear weak and friable in outcrop and promote the termination of vertically propagating fractures. Since many fractures appear to abut against organic horizons, we encourage future descriptions of sedimentary stratigraphy to note the location of these thin organic deposits. Although mud horizons do not appear to be as weak and friable as organic horizons, fractures also frequently abut against these types of cycle boundaries.

Fracture pattern differs dramatically between the massive middle shelf facies association of the Manistique Formation and the more thinly-bedded inner shelf facies association of the Byron and Hendricks Formations. The massive middle shelf facies association contains longer (up to 8 m) and more widely spaced (5-7 m) fractures; fractures are not contained to distinct stratigraphic horizons because of the overall absence of weak interfaces (Underwood, 1999).

Transitions in fracture pattern coincide with the transitional inner-middle shelf facies association (Figure 13c). Vertical fractures appear to terminate both at mud cycle boundaries and at horizons within cycles. The faunal-bearing base of many cycles in this facies association often fracture independently from the thinner laminated mudstone top of the diagenetic cap which results in abundant fracture tips within individual cycles (e.g. 19.5 m; Figure 13c). Fracture density within an individual cycle is higher in the thinner, mudstone top than in the thicker faunal-bearing base. Although the inner-middle shelf facies association exhibits continuous and distinct bedding, in some cases, fractures appear to span several shallowing upward cycles.

### *Stiffness Variations Among Facies*

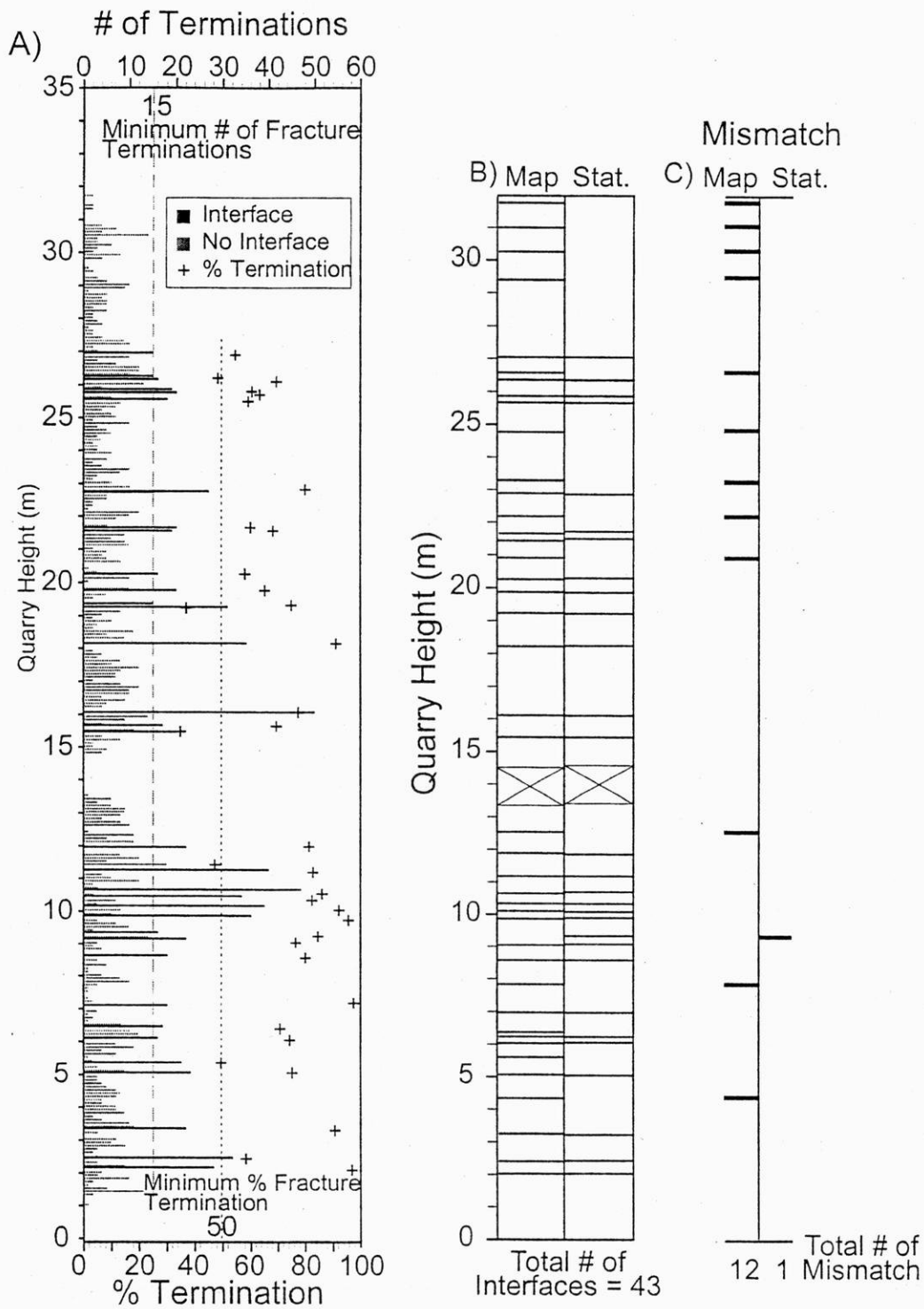
Maps of vertical outcrops show that fractures are largely contained within distinct stratigraphic units and abut against stratigraphic horizons acting as mechanical interfaces (Figures 12c & 13c). Because either contrasts between layer stiffness or weakness of stratigraphic horizons can control fracture patterns (e.g. Cook and Erdogan, 1972; Huang and Angelier, 1989), we first assess the variation of stiffness between facies associations of the Silurian dolomite.

The *in situ* stiffness tests yield average stiffness of  $57.2 \pm 5$  GPa,  $52.8 \pm 5$  GPa, and 60.9 GPa for inner, inner-middle, and middle shelf facies associations, respectively. The stiffness variation between facies associations throughout the Silurian does not exceed the error of this testing method. We suspect that dolomitization may have contributed to present-day uniform properties and that fracturing likely occurred post-dolomitization. Since stiffness changes are minimal throughout the Silurian dolomite, fracture termination is unlikely the result of material property differences between mechanical units. Consequently, the termination of vertical fractures is more likely controlled by the nature and distribution of stratigraphic horizons that act as weak mechanical interfaces.

### *Identification of Mechanical Interfaces*

Mapping mechanical interface distribution allows us to develop a mechanical stratigraphic section for mapped intervals (e.g. Figure 12b); a mechanical stratigraphic section is similar to stratigraphic sections used by sedimentologists. Whereas the horizontal axis of a traditional stratigraphic section is defined by the texture of the lithostratigraphic unit (Figure 12a), in our mechanical stratigraphic sections, the horizontal axis shows the fracture density of the mechanical unit (e.g. Figure 12b).

Interfaces mapped at Big Quarry have been compared to quantitatively determined interface locations in order to assess visual bias. The quantitative method did not identify any mechanical interfaces in the Mathey Quarry outcrop (Figure 14). Additionally, only one interface was visually identified in the unit. Therefore, no comparison of the two methods can be performed for the Manistique and Engadine formations. In general, interface locations determined from our quantitative criteria correspond well with those qualitatively assessed from fracture maps (Figure 17) suggesting that little visual bias occurred during the mapping process. Only one subtle interface that passed the quantitative criteria was missed in the visual identification (at 9.3 m; Figures 12 & 17). Additionally, only one visually distinct mechanical interface delineated during fracture mapping at Big Quarry does not pass the quantitative definition of a mechanical interface (at 12.65 m in Figure 17). Interestingly, the visual identification approach was better



$$\% \text{ Difference} = \frac{\# \text{ Mismatch}}{\text{Total \# of Interfaces}} = 30\%$$

**Figure 17.** A) Bold lines represent stratigraphic horizons which pass the mechanical interface criterion: greater than 15 fracture tips and >50% termination within 10 cm interval spanning 13 m. B) Comparison of visually mapped interfaces (left) with interfaces that meet our quantitative criteria (right) for the Byron/Hendricks Formations. C) Differences between the two methods are highlighted by mismatches between mapped and statistically determined interfaces.

suited for areas with highly undulating stratigraphic horizons or areas where the photographs used to aid in fracture mapping developed vertical distortion. The quantitative method failed to identify several horizons with greater than 10 cm undulations, such as the prominent surface (a sequence boundary) at 4.35 m (Figures 12 & 17) and an interface at 7.8 m (Figures 12 & 17). Since the photographs of regions high along the quarry walls (>20 m) developed vertical distortion, some apparent interface undulations are greater than the 10 cm sampling interval in the upper portion of mapped interval. The results from the two methods are merged by modifying the distribution of mechanical interfaces mapped in the field so that each interface conforms to the new quantitative definition with special consideration for undulating surfaces.

The close correlation of the visually and quantitatively determined distribution of non-undulating mechanical interfaces (Figure 17) suggests that the cutoff used for number of terminating fractures does not greatly over-restrict mechanical interfaces. Although the two methods of identifying mechanical interfaces produced similar results, the application of a quantitative criterion provides rigor to the analysis since we require that all interfaces pass the same objective definition of a mechanical interface.

### *Classification of Mechanical Interfaces*

We have identified two types of mechanical interfaces: cycle and intracycle interfaces. Cycle interfaces occur at the top of cycles, whereas intracycle interfaces are within an individual cycle. Each type of interface includes several distinct subcategories.

Cycle interfaces (C) are most abundant in sections of the Silurian dolomite consisting of thinly bedded inner and inner-middle shelf facies associations. Thin, weak deposits such as organic partings (ORG) and thin mud layers (MUD) often separate cycles. Organic cycle interfaces (C-ORG) are generally characterized by brown, thinly laminated organic material, with a thickness generally ranging from 0-1 cm along any one interface. In outcrop, the organic interface is very friable, poorly cemented and often iron-stained. Organic cycle interfaces are less abundant than other interface-types and are observed only within inner shelf facies association (Figure 12).

Mud cycle interfaces (C-MUD) vary in thickness from <0.5 cm to 4 cm; thickness is relatively uniform along individual horizons, but larger variations occur between horizons. These interfaces are generally platy and often mudcracked or associated with storm deposits. Mud interfaces associated with storm deposits often undulate with amplitudes ranging from 1-10 cm and are usually distinct and easily identifiable in the field. Cycles in the Engadine Formation (at 9.4 m; Figure 14) are separated by lithologic cycle interfaces (C-LTH) without intervening mud or organic material.

Intracycle interfaces (IC) separate portions of individual depositional cycles that fracture independently of one another. Two subcategories of intracycle interfaces were observed: thin mud layers (MUD) and contacts between layers of contrasting lithology (LTH). Mud intracycle interfaces (IC-MUD) resemble C-MUD interfaces, but are generally thinner and more planar. This interface type is observed in both the inner and inner-middle shelf facies associations. Lithologic intracycle interfaces (IC-LTH) typically separate coarse-grained, faunal-bearing lithologies, which are deposited in a more open marine environment, from fine-grained, thinly laminated lithologies deposited in a more restricted marine environment. This interface type is observed only in the inner-middle shelf facies association (e.g. at 19.8 m; Figure 13).

Occasionally, we identified a mechanical interface within a shallowing upward cycle that does not correlate to any specific stratigraphic horizon noted in previous stratigraphic studies; we denoted such interfaces by the symbol IC\* (e.g. at 5.6 m; Figure 12). More detailed stratigraphic description is required in order to classify these interfaces.

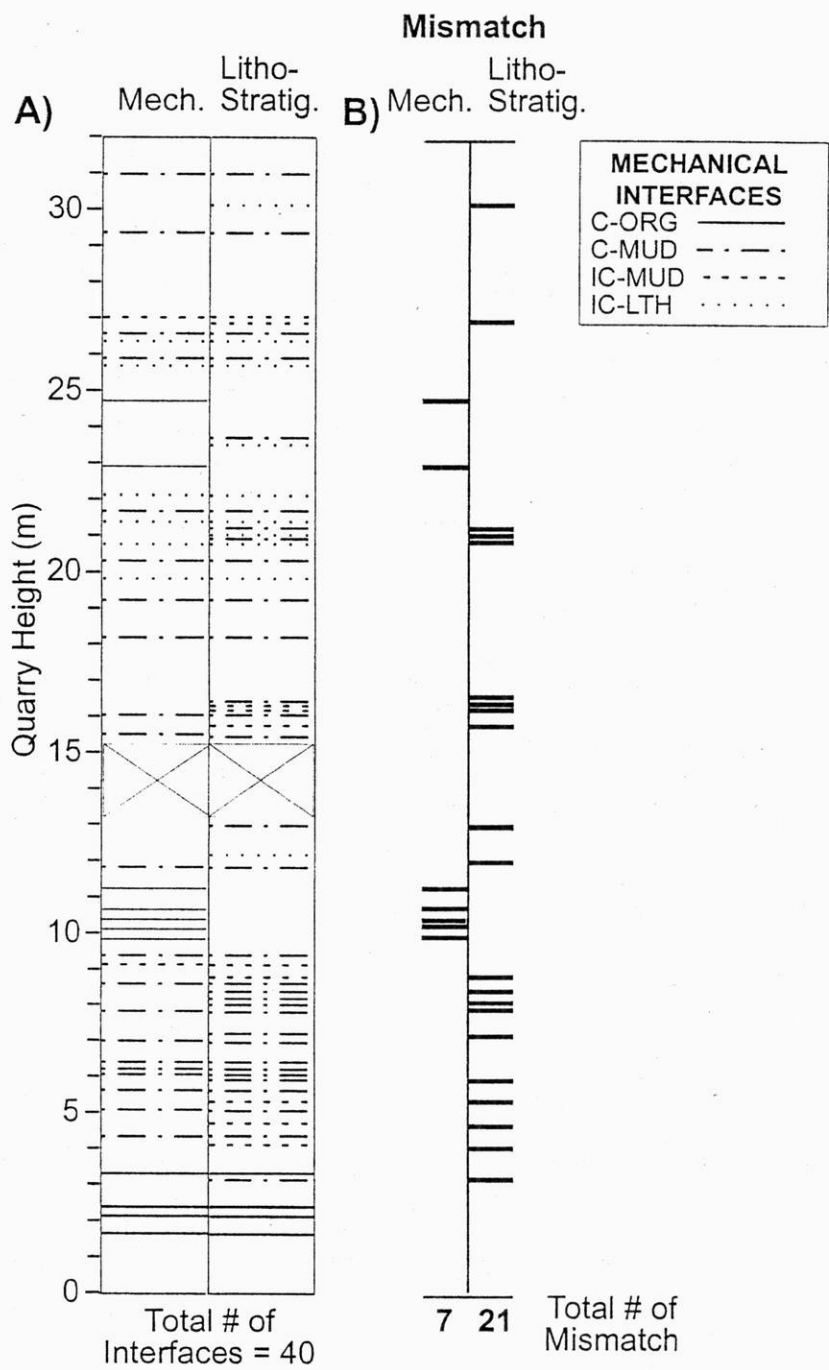
It should be noted that although mechanical interfaces correlate well with stratigraphy, not all stratigraphic horizons contribute to fracture pattern development. For example, some fractures propagate across mud horizons that appear no different from nearby horizons along which the fractures terminate.

## Mechanical Stratigraphy Prediction

The vertical length of fractures in horizontal sedimentary strata is controlled by the spacing of mechanical interfaces which effectively terminate vertically propagating fractures. The vertical length of fractures, in turn, controls the fracture density as longer fractures produce larger stress shadows that inhibit nearby fracture growth (Pollard and Segall, 1987; Gross, 1993). Since the length (vertically) and density of fractures in the Silurian dolomite are ultimately controlled by the distribution of mechanically weak interfaces, determining the distribution of these interfaces is an *a priori* requirement to predict fracture patterns at depth. In this section, we develop and test empirical relationships to predict the distribution of mechanical interfaces and subsequent fracture patterns using only stratigraphic data (i.e. data from rock core). This would allow us to predict fracture pattern within sections of the Silurian dolomite that are not exposed in outcrop. First, we establish quantitative relationships between mechanical stratigraphy, then we utilize quantitative relationships between mechanical stratigraphy and fracture pattern to develop a predicted mechanical stratigraphic section.

The quantitative relationships between lithostratigraphic and mechanical stratigraphy are based on outcrop observations in Big Quarry (Figure 18). This comparison reveals that not all stratigraphic horizons effectively terminate fractures. If we assume that each stratigraphic horizon acts as a mechanical interface (i.e. each recognized horizon is abutted by many fractures), we would predict many more closely spaced interfaces. This would yield shorter and more densely spaced fractures than those observed and mapped (Figures 12 and 13). Since this method greatly over-predicts the distribution of mechanical interfaces, lithostratigraphy should not be directly used to predict fracture patterns rather, statistically developed empirical relations can guide the prediction of mechanical stratigraphy from lithostratigraphy.

We have evaluated the probability of each type of stratigraphic horizon to act as a mechanical interface and have assessed whether facies association influences the degree of fracture termination at the stratigraphic horizon (Figure 19; probability = # mechanical interfaces / # stratigraphic horizons). Since the middle shelf facies association is not well represented in the



$$\% \text{ ERROR} = \frac{\# \text{ Mismatch}}{\text{Total \# of Interfaces}}$$

$$= 70\%$$

**Figure 18.** **A)** Comparison of observed mechanical interface distribution (left) with all noted stratigraphic horizons (right) for the Byron/Hendricks Formations. Mechanical interfaces are identified from both visual inspection and from our quantitative criterion determined. **B)** Not all stratigraphic horizons act as mechanically interfaces. Some mechanical interfaces occur where no sedimentary horizons had been noted.

Big Quarry section used for this analysis, our statistical analyses group middle shelf and inner-middle shelf facies associations in order to create larger sample groups. Within the inner shelf, and inner-middle/middle shelf facies associations, cycle boundaries ( C interfaces) frequently act as mechanical interfaces and intracycle horizons are less effective (Figure 19). Intracycle horizons (IC interfaces) between contrasting lithologies mostly occur within the inner shelf facies association and arrest fractures as effectively as cycle-bounding muds (Figure 19).

We use the probabilities developed for each mechanical interface-type in each facies association to stochastically predict the distribution of mechanical interfaces from only stratigraphic descriptions. To illustrate our predictive method, a cycle-bounding mud horizon (classified as C-MUD) within the inner-middle/middle shelf facies association has a 63% chance of acting as a mechanical interface that effectively stops fractures. Among all of the observed stratigraphic horizons that are cycle bounding mud layers (C-MUD), only 63% are randomly chosen to act as mechanical interfaces. This process is repeated for each mechanical interface type.

Some intracycle interfaces do not correlate to specific stratigraphic features (IC\*). Because there is no correlation with stratigraphy, the location of these interfaces cannot be predicted using the approach outlined above. For the purpose of testing our model predictions against observed mechanical interfaces, these interfaces that do not correlate to distinct stratigraphic horizons are not considered. Since these horizons are relatively infrequent (Figures 12 & 13), the misallocation of these mechanical interfaces will not greatly influence overall fracture distribution.

We test our method by comparing the predictions based on the measured lithostratigraphic sections of Big Quarry (Waldhuetter, 1994; Simo and others, 1998) to the field-mapped mechanical stratigraphy of the same interval. The model is stochastic since each realization, based on random assignment of mechanical interfaces, can produce different interface distributions.

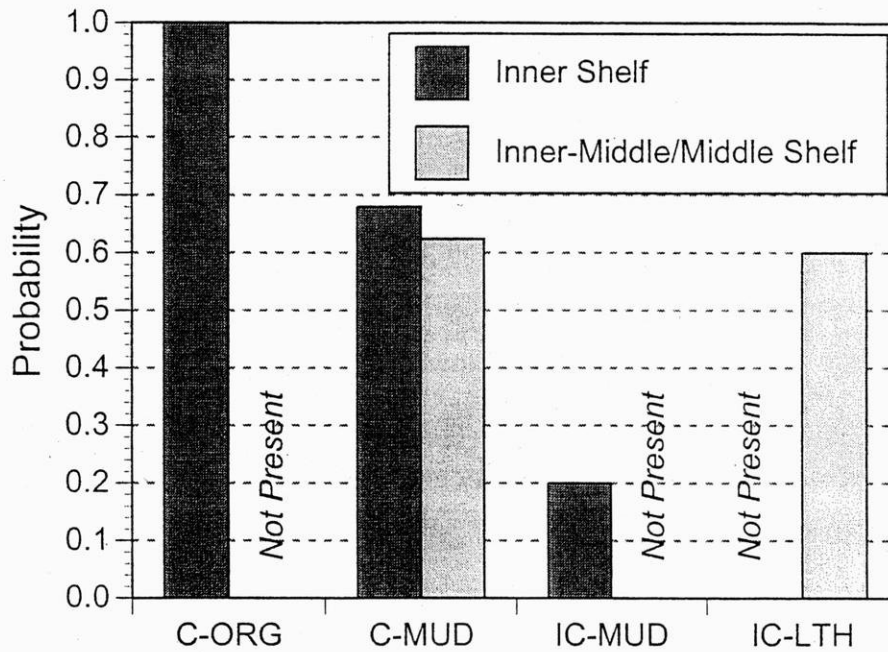


Figure 19. Probability of a stratigraphic horizon acting as a mechanical interface.

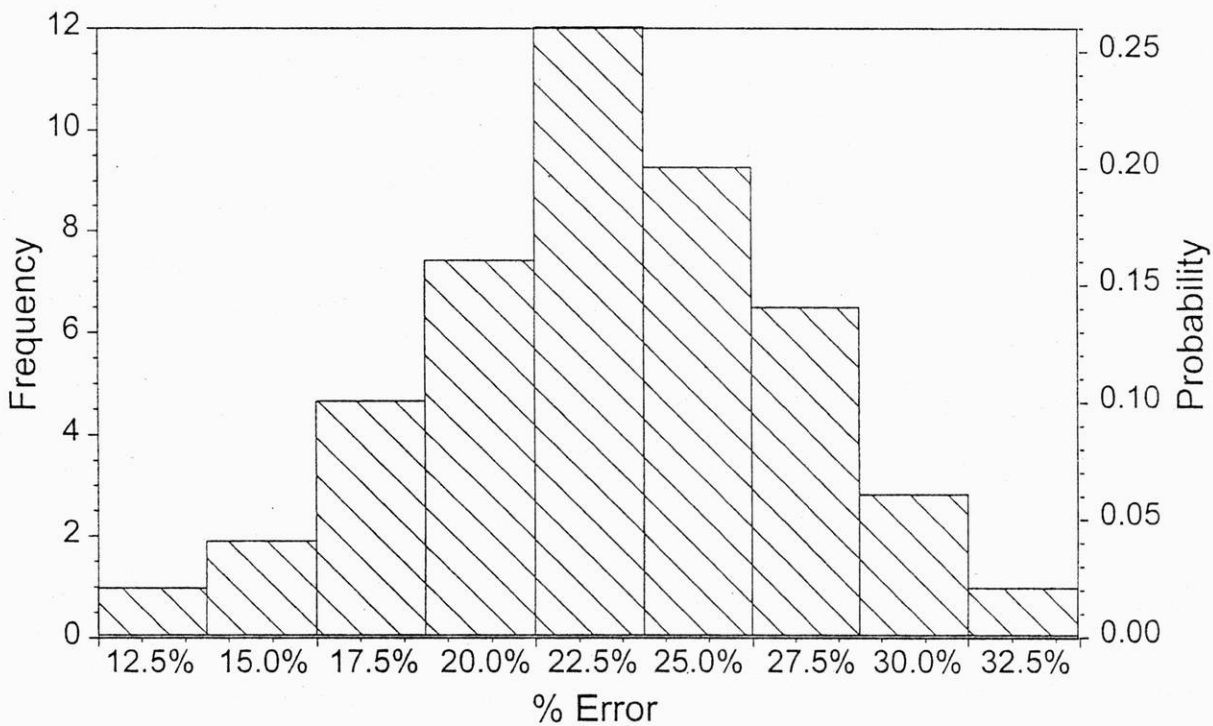


Figure 20. The average percent error for 50 realization is  $23\% \pm 4\%$ . The probability of encountering a given error value is computed by dividing the error frequency (left vertical axis) by the total number of realizations used in the analysis (50). The probability of extreme minimum and maximum error of 13% and 33%, respectively, is only 0.02. We are 96% certain that the percent error in any model run will fall within the range of 13-33%; this certainty is based on integrating the area under the probability curve.

In order to better assess the error of our model predictions, we ran a Monte Carlo simulation using fifty realizations (e.g. Herbaugh and others, 1977). This predictive method has 0.32 probability of having the average error within the fifty model realizations ( $23\% \pm 4\%$ , Figure 20). Although significant error (13-33%) occurs in predicting the exact location of mechanical interfaces, an example realization demonstrates important similarities between predicted and observed mechanical stratigraphy (Figure 21). Correlation between observed and predicted mechanical interface distribution is best for the lower part of the section where the dominant interface types are C-MUD and C-ORG; which have high overall probabilities of acting as mechanical interfaces (Figure 19). The degree of correlation decreases higher in the section where intracycle interfaces (IC-LTH, IC-MUD) are more prevalent; these interfaces have lower overall probabilities of acting as mechanical interfaces (Figure 19). Overall, the empirically predicted mechanical interface distribution equally over-predicts and under-predicts the location of mechanical interfaces (Figure 21). The error of our stochastic method for predicting mechanical stratigraphy from sedimentary stratigraphy is less than the error if we assume that each and every stratigraphic horizon acts as a mechanical interface ( $23\% < 70\%$ , see Figures 18 & 20).

## **Discussion**

Since groundwater in the Silurian aquifer of Door County flows primarily through the fracture network, prediction of flow characteristics, requires thorough understanding of the subsurface fracture pattern. Developing a method for predicting vertical fracture patterns at depth is an important step towards understanding groundwater flow processes in Door County.

The presence of horizontal high-flow features in Door County generally correlate with changes in stratigraphy, such as cycle boundaries (Muldoon and others, in review). Since vertical fracture pattern is also controlled by changes in stratigraphy, we propose that variations in vertical fracture patterns between units may contribute to the presence of hydrogeologic anomalies. For example, horizontal high-flow features may develop at mechanical interfaces where abundant

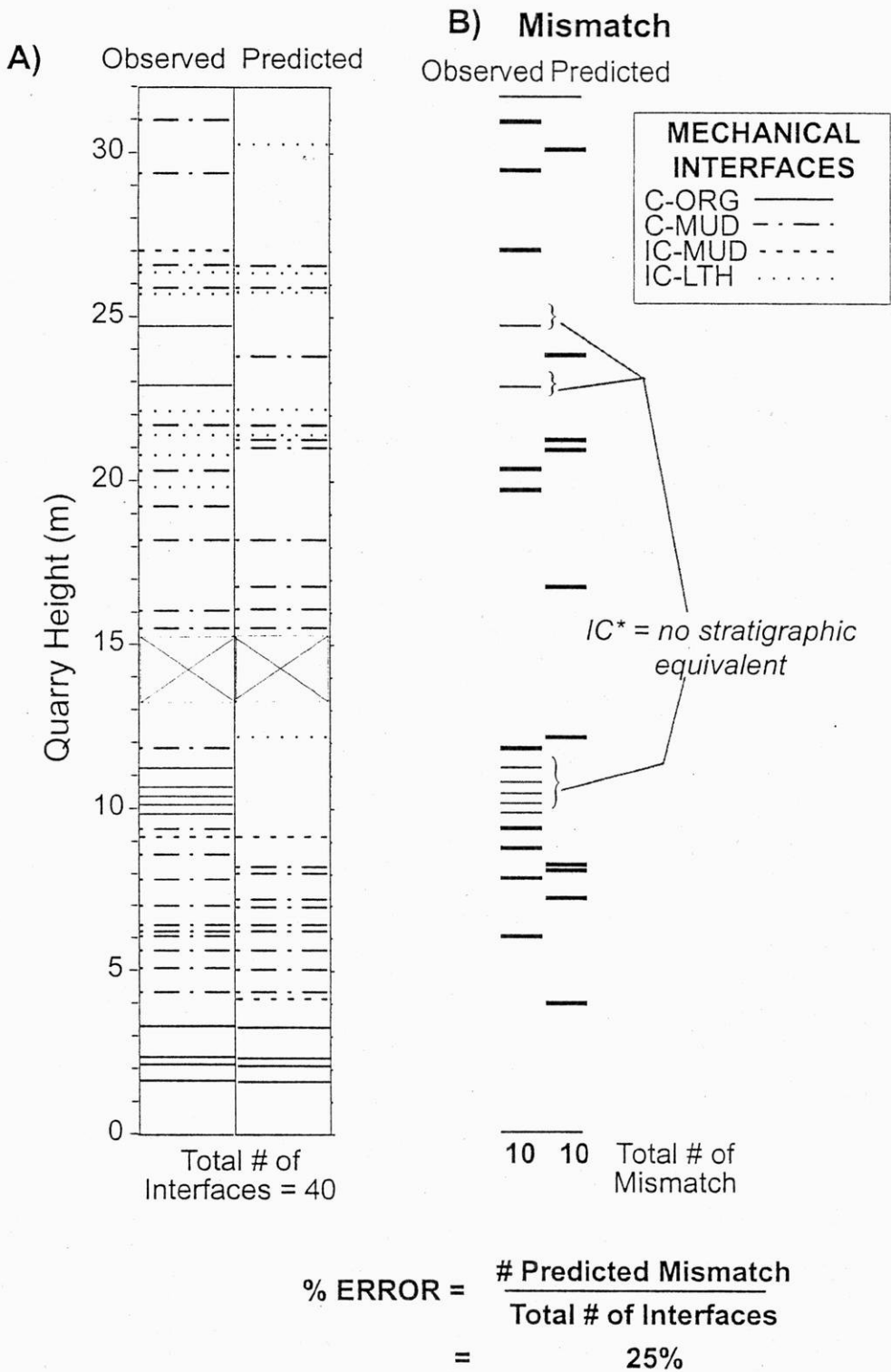


**Figure 21.** A) One realization of predicted mechanical stratigraphy (right) versus observed mechanical interface distribution (left) for the Byron/Hendricks Formations. B) The percent error of 25% is evaluated from mismatches between predicted and observed mechanical interface distribution. Interfaces with no stratigraphic correlation are not included in the analysis.

vertical fractures terminate. In addition, a decrease in fracture density below an interface reduces the number of vertical flow paths.

Through correlation of mapped vertical fractures with stratigraphy, we have identified several stratigraphic controls on fracture patterns within exposed intervals of the Silurian dolomite in Door County. The stratigraphic features which control fracture pattern in a sedimentary rock mass can be described in terms of mechanical stratigraphy; this includes the thickness and properties of the mechanical units and the properties of the mechanical interfaces (e.g. Gross et al., 1995). The thickness of mechanical units is constrained by the distribution of mechanical interfaces throughout the Silurian. Mechanical interfaces correspond to many but not all of the stratigraphic horizons described by Waldhuetter (1994) and Hegrenes (1996).

The identification of mechanical interfaces through quantitative means can minimize the visual bias involved in conventional identification. Stratigraphic horizons that have both a majority of abutting fractures and exceed a cutoff number of abutting fractures are considered to act as mechanical interfaces. This method is sensitive to undulation of surfaces and under-identifies mechanical interfaces when stratigraphic horizons undulate excessively.

Qualitative relationships between the stratigraphy and fracture patterns were developed through detailed fracture mapping of several quarry walls. The stratigraphic controls on fracture patterns were then quantified from observed fracture patterns to assess the relative effectiveness of various stratigraphic horizon types at terminating fractures. Cycle bounding organic partings and mud horizons are more effective at terminating fractures than intracycle mud horizons or horizons between contrasting lithologies.

Mechanical stratigraphic relationships based on field observations were used to develop a method for predicting mechanical stratigraphy and vertical fracture patterns at depth. Although mechanical interfaces correlate well with distinct stratigraphic horizons, not all stratigraphic horizons are effective at terminating vertical fractures. As a result, predicting mechanical

stratigraphy can not utilize each observed stratigraphic horizon. The following guidelines can be used for predicting fracture patterns. All observed organic shallowing upward cycle boundaries (C-ORG) in inner shelf facies association terminate abundant fractures (probability,  $P = 1.0$ ). Cycle bounding mud horizons in the inner shelf and inner-middle/middle shelf facies associations have lower probabilities ( $P = 0.68$  and  $0.63$ , respectively) of acting as mechanical interfaces. In the inner-middle/middle shelf facies association, intracycle horizons appear as lithologic contacts (IC-LTH) within a shallowing upward cycle. These horizons are more likely to act as mechanical interfaces ( $P = 0.60$ ) than the intracycle mud horizons that appear in the inner shelf facies association ( $P = 0.20$ ).

We predict mechanical stratigraphy using the probability of a stratigraphic horizon acting as a mechanical interface. Mechanical interface distribution is based on the distribution of corresponding stratigraphic horizons. Since all stratigraphic horizons do not act as mechanical interfaces, interface locations are chosen stochastically based on the empirically developed relationships for each interface type. Model predictions are compared to observed mechanical stratigraphy and the error in predicted interface locations is evaluated. Based on 50 model realizations within a Monte Carlo simulation, we ascertain a 96% certainty that any given model run will assign 13-33% erroneous mechanical interface locations.

# STATISTICAL CHARACTERIZATION OF FRACTURE PROPERTIES

Numerical models of groundwater flow through fracture networks require statistical descriptions of fracture characteristics including orientation, dip, length, and density. One of the initial objectives of this project was to simulate fluid flow through a coupled fracture-flow/reactive-transport model. To that end, we have developed statistical characterizations of the regional fracture network in Door County.

Several previous projects have collected data of fracture characteristics in Door County (e.g. Stieglitz and Johnson, 1986; Bradbury and Muldoon, 1993; Stieglitz and Dueppen, 1994; Roffers, 1996). Other than Roffers (1996), the previous investigators did not address the question of whether lithostratigraphy affected fracture patterns. Based on a comparison of fracture trace maps from color 35 mm aerial photographs (scale 1:3,000) and black and white air photos (scale 1:20,000) Roffers concluded that fracture orientation did not vary between the various mapped formations of the Silurian dolomite (see Figure 1 for map units). He did note that fracture orientations varied spatially and appeared to be a function of position in the county. Since one of the goals of this project was to address how lithostratigraphy affected mechanical stratigraphy and the resulting fracture patterns, we used some of Roffers (1996) existing data and collected several new data sets designed to address that question.

## **Methods**

Scanline surveys, described in detail below, and areal mapping (Laslett, 1982; LaPointe and Hudson, 1985) are two standard methods for obtaining statistical descriptions of fracture characteristics. Maps of fractures on quarry floors were available from Bissen Quarry (Roffers, 1996) and Big Quarry (Roffers, 1996). Maps of fractures on vertical quarry walls, described in the previous chapter, were completed as part of this study for lower and upper Big Quarry as well

as the Mathey Road Quarry. In order to obtain a representative sample of fracture characteristics from as wide a range of facies associations as possible, scanline surveys were completed at 15 outcrop sites throughout Door County as part of this project. Locations of scanline surveys are shown in Figure 9 and Figure 11 shows the stratigraphic position of each scanline site.

While scanline surveys and areal mapping can provide useful information on fracture orientation, dip and length, there is always concern that fracture densities measured on surface outcrops may not be representative of fracture densities in the subsurface. In order to address this issue we drilled a horizontally-oriented core at Big Quarry. The detailed fracture maps of outcrop faces in lower and upper Big Quarry provided one measure of fracture density (described below). By drilling a horizontally-oriented 15-m core into lower quarry face, we were able to assess whether vertical fracture density varied with distance from the outcrop face.

#### *Measurements of Fracture Density*

Fracture density is a critical parameter for numerical models of fracture flow. In relatively homogeneous layered sedimentary formations, the spacing of weak mechanical interfaces controls mechanical unit thickness and unit thickness, in turn, controls fracture density. Understanding fracture density relationships therefore requires knowledge of the distribution of mechanical interfaces which control fracture initiation and propagation. Field investigations indicate that the product of fracture density and bed thickness is approximately 1.0 (Price, 1966; Hobbs, 1967; McQuillan, 1973; Huang and Angelier, 1989; Narr and Suppe, 1991; Gross, 1993; Gross and others, 1995; Wu and Pollard, 1995; Becker and Gross, 1996; Bai and Pollard, 2000). One explanation for this relationship relies on the concept of a stress shadow (Lachenbruch, 1961; Nur, 1982; Pollard and Segall, 1987; Gross and others, 1995); new fracture growth is inhibited within a zone of decreased stress adjacent to an open fracture (Pollard and Segall, 1987). The size of the stress shadow is directly proportional to the height of the fracture, so that thicker mechanical units will have longer and more farther spaced fractures than thinner units (Pollard and Segall, 1987; Gross, 1993). Furthermore, within sedimentary strata, the length of

vertical fractures is controlled by mechanical unit thickness (e.g. Gross, 1993) so that thicker mechanical units will have longer and more widely spaced fractures than thinner units.

Given this general framework, we have tried to estimate fracture densities for the various facies association within the Silurian by multiple methods including 1) scanlines across vertical quarry faces to determine fracture densities for the mechanical stratigraphic units (described in the previous section), 2) maps of fractures on quarry floors at Bissen Quarry and Big Quarry (Roffers, 1996), and 3) a 15-m long horizontal core drilled into the lower quarry face at Big Quarry.

For the scanlines across vertical quarry faces, fracture density was measured as the number of vertical fractures per meter along bed-parallel transects across the vertical quarry exposures. We only report the number of fractures that, at a minimum, span the entire thickness of each mechanical unit. Roffers determined a fracture density from his map of Bissen Quarry. He summed the length of fractures exposed within each square meter and reported a fracture density in units of  $m/m^2$ . The horizontal core was examined by M. Cooke who noted which breaks appeared to be caused by the drilling process and which appeared to be pre-existing fractures. Fractures that showed evidence of staining, precipitation of secondary minerals, or discoloration "halos" were considered pre-existing fractures. By counting only the "pre-existing" fractures, we determined the number of fractures per meter of core.

### *Scanline Surveys*

A complete discussion of scanline mapping and some of the problems associated are summarized by LaPoint and Hudson (1985); we used data from these surveys as a means of characterizing the orientation and length distribution of the regional fractures. In a scanline survey, a tape or string is placed across the outcrop face and the fractures that intersect this line are characterized and recorded. The length and orientation of the scanline are also recorded. For each fracture that crossed the scanline we recorded the location along the scanline, orientation, length, dip (if possible), and termination. Generally we assumed that the fractures being mapped were vertical

or nearly vertical. Fractures can either terminate into the rock or the end of the fracture can be covered or obscured by overlying soil. The termination of each end of the fracture was classified into one of the following categories: (F)= terminates into another fracture, (C)= covered, (B)=terminates into a blast hole, (R)= terminates in rock, or (S)= terminates as a splay fracture. If the termination was into another fracture (F), we noted whether the termination was perpendicular (P) or parallel (L) to the intersected fracture.

Fractures that are oriented approximately perpendicular to the scanline are more likely to be intersected than those fractures that are sub-parallel to scanline. In the surveys conducted for this study, the scanlines were orientated approximately perpendicular to major fracture sets rather than at random orientations. Thus with a minimum of two perpendicular scanlines, both of the major fracture sets could be characterized while introducing a minimal amount of error. At some scanline sites the exposed fracture pavement was somewhat limited in size, for these sites we often collected data along several short scanlines, which were oriented approximately parallel to each other, in order to intersect enough fractures to have a statistically representative sampling of a given fracture set. Table 1 summarizes location, orientation, and length of each scanline as well as the number of fractures intersected by the scanline; more complete data from all scanline surveys are included in Appendix A.

## **Fracture Density**

### ***Summary of Fracture Density Data Collected Previously***

The data set developed by Roffers (1996) is probably the most complete analysis of fracture density data from Door County. As part of a tracer study conducted at Bissen Quarry (Muldoon and Bradbury, 1998) a map of all fractures greater than 1 ft in length was developed. Roffers (1996) uses this map as well as fracture traces from color slides, and fracture traces from black and white airphotos, to calculate fracture densities in terms of the cumulative length of all fracture traces within a given area (reported as m/m<sup>2</sup>). These values are not directly comparable to the fracture densities determined in this study, however, it is useful to review Roffers analysis

Table 1. Summary of location, orientation, and length of scanlines.

Scanline Site		Facies Association	Orientation	Length (m)	Total # Fractures Intersected
<i>Big Quarry</i>	Level 1	Inner Shelf	72	6.62	50
			339	9.5	50
	Level 2	Inner Shelf	52	39.3	45
			52	10	6
			340	22	32
			340	10	7
			340	5.1	11
	Level 3	Inner-Middle	44	6.3	15
			49	5.5	10
			51	12.1	25
			311	5.2	8
			340	22.2	33
			340	5.3	9
<i>Cave Point Rd Quarry</i>		Middle	62	3.5	5
			76	15.56	12
			76	10	6
			345	5.1	7
			355	9.5	12
			358	6.8	4
<i>Cave Point Park</i>		Middle	330	15	3
<i>First Lane</i>		Middle	74	17.5	3
			338	10	5
<i>Garret Bay</i>		Inner	73	9	9
			325	7	5
<i>Gibson Lane</i>		Middle	69	24	2
			80	10	2
			85	17	4
			339	22.4	5
			348	12	2
			358	16	5

Scanline Site	Facies Association	Orientation	Length (m)	Total # Fractures Intersected
<i>Hwy 42</i>	Middle	0	10	15
		66	11.5	13
<i>Kisser South</i>	Middle	70	12	25
		337	13.9	14
<i>Lily Bay Rd. Quarry</i>	Middle	64	11	7
		338	8	15
<i>Little Quarry</i>	Middle	62	13.8	50
		342	11.69	50
<i>Mathey Rd. Quarry</i>	Middle	75	11	1
		75	27.5	5
		335	33	11
<i>Newport State Park</i>	Middle	77	23	17
		331	10.5	12
		343	6.2	9
<i>Penin Players' Quarry</i>	Middle	74	15	10
		75	5	8
		347	18.4	21
<i>Spring Rd.</i>	Inner-Middle	65	5	22
		334	3	22
<i>Toft's Point</i>	Middle	82	15	11
		82	16	9
		83	11.7	8
		338	13.8	14
		356	10	12

of fracture density. The map of Bissen Quarry yielded the highest density (1.92 m/m<sup>2</sup>) which is not surprising. It is expected that mapping at the outcrop scale will yield a higher density than mapping at the scale of the airphotos (1:20,000).

Roffers prepared a map of fracture densities determined from black and white airphotos to look for spatial trends (Roffers, 1996, fig 4-9) and also completed a statistical analysis of fracture density in relation to depth to bedrock, surficial geology, and land use. He concluded that while mapped fracture densities were higher in the northern portion of the county, especially in agricultural fields with a thin soil cover, it is likely that the actual fracture density is relatively uniform.

### ***Observed Fracture Density***

*Scanlines across vertical quarry faces* -- We assume that the entire Silurian section has undergone similar burial and strain conditions, and so we focused our initial analysis of fracture density on layer thickness and material property differences. Fracture densities based on observations from scanlines across vertical quarry faces are illustrated in Figures 12b, 13b, and 14b and summarized in Figure 22. This is the only method by which we can observe the relationship between mechanical unit thickness and fracture density as the other two methods of estimating density consist of data collected within a specific mechanical unit the thickness of which could not be easily determined.

Examination of fracture maps (Figures 12, 13, and 14) indicates that average fracture density is generally high in the Byron Formation ( 1.41 fractures/meter for inner shelf facies association; 1.69 fractures/meter for the inner/middle shelf facies association) and gradually decreases to a low value of 0.17 fractures/meter in the middle shelf facies association of the Manistique Formation (Figure 22). The alternating restricted/open marine intervals of the Hendricks Formation exhibit intermediate fracture density values (Figure 22). The lack of consistent fracture densities within individual facies associations suggest that fracture density may be influenced less by lithology and more by other factors such as bed thickness.

To test the role of mechanical unit thickness in observed fracture density, we plot fracture density versus the thickness of mechanical units at Big Quarry (Figure 23). Fracture density in the inner, inner-middle, and middle shelf facies associations in the Byron/Hendricks Formations decreases

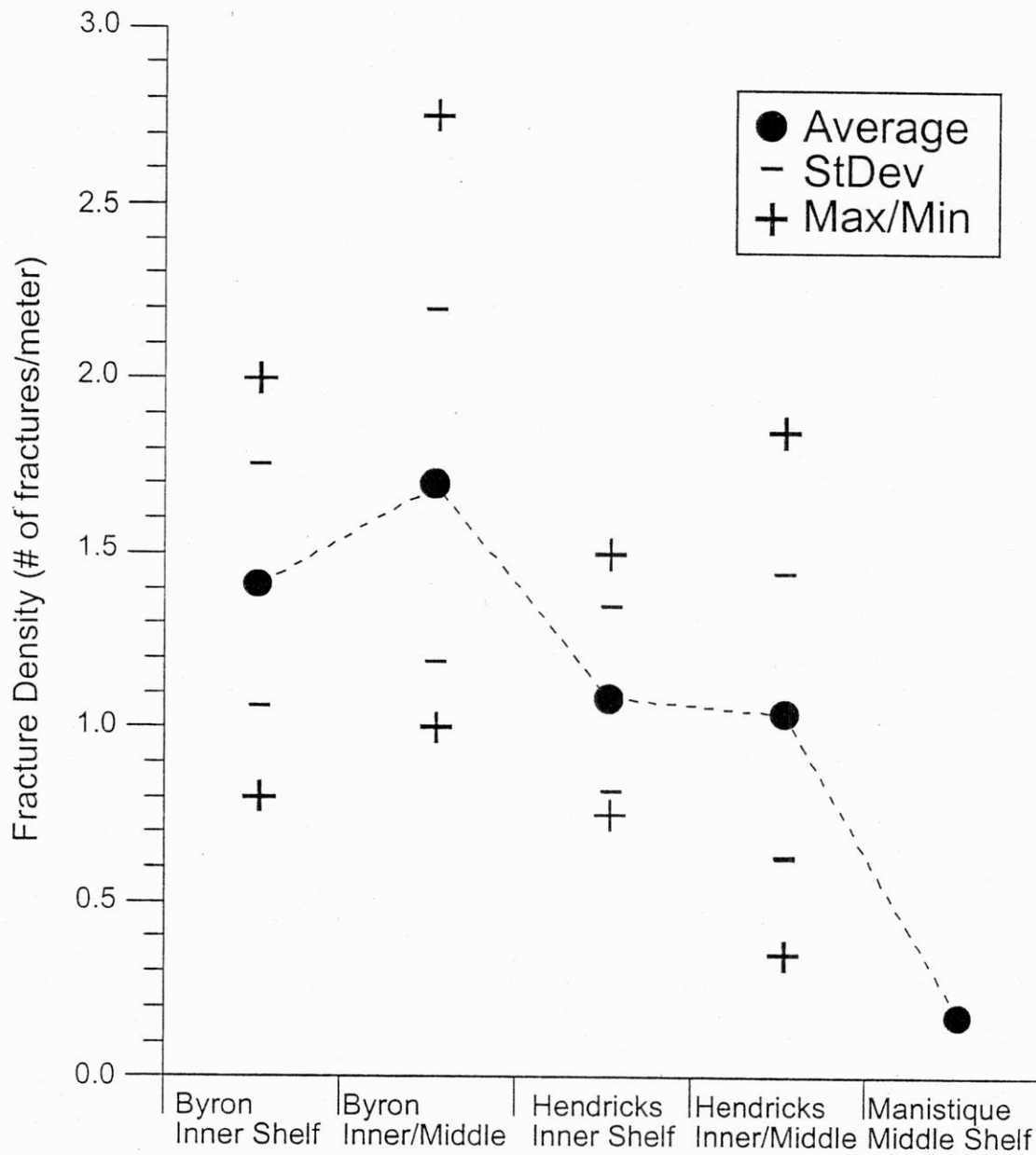


**Figure 22.** Average fracture densities for various facies associations of the Silurian dolomite. Fracture densities are based on the fracture maps (figures 12, 13, and 14). Lack of consistent fracture density within each facies association is probably due to differences in bed thickness.

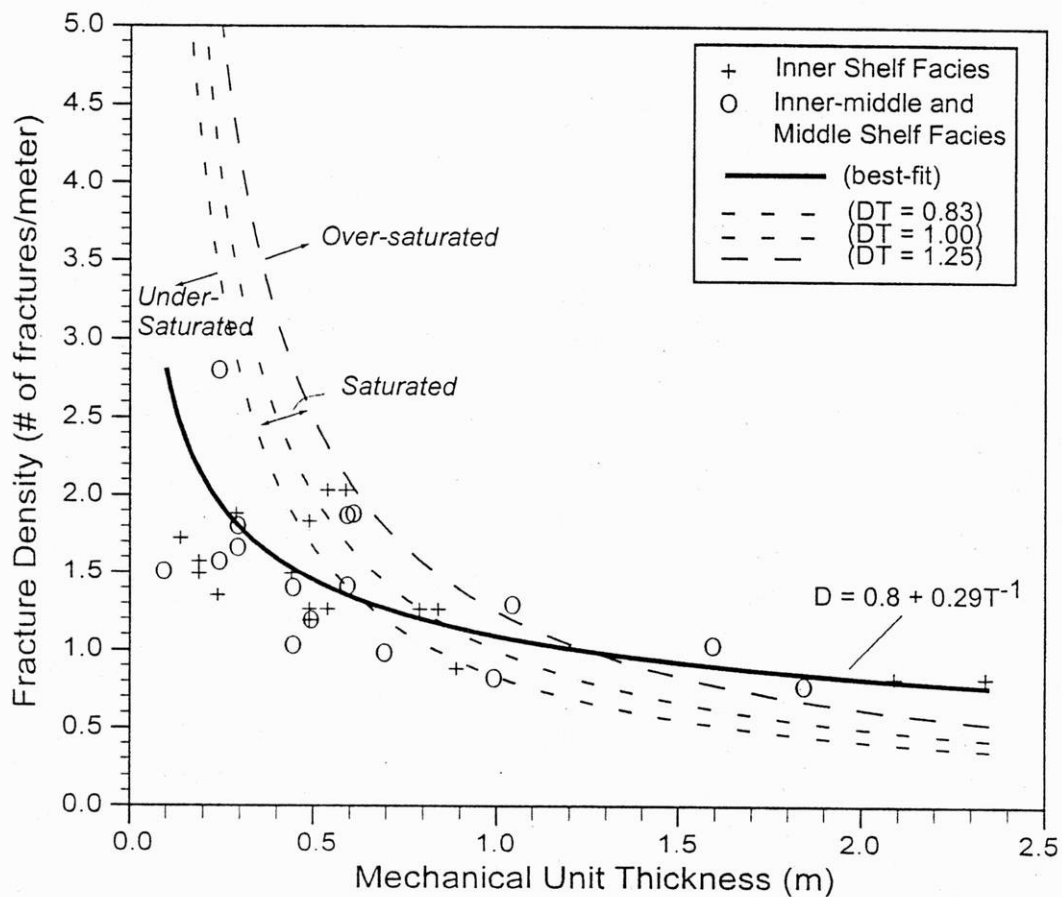


**Figure 23.** Fracture density versus mechanical unit thickness for units in the Byron/Hendricks Formations: Fracture density is calculated from fracture maps (figures 12c & 13c). The bold line represents the best-fit line though all of the data. Dashed curves represent density times mechanical unit thickness (DT) of 0.83, 1.00, and 1.25.

with increasing bed thickness but does not follow the expected density (D) times thickness (T) equals 1.0 curve which is based on numerous field observations (e.g. Price, 1966; Hobbs, 1967; McQuillan, 1973; Huang and Angelier, 1989; Narr and Suppe, 1991; Gross, 1993; Gross and others, 1995; Wu and Pollard, 1995; Becker and Gross, 1996; Bai and Pollard, 2000). If fracture density conforms to the relationship,  $DT = 1$ , then the beds are considered to be fracture-saturated. However, within some tectonic regimes, beds may have experienced high levels of strain that enhance fracture density by sequential in-filling (e.g. Becker & Gross, 1996; Wu & Pollard, 1992); such beds can be considered over-saturated. Contrastingly, beds that experience low levels of tectonic strain are expected to be under-saturated with respect to fractures. Bai and Pollard (2000) suggest cutoff values for under- ( $DT=0.83$ ) and over-saturation ( $DT=1.25$ ) based on layer-parallel stresses between adjacent fractures (Figure 23). Ladeira and Price (1981) note that thicker beds have lower than expected fracture density and tend towards under-saturation. Additionally, fracture density becomes nearly constant with bed thickness at values greater than 1.5 m (Ladeira and Price, 1981; e.g. Figure 23). As a result, this method may not be an appropriate method to predict fracture density in thick (>1.5-2.0 m) mechanical units. Fracture density data from the Byron/Hendricks Formations (Figure 23) indicate that mechanical units are generally under-saturated with respect to fracturing; this is expected due to the low strain tectonic environment. As mechanical unit thickness increases, fracturing tends towards over-saturation, however very few data points define this portion of the graph on Figure 23.

Fracture density has also been shown to correlate with the stiffness of mechanical units (e.g. Gross, 1993; Huang and Angelier, 1989). While the Schmidt Hammer did not detect systematic stiffness differences between facies associations, some variation was detected within each facies association. Similarly, little distinction could be made between the trend of fracture density for the inner shelf facies association and that for the inner-middle and middle shelf facies associations. The observed scatter of data in Figure 23 may be due to stiffness variation within each facies association.

*Analysis of Vertical Core Data* — The above fracture density relationships are based on outcrop observations, however, fractures observed in core also show increased density with thinner beds. Vertical rock cores typically shed little insight into vertical fracture patterns at depth because the probability of intersecting vertical fractures is very low (Narr and Lerche, 1984). A vertical core, however, has a higher probability of intersecting a vertical fracture in units containing dense fractures than in units with low fracture density. A vertical core, penetrating almost the entire Silurian section, was collected at the Jarmen Road research site in the summer of 1995 by Mark Harris of UW-Milwaukee. Hegrenes (1996) recorded the number of vertical fractures for each formation in the Jarmen Road core (Figure 24). Since fracture density is higher in thin beds, intervals of the aquifer that contain more numerous thin beds will likely contain more fractures. If fracture density were consistent throughout the Silurian section (i.e. probability of core/fracture intersection is constant), the core would be more likely to intersect vertical fractures in a thicker formation because a thicker formation contains more numerous beds. As a result, we divide the number of fractures recorded by the thickness of the formation. Different values of the number of fractures divided by formation thickness will identify differences in the probability of core/fracture intersection.

Within the Jarmen Road core, vertical fractures occur more frequently within the thinly bedded inner shelf and inner-middle shelf facies associations of the Hendricks, Byron, and upper Mayville Formation than in the more massive middle shelf facies association of the Engadine, Manistique, and lower Mayville Formations (Figure 24). Since a higher occurrence of core/fracture intersection suggests a higher fracture density (Narr and Lerche, 1984), core observations are consistent with field results which show that the more thinly bedded inner shelf and inner-middle shelf facies associations exhibit higher fracture density than middle shelf facies association. Consistent relative fracture density behavior in outcrop and at depth suggests that observed fracture density from scanlines across quarry faces is not greatly affected by surficial weathering processes or blasting associated with quarry operations. Therefore, relative relationships developed for fracture densities observed in outcrop should also be valid at depth.

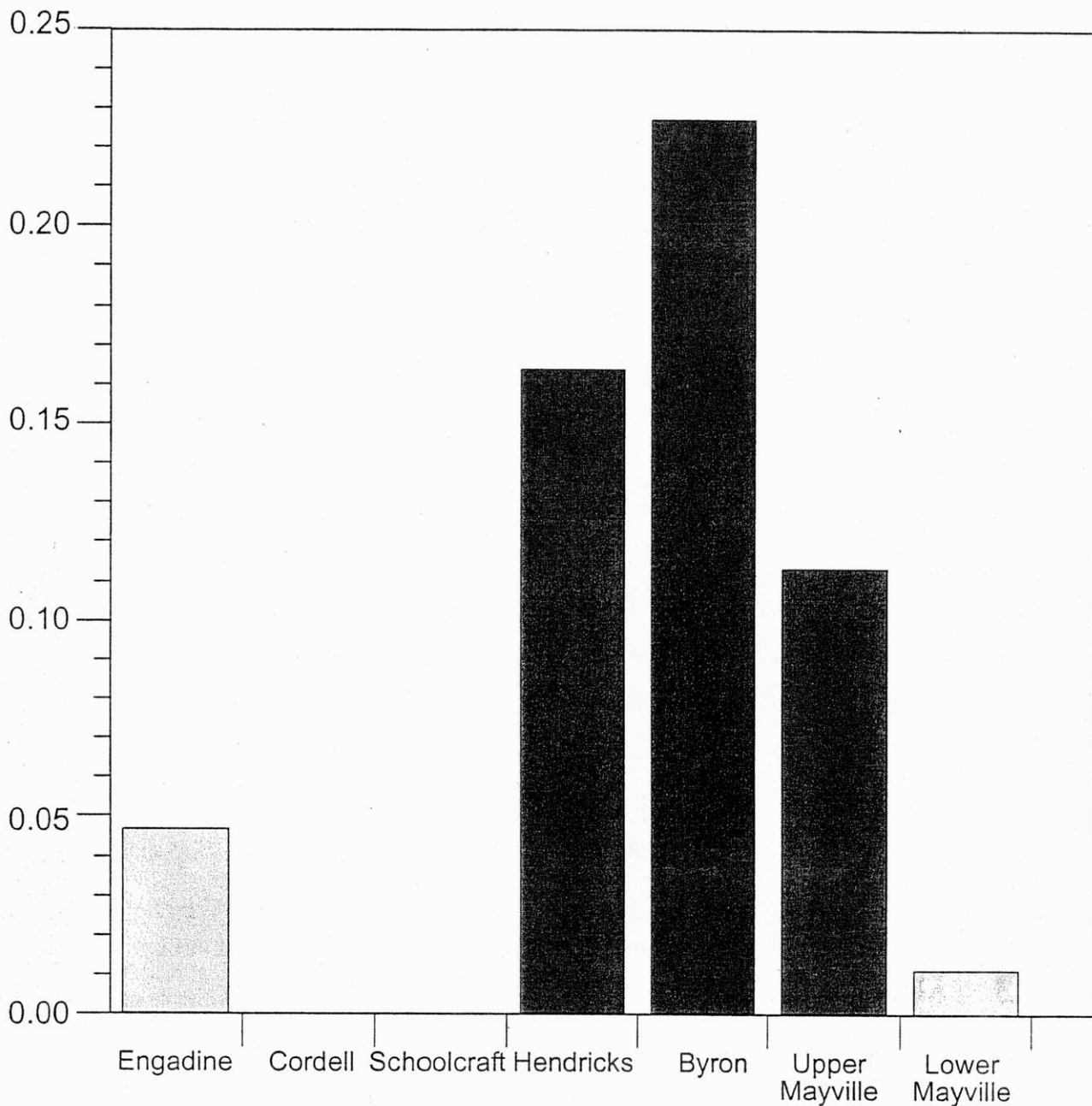


**Figure 24.** Fracture density based on observations of vertical fractures in the core collected from the Jarmen Road research site (Hegrenes, 1996). The number of fractures observed in each lithostratigraphic unit has been normalized by dividing by unit thickness. The inner shelf and inner-middle shelf facies association (dark gray units) are more thinly bedded and contain more vertical fractures than the more massive middle shelf facies association (light gray units).

*Horizontal Core* — The horizontal core, collected from the Byron Formation (inner shelf facies association) exposed in lower level of Big Quarry, was drilled as another means of assessing whether the fracture densities determined from the fracture maps of quarry faces were realistic. There is always concern that surface exposures, especially quarry faces, will be more densely fractured due to 1) removal of the lateral confining stress, 2) surficial weathering, and 3) blasting effects. Appendix B contains a graphic log of the core in which the location of each fracture is noted. Visual examination of the log does not suggest that fracture density varies in any systematic way with distance from the quarry face. In order to quantify the density relationships, we tallied the number of fractures along each meter of core. For the purpose of this analysis, sub-vertical fractures were included and their location was taken to be the mid-point of the fracture. Fracture densities, summarized in Figure 25a, range from 2 to 9 fractures per meter with an average of 5.2 fractures/meter. There does not appear to be any systematic variation in fracture density with distance from the quarry face.

We were somewhat surprised that the core yield higher fracture densities than the scanlines across vertical quarry faces (described above). In order to explore this result further, we decided to collect scanline data from the pavement exposed on the first bench in Big Quarry. This pavement exposes the inner shelf facies association contained within the Byron Formation, the same lithofacies penetrated by the core. Generally, scanlines across fracture pavements are not considered a good estimate of fracture density since the degree of weathering of the pavement greatly affects the results. The pavements in Big Quarry are relatively unweathered and show few blasting effects and thus we felt that it would be a good comparison. Two 10-m scanlines were laid out perpendicular to the quarry face; the origin, or zero-point, for these lines was at the quarry face. Data from these lines are included in Appendix A and summarized in Figure 25b. Densities were determined by counting the number of fractures in each meter of the scanline. These scanlines also seem to indicate that there is no systematic variation in fracture density as one moves back from the quarry face. Fracture densities along the two scanlines ranged from 1 to 5 fractures/meter with an average of 2.4 for line 1 and 1.5 for line 2. If we determine a density by summing the total number of fractures ( $n=43$ ) and dividing by the total length on both

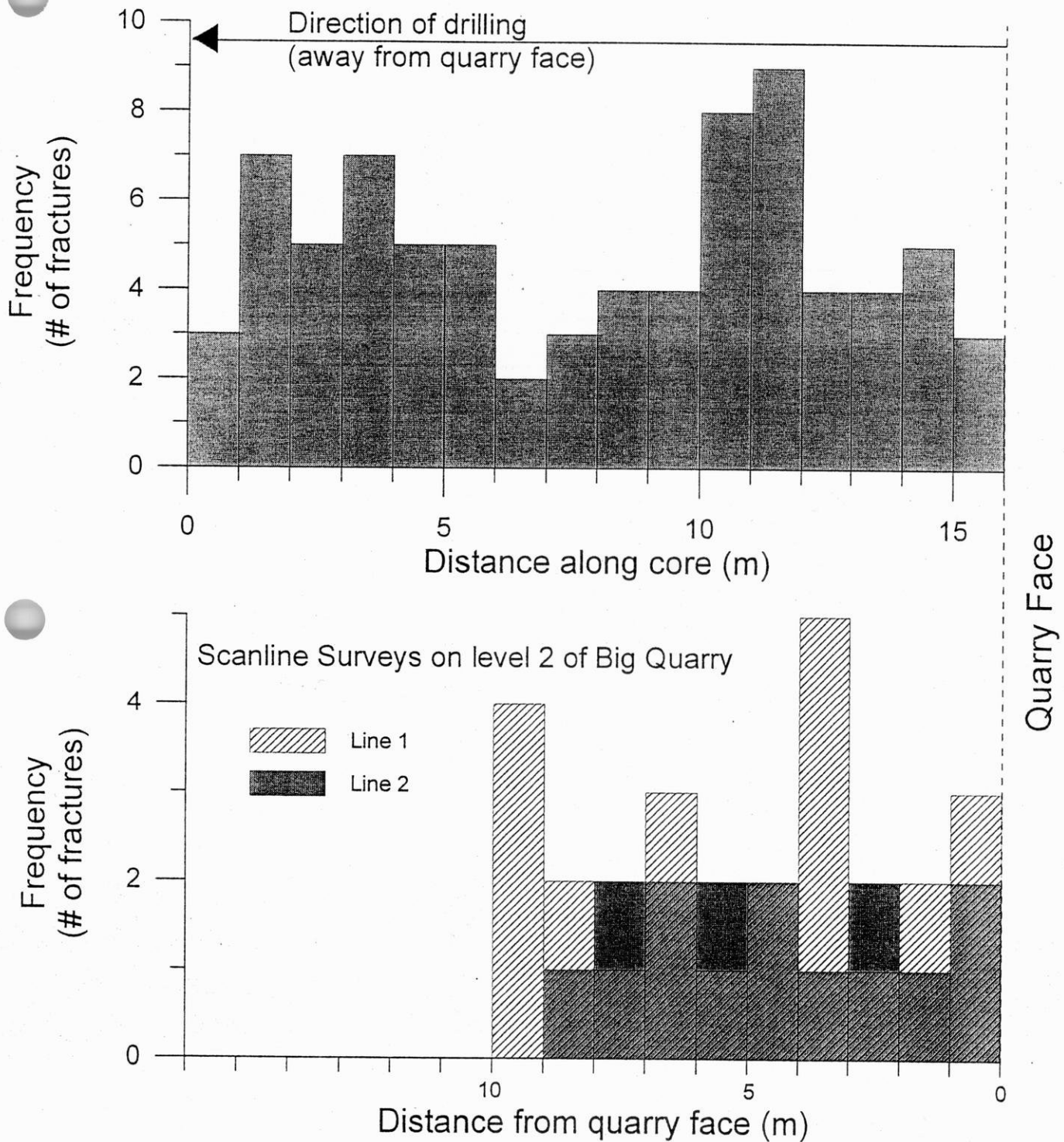


Figure 25. Fracture density in lower Big Quarry as determined from A) horizontal core and B) two scanline surveys. The core was collected from the lowest level in Big Quarry. Fracture density was determined by counting the number of fractures in each (1 meter) interval. The scanlines were 10-m in length, with the origin (0.0 m) being the quarry face.

scanlines (20 meters) we calculate an average density of 2.15 fracture/meter. Table 2 summarizes the average fracture density determined by a variety of methods in Big Quarry.

**Table 2. Observed fracture densities for the Inner Shelf Facies Association exposed within the Byron Formation (Big Quarry)**

	<b>Average Density fractures/meter</b>	<b>Range</b>
<b>Horizontal Core</b>	5.2	2-9
<b>Scanlines</b>		
<i>Vertical quarry faces</i>	1.41	0.8-2.0
<i>Fracture pavement</i>	2.15	1-5

The range of fracture densities determined by the three methods was larger than expected and required some evaluation as to which method provided the most appropriate estimate of fracture density for future numerical modeling. The fact the fracture density from the horizontal core was the highest of the three estimates suggests that faint fractures, which might not be visible in the scanlines, were detected in the core because the process of coring may have enhanced the aperture of these fractures. It is not surprising that the density from the scanline across the quarry face was less than the density from the scanline across the fracture pavement. Densities calculated from the scanlines across the quarry face only included those fractures that cross cut the entire thickness of the mechanical unit; since not all fractures do so, this method is expected to yield lower estimates of fracture density. If we consider which fractures are most likely to be well-connected to the overall fracture network it seems probable that those crossing mechanical units and terminating at a bedding-plane fracture would be the most significant. Given this, we use the densities estimated by the scanlines across quarry faces to develop the statistics required for prediction of fracture densities in the subsurface.

### *Predicting Fracture Density*

In the Silurian dolomite, fracture density seems more dependant on mechanical unit thickness (Figure 23) than the facies association (Figure 22). Once the distribution of predicted mechanical interfaces is known (described in previous chapter), fracture density can be estimated using mechanical unit thickness, defined by the distance between predicted mechanical interfaces. We use a best fit through the density-thickness data to make this prediction (Figure 23); this best fit was produced using a relationship similar in form to the theoretical  $DT=1$  relationships. Comparing the predicted results with the observed fracture density within this interval reveals small error in the analysis (Figure 26). Regions of relatively low fracture density ( $<1$  fracture/meter) correlate well from observed to predicted fracture density distributions. Maximum predicted fracture densities are greater than maximum observed fracture densities because the best-fit line used to predict densities (Figure 23) is skewed upward at low values of mechanical unit thickness.

Since our method reasonably predicts the mechanical stratigraphy and fracture density for the mapped intervals, this predictive method will provide valuable inferences regarding fracture pattern at depth using detailed stratigraphic descriptions of available core.

### **Fracture Orientation**

The scanline surveys, conducted in the summer of 1999 by Anne Ebenreiter, provide the data that we use to look at the variation in fracture orientation and length in relation to the various facies associations. Many data on fracture orientation and length have already been collected in Door County (e.g. Stieglitz and Johnson, 1986; Bradbury and Muldoon, 1993; Stieglitz and Dueppen, 1994; Roffers, 1996), however, none of these data sets contain the necessary lithostratigraphic information that we required in order to relate fracture orientation and length to facies associations. The locations of the scanlines surveys are shown in Figure 9 and their stratigraphic position is summarized in Figure 11.

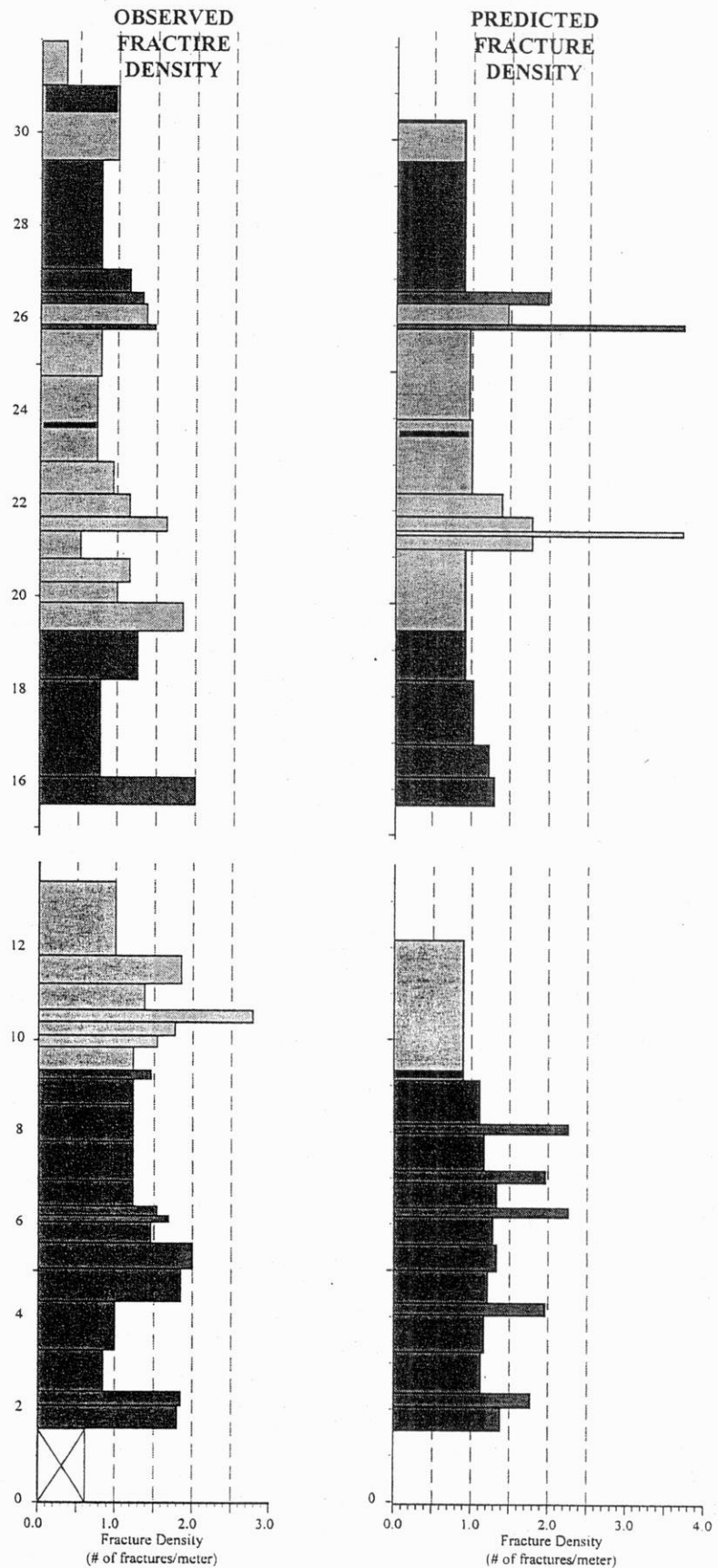


**Figure 26.** Predicted fracture density for the units exposed in Big Quarry. Mechanical interfaces represent the same realization as shown in Figure 21. Fracture density predictions for intervals less than 2 m utilize empirical relationships with mechanical unit thickness (Figure 23). Dark gray layers represent inner shelf facies association, while lighter gray layers represent inner-middle/middle shelf facies association.

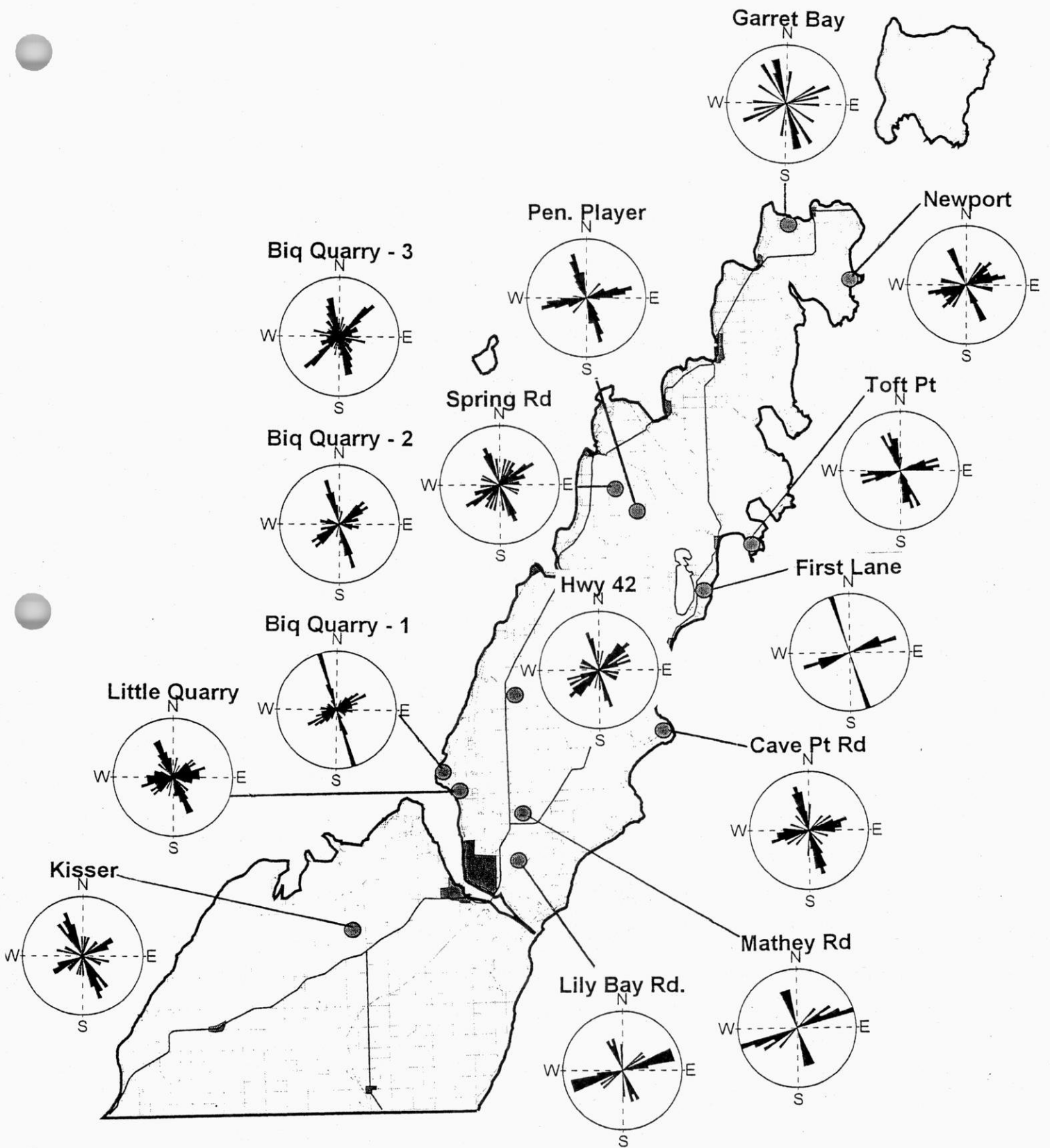


Figure 27. Rose diagrams of fracture orientations from scanline surveys across fracture paements.

A common way of presenting and comparing fracture orientation data is a rose diagram which is simply a circular histogram with frequency plotted as distance from the center. Rose diagrams for each site are shown in Figure 27. All of the rose diagrams use a 5-degree sector and are plotted as equal-area plots rather than arithmetic plots so as to preserve the relationship between area and frequency. The majority of the rose diagrams have a maximum frequency of 25% , however, a few of the plots have frequencies greater than 25% for one of the sectors; these statistics are summarized in Table 3.

**Table 3. Statistics for rose diagrams**

Scanline Site		Facies Association	# of Points	Maximum Percent
<i>Big Quarry</i>	Level 1	Inner Shelf	100	35
	Level 2	Inner Shelf	101	25
	Level 3	Inner-Middle	100	25
<i>Cave Point Rd. Quarry &amp; Park</i>		Middle	49	25
<i>First Lane</i>		Middle	8	37
<i>Garret Bay</i>		Inner	14	25
<i>Gibson Lane</i>		Middle	19	25
<i>Hwy 42</i>		Middle	28	25
<i>Kisser South</i>		Middle	39	25
<i>Lily Bay Road Quarry</i>		Middle	22	25
<i>Little Quarry</i>		Middle	100	25
<i>Mathey Road Quarry</i>		Middle	17	25
<i>Newport State Park</i>		Middle	38	25
<i>Peninsula Players' Quarry</i>		Middle	39	25
<i>Spring Rd.</i>		Inner-Middle	44	25
<i>Toft's Point</i>		Middle	54	25

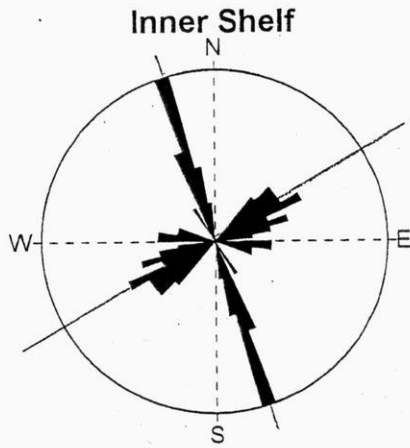
Examination of Table 3 reveals that some of the rose diagrams presented in Figure 27 are based on a small number of data points. Despite that limitation, the rose diagrams provide a general overview of fracture orientations that is consistent with the geographic variation noted by Roffers

(1996). Based on an analysis of fracture orientations mapped at multiple scales Roffers (1996) determined that fracture orientations were consistent across the geologic units mapped by Chamberlain (see Figure 1 for map of units) and that variations in fracture orientation were primarily a function of geographic position in the county. Since we are most interested in the characteristics of the various facies associations, we chose to analyze the scanline data in that context. For each of the facies associations, we combined the data from all scanline surveys conducted in that facies association and generated rose diagrams with those data sets. While the rose diagrams in Figure 28 are not identical, the variation in fracture orientations within the three facies associations does not appear significant and does not suggest any systematic trend. This is to be expected given that all of the lithostratigraphic units experienced similar stress histories.

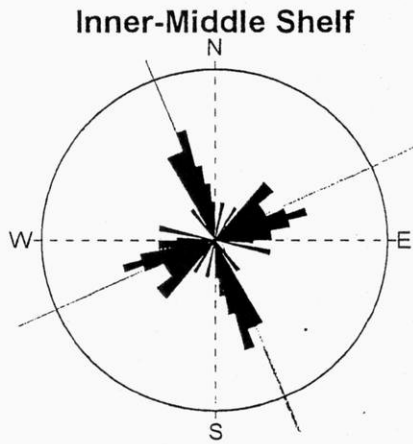
### ***Predicting Fracture Orientation***

Numerical models of flow through fracture networks vary widely in terms of 1) statistical models used to generate fracture locations, 2) statistical descriptions of fracture orientations, and 3) fracture shapes. While we have not yet found a coupled code capable of simulating flow through the fracture network and the ongoing dissolution/widening of the fracture aperture; we are interested in pursuing this research in the future. To that end, we will use Golder and Associates FracMan family of codes to simulate fracture orientations. The following section described how data from the scanline surveys and fracture map of Bissen quarry can be used to develop a statistical description of fracture orientations.

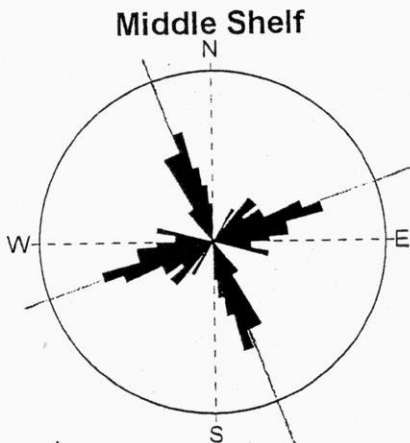
FracSys, the data analysis package, provides modules for fracture set definition (ISIS), for analysis of fracture trace maps as a method for choosing one of six fracture generation models (HeterFrac) and for determining fracture set size distribution (FracSize). The results of the FracSys analysis are used to generate fracture networks using the FracWorks package.



Equal Area Plot  
 Number of Points: 215  
 Class Size: 5  
 Maximum Percent: 25



Equal Area Plot  
 Number of Points: 418  
 Class Size: 5  
 Maximum Percent: 25



Equal Area Plot  
 Number of Points: 274  
 Class Size: 5  
 Maximum Percent: 25

**Figure 28.** Rose diagrams of fracture orientations for the three facies associations within the Silurian dolomite.

## Fracture Length Distribution

Numerical models of fluid flow through a fracture network require statistical characterization of the length distribution for each fracture set. Since we were most interested in predicting fracture characteristics for specific facies associations, we have combined the data from the individual scanline surveys into three data sets. The length distribution for each facies association is shown in Figure 29; we have plotted both fracture length and log fracture length. From these data it appears that fracture length is well-represented by a log normal distribution. The descriptive statistics for each distribution are included in Figure 29.

### *Predicting Length Distributions*

While scanline surveys provide valuable information about fracture length, there are some concerns that must be addressed. One problem with scanline data is that the termination of the fracture may be censored and thus the maximum fracture length at the site would be censored. In addition, since scanline have a higher probability of intersecting long fractures they tend to under sample short fractures. The under sampling of short fractures can make a negative exponential distribution of fracture length appear to be log normal (LaPointe and Hudson, 1985). Priest and Hudson (1981) analyzed this problem in depth and developed a mathematical technique to deal with censoring. In their analysis, they presented the following equation to determine the uncensored mean fracture length from the censored data:

$$u = \frac{-\log\left[\frac{n-r}{n}\right]}{c}$$

where:      1/u = mean uncensored trace length  
              n = number of fractures sampled  
              r = number of uncensored fractures  
              c = length at which censoring occurs

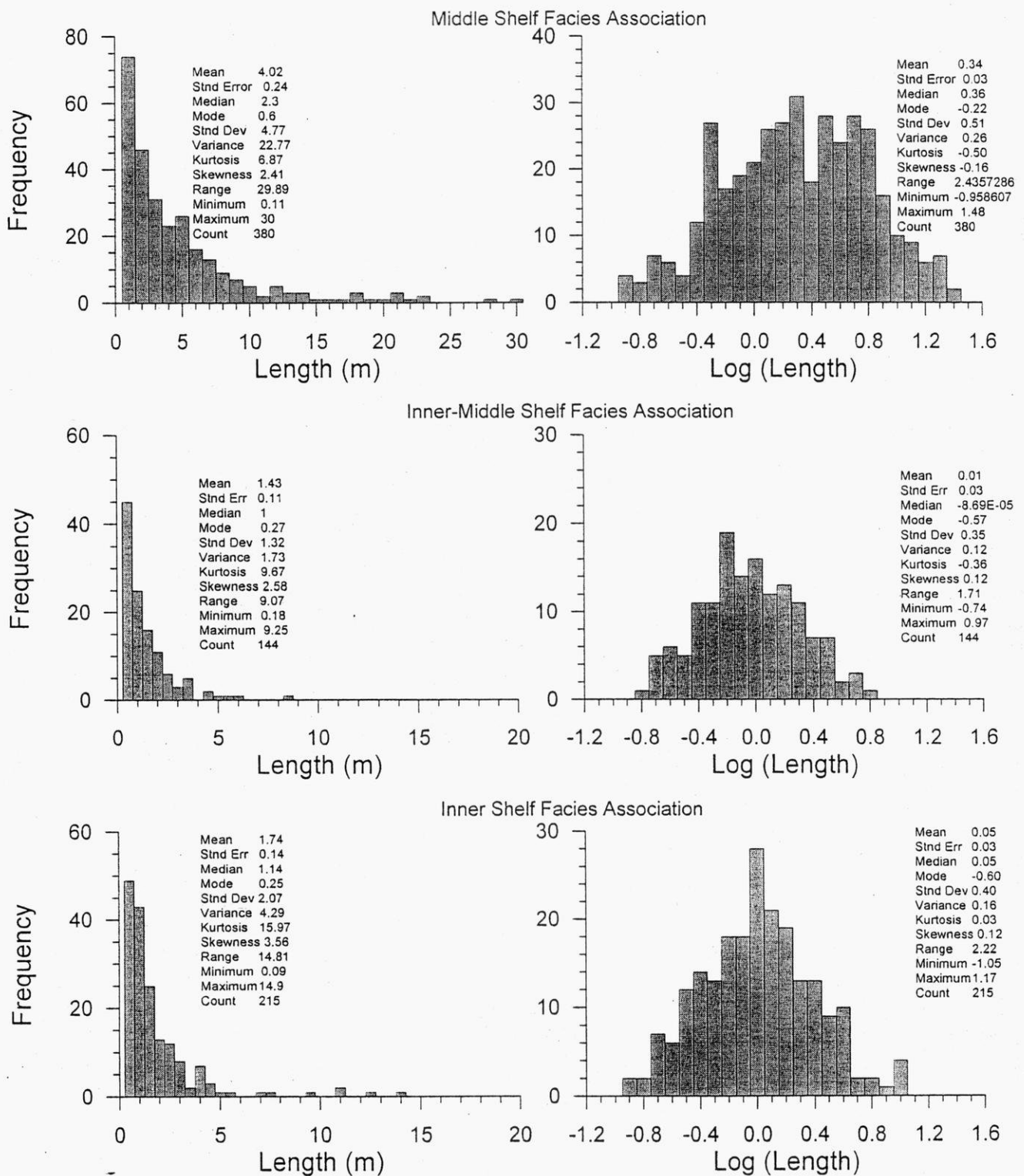
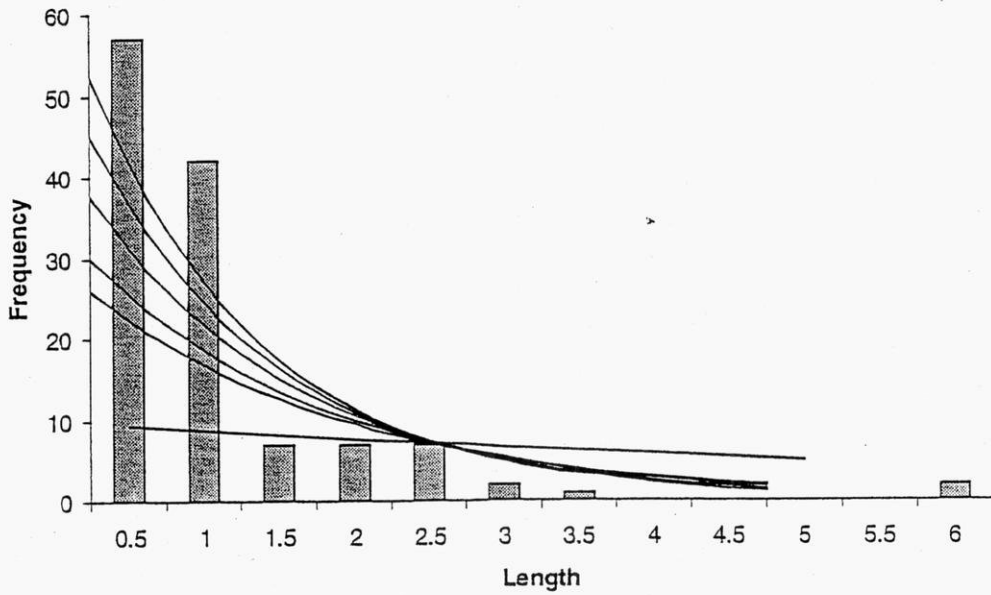


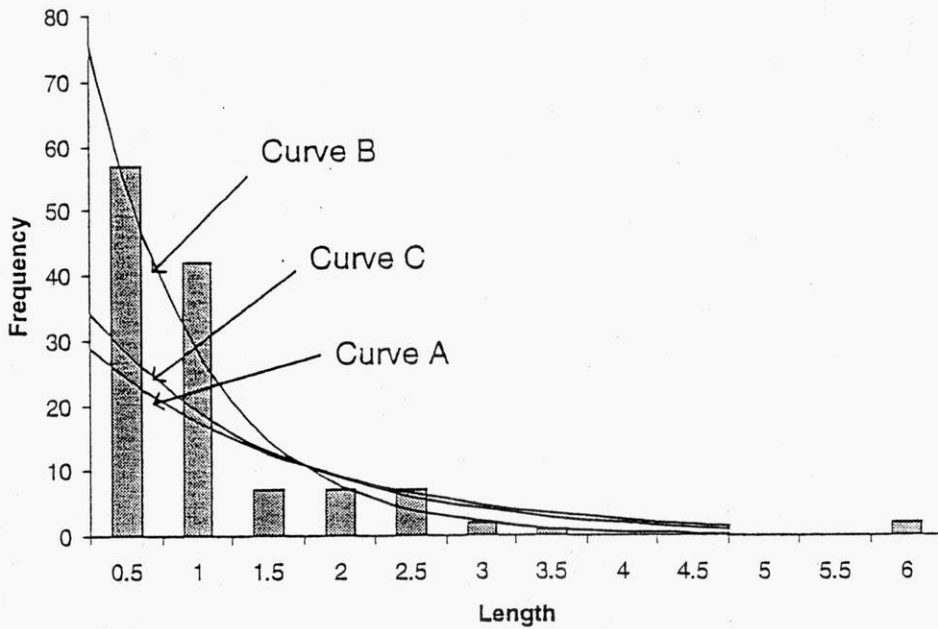
**Figure 29.** Histograms of fracture lengths for the three facies associations in the Silurian dolomite. Raw length data are shown on the left side of the figure and log-transformed lengths are shown on the right-hand side. Descriptive statistics are included with each histogram.

This relationship provides a good method of determining the uncensored mean fracture length. An example from Big Quarry, where two of the longest fractures (i.e. more than 11 m) were censored on both ends, illustrates the issue. The mean fracture length for "uncensored" fractures at Big Quarry is 2.42 m; for our analysis the mean fracture length is not as important as the distribution of fracture lengths. However, there are an infinite number of distributions with same average fracture length. For example, all of the negative exponential distributions in Figure 30a have a mean fracture length of 2.42 meters. This figure demonstrates the wide range of distributions that have the mean trace length determined by the Priest and Hudson method. However, it is obvious from Figure 30a that not all of these distributions provide an accurate representation of the fractures lengths that are present at Big Quarry. An upper and lower limit can be placed on the range of distributions by making a few assumptions. First, it can be assumed that the censored fractures terminated just out of sight and thus for all practical purposes the length measured is the actual length of the fracture. This distribution for this scenario is labeled A in Figure 30b. The second boundary can be created by assuming that the two fractures do not affect the distribution and can be ignored, which is shown by curve B. It is likely that the actual distribution of fracture lengths lies somewhere between these extremes. Therefore, the curve labeled C will be considered representative of the fracture lengths at Big Quarry. This distribution was created by assuming that one of the fractures had a length that was very close to that reported while the other length of the other fracture did not significantly affect the distribution.

The fracture length data appear to well-represented by both a log-normal distribution and a negative exponential distribution. Given that scanlines are known to under sample short fractures, it appears more appropriate to use a negative exponential distribution. Using the length data for the facies associations, which include both uncensored and censored fracture lengths, we calculated a best-fit line for the distribution. As in the above analysis we wanted to minimize the impact of the few "long" fractures in each distribution. To do so we excluded any data within the last two standard deviations from our analysis. The resulting equations for the three negative exponential distributions are shown in figure 31.



(a)



(b)

**Figure 30.** Histograms of “uncensored” fracture lengths from Big Quarry which serve to illustrate the problem of “censored” data. A) All of the distributions shown in this histogram have a mean fracture length of 2.42 m. B) By making certain assumptions, we can limit the range of possible distributions which best describe the fracture length data.

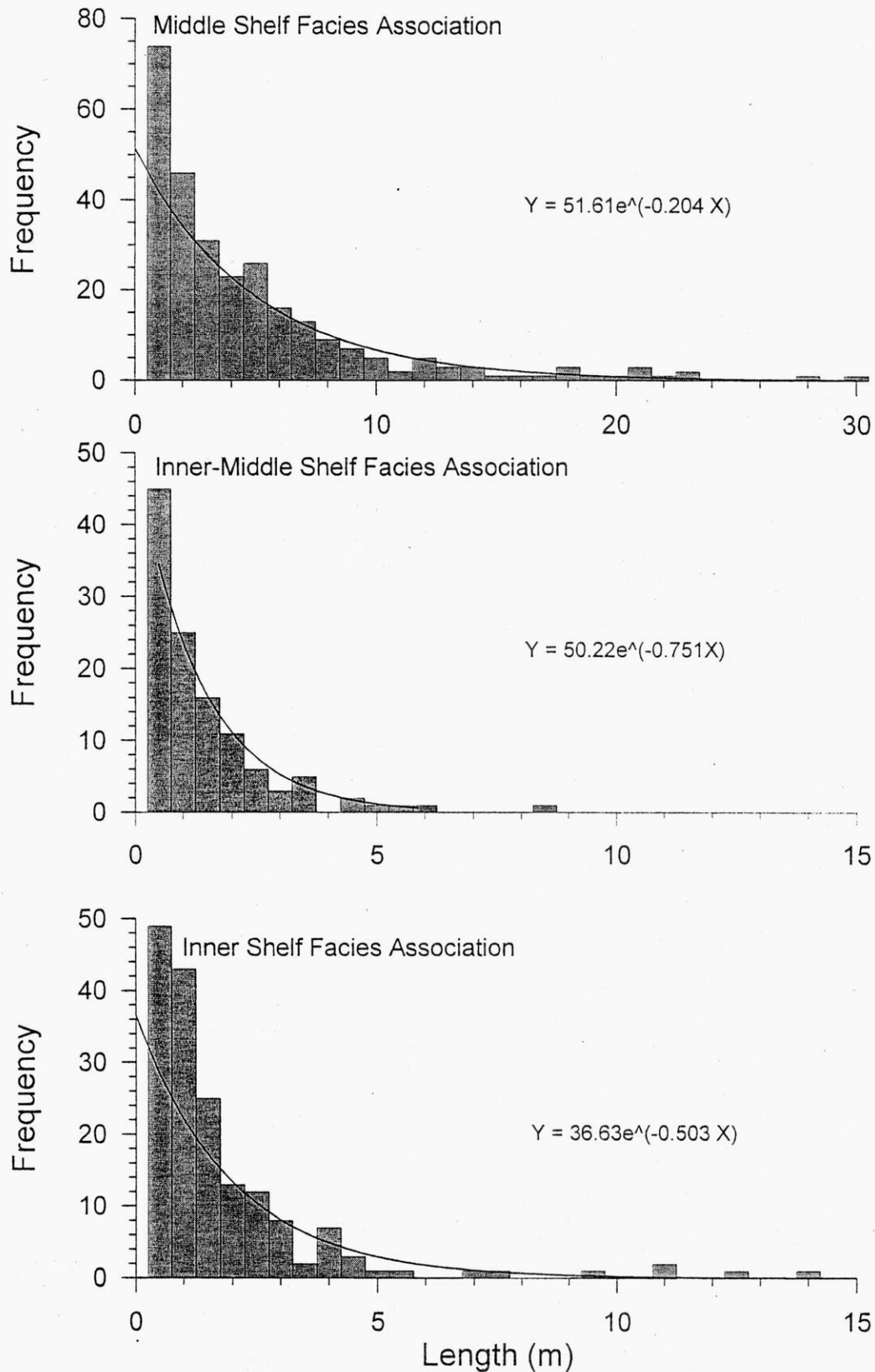


**Figure 31.** Histograms of fracture lengths for the three facies associations in the Silurian dolomite shown with the “best-fit” line for a negative exponential distribution. In order to minimize the impact of the long fractures, which tend to be over sampled by scammonies, we excluded from our analysis the fractures within the last two standard deviations.

## Fracture Aperture

Discrete fracture flow models vary in how they calculate flow. Some codes are based on Darcy's law and require a distribution of fracture transmissivities; others are based on the cubic law and require a distribution of fracture apertures. In our future modeling we will need some estimate of the initial aperture of the fractures; this aperture distribution will be modified as dissolution progresses over time. Surface exposures, which are weathered, provide very poor estimates of fracture aperture and therefore we did not collect quantitative aperture data as part of the scanline surveys. Many researchers have noted a relationship between fracture length and fracture aperture and it makes intuitive sense that longer fractures have larger apertures. Prior to any modeling, we will conduct a literature search to identify aperture/length relationships published by other researchers.

# SIMULATION OF FRACTURE FORMATION\*

\* summarized from Cooke and Underwood (2001). 'Fracture Termination and Step-over at Bedding Interfaces Due to Frictional Slip and Interface Opening' Journal of Structural Geology, vol 23, p. 223-238.

## **Introduction**

In sedimentary rocks, opening-mode fractures have been observed to abut against bedding contacts (Baer, 1991; Narr and Suppe, 1991; Gross and others, 1995; Becker and Gross, 1996; Ji and Saruwatari, 1998; Underwood, 1999), cross through contacts (e.g. Becker and Gross, 1996), and jog or step-over at bedding contacts (Helgeson and Aydin, 1991). These types of fracture intersection with bedding are readily recognized in field, but the mechanisms that control the development of one over the other are not yet well understood. This section investigates different modes of bedding contact deformation to better understand the parameters that control the fracture termination at, propagation through, or step-over at bedding contacts such as within the Silurian dolomite of Door County.

## ***Previous work on fracture termination***

Previously, field investigations have largely focused on fracture termination in strata consisting of interbedded brittle and ductile rocks (Corbett and others, 1987; Baer, 1991; Helgeson and Aydin, 1991; Narr and Suppe, 1991; Gross and others, 1995; Becker and Gross, 1996; Hanks and others, 1997; Ji and Saruwatari, 1998; Rijken and Cooke, in review). However, the sedimentary horizons that terminate fractures within the Silurian dolomite occur between brittle beds. Only a few field studies (Dyer, 1988; Baer, 1991; Helgeson and Aydin, 1991; Narr and Suppe, 1991; Gross, 1993; Underwood, 1999) discuss the importance of weak bedding contacts on fracture termination.

Most of our present mechanical understanding of the effects of weak mechanical interfaces on fracture development comes from theoretical and laboratory work on Plexiglas™ (Biot and others, 1983), composite materials (e.g. Budiansky and Hutchinson, 1986) and rocks (Weertman, 1980; Teufel and Clark, 1984; Theircelin and others, 1987; Renshaw and Pollard, 1995). An interface that has a low tensile strength is expected to fail by debonding and subsequently open in the presence of the fracture tip stress field (Figure 32b). It is postulated that when the interface opens as the fracture intersects it, the stress singularity at the fracture tip is lost and the fracture may not propagate across the interface. Additionally, a fracture may terminate against a sliding interface when the shear stress at the interface exceeds its shear strength and the interface slips (Figure 32c). Slip along the interface acts to blunt the fracture tip.

#### *New fracture initiation along bedding contacts*

Not only can fractures terminate at bedding contacts but new fractures may initiate within intact rock across the contact. We investigate the potential for fracture propagation across, termination at, or step-over at a bed contact by examining the stresses along this contact as the fracture approaches the contact. If the stresses are great enough, a new fracture will initiate along the intact side of the bedding contact resulting in either fracture step-over or fracture propagation across the contact. Generally, a new fracture initiates if the maximum tensile stress (maximum principal stress) on the intact side of the interface exceeds the tensile strength of the material (e.g. Jaeger and Cook, 1979). This study utilizes the tension positive sign-convention to ease analysis of fracture propagation and initiation, which develop under tensile stresses.

Field (Helgeson and Aydin, 1991), experimental (Renshaw and Pollard, 1995), and numerical studies (Helgeson and Aydin, 1991) suggest that deformation along interfaces may promote both new fracture initiation away from the fracture tip as well as fracture termination at the interface. While the laboratory experiments focused on interlayer slip, interface opening also likely occurred. Consequently, both mechanisms of interface deformation (sliding and opening) are further explored within our study.

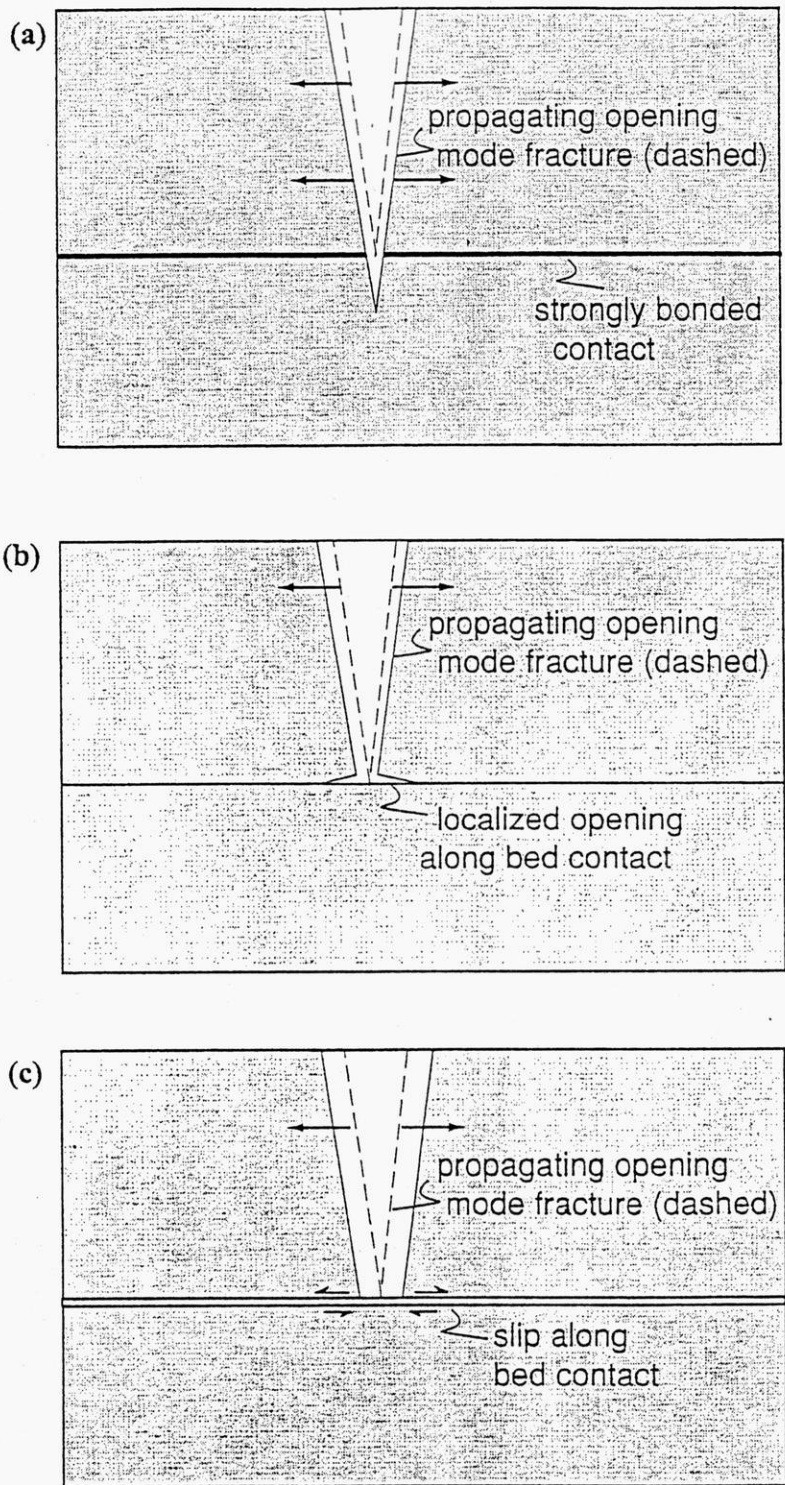


**Figure 32.** Postulated mechanisms for fracture propagation through and termination at bedding contacts. (a). Fracture Propagation through a strong well-bonded contact within a homogeneous material. (b) Fracture termination at a weakly bonded bedding contact due to local opening of the contact. (c) Fracture termination at a bedding contact due to slip along the contact.

We use numerical experiments to investigate two potential mechanisms for fracture termination at, propagation through, and step-over at bedding contacts: (1) debonding and subsequent opening of bed contacts (Figure 32b); and (2) slip along contacts (Figure 32c).

### **Numerical modeling**

One of the most successful numerical modeling techniques used in rock fracture mechanics applications is the Boundary Element Method (BEM), which solves the governing differential equations of continuum mechanics for a Boundary Value Problem (Crouch and Starfield, 1990). Boundary Element Method simplifies the problem by only requiring the external and internal boundaries of the domain to be discretized. A subset of BEM, the displacement discontinuity method, is particularly well-suited for fracture investigations in homogeneous materials (Crouch and Starfield, 1990).

In order to numerically model a fracture approaching a frictional interface, we used the Boundary Element Method code called FRIC2D (Cooke, 1996), which uses the displacement discontinuity BEM method. FRIC2D analyzes frictional slip and associated opening-mode fracture propagation in two dimensions via special constitutive interface elements that simulate frictional slip along weak bedding surfaces (Cooke, 1996).

Unlike regular boundary elements that require specification of stresses or displacements, these constitutive interface elements require prescription of constitutive properties (Crouch and Starfield, 1990). The constitutive properties of these elements include shear stiffness, normal stiffness, cohesion ( $c$ ), and the coefficient of friction ( $\mu$ ). The elastic interface parameters, normal and shear stiffness, are analogous to the shear and Young's moduli for bulk material, because the normal and shear stiffness relate the normal ( $\sigma$ ) and shear ( $\tau$ ) stresses to the normal and shear displacements along the interface. At low stresses, the interface deforms elastically, whereas at greater shear or tensile stress the interface may slip or open inelastically (i.e. non-reversibly). Within FRIC2D, interface elements slip where the Coulomb friction criterion is met,

(Eq. 1)

$$|\tau| \geq c - \sigma\mu.$$

In the presence of tensile stresses, the interface may open. Within FRIC2D, the interface elements open where the normal stress across the interface exceeds the tensile strength of the interface,  $T$ ,

(Eq. 2)

$$\sigma \geq T.$$

If  $T < (c/\mu)$  this opening criterion is implemented as a tensile cutoff to the frictional slip criterion (Figure 33) in a similar fashion as the tensile cutoff of the Mohr-Coulomb failure envelope for intact rock (e.g. Goodman, 1989). Once the tensile strength of the interface is exceeded, the bonding and/or cementation of the interface is broken, subsequently reducing the tensile strength of the interface.

Once any element slips or opens, the stress state of the entire system must be recalculated because slip or opening of one element will change the state of stress on neighboring elements, which in turn may also slip or open (Cooke and Pollard, 1997). This process is repeated until the differences in shear stresses and normal stress of successive iterations falls below a prescribed tolerance level (Cooke and Pollard, 1997). For this study, we used a tolerance of 0.1% in all models. Once the tolerance is met for both slip and opening, the solution is considered to have converged.

### *Model Set-Up*

To evaluate the contributions of interface slip and debonding to fracture termination and step-over at bedding contacts, we perform numerical experiments on each of these processes as well as the combination of sliding and opening. The two-dimensional model contains a vertical opening-mode fracture that increases in length as it approaches a horizontal interface representing a bedding contact (Figure 34). To investigate the fracture approach to the interface, the distance between the interface and the fracture tip,  $s$ , and the fracture length,  $2a$ , are varied so

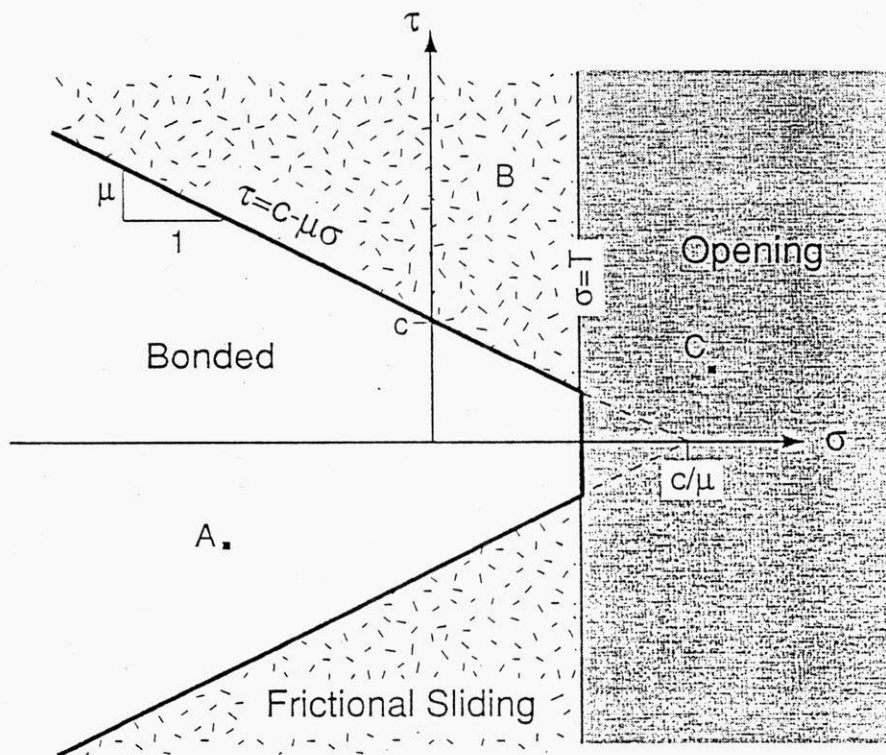


**Figure 33.** Conceptualization of the interface constitutive properties in shear-normal ( $\tau$ - $\sigma$ ) stress space. Where the shear stress does not exceed the Coulomb friction criterion, for example point A, the interface element is bonded. Point B lies within the ornamented region where shear stress exceeds the frictional sliding criterion and the element represented by B slips. Where the normal stress exceeds the tensile strength of the interface, T, within the dark shaded region (e.g point C), the interface opens.

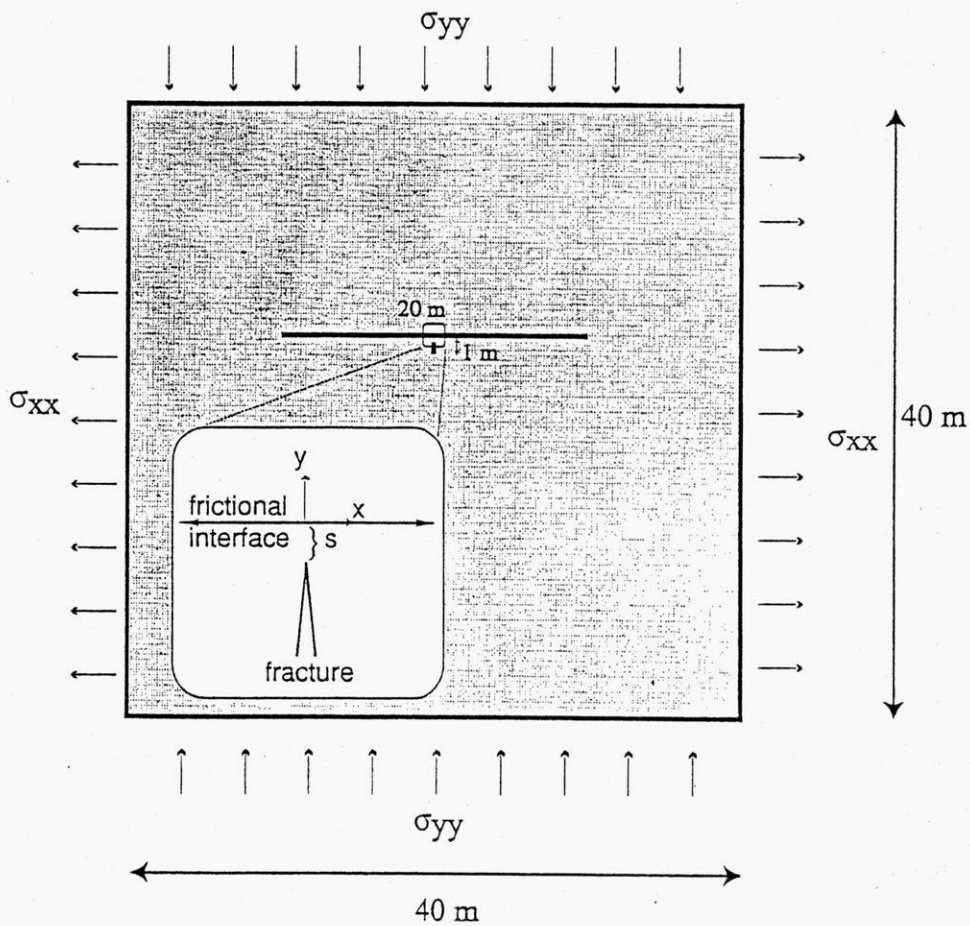


**Figure 34.** Model used to examine fracture termination at weak mechanical interfaces. The model includes four outer boundaries along which remote stresses ( $s_{xx}$  and  $s_{yy}$ ) are specified, a horizontal interface and a vertical fracture that grows longer as it approaches the interface. The distance from interface to far tip of fracture is 1m. The inset shows an enlargement of the fracture tip region.

that  $2a + s = 1\text{m}$  (Figure 34). Uniform remote vertical compression simulates overburden loading while propagation of the vertical fracture is driven by remote horizontal tension.

Material properties and boundary conditions are chosen to simulate fracture conditions within the Silurian dolomite. The fractures within the Silurian dolomite may have formed during uplift and subsequent horizontal extension of the strata in the presence of elevated pore pressures (Underwood, 1999). We estimate the depth of burial during fracture development to be around 200 m (-5 MPa) and the effective horizontal tension to be around 5 MPa. Although pore pressure is not explicitly considered within this model, the effective horizontal tension may incorporate the influence of pore pressure on fostering fracture propagation. Material parameters for the Silurian dolomite (Young's Modulus: 65 GPa; Poisson's Ratio: 0.35) were assigned based on published results from analogous materials (Birch, 1966).

We assessed end-member conditions for fracture intersection with bedding contacts by investigating first the case of interface slip with no opening (sliding-only) and then the case of debonding and subsequent opening along the interface with no sliding (opening-only). The combination of opening and slip is investigated in the third suite of models.

The three suites of models seek to isolate the influence of interface slip and interface opening on fracture propagation through, termination at and step-over at bedding interfaces. Because the models strive to isolate one or other mechanism of interface deformation rather than simulating natural conditions, all three suites of models incorporate interface shear and normal stiffnesses several orders of magnitude greater than the rock stiffness. The high interface normal and shear stiffness minimizes elastic deformation along the interface so that the resulting behavior is limited to slip and opening due to stresses that meet the prescribed interface sliding and opening criteria.

Within each suites of models, several different interface conditions are examined to explore the nature of fracture propagation, termination or step-over with respect to different strength

interfaces. Strong interfaces are simulated with very high values of friction coefficient, cohesion and tensile strength (Table 4). Since these strong interfaces neither open nor slide within the model, the interfaces are considered to be bonded or welded. In contrast, very weak interfaces will slide easily under non-zero shear stress and open easily under interface tension (Table 4). Between the end-members of bonded and weak interfaces lies what we have termed moderate-strength interfaces. For the purpose of this study, moderate-strength interfaces are simulated with friction coefficient based on rock contact friction experiments (Byerlee, 1978; Table 4). Because strength data for bedding interfaces is not available, we use values that are fractions of the average strength of intact rock (~10 MPa, Goodman, 1989; Suppe, 1985; Table 4). Moderate-strength interfaces slip only where the frictional slip criterion (Eq. 1) is met in the sliding-only and combination models, and open only where the tensile stress across the interface exceeds  $T$  (Eq. 2) in the opening-only and combination models.

**Table 4: Strength Properties of Interfaces**

	C	$\mu$	T
Strong interface	>> 10 Mpa	>> 1	>> 10 MPa
Moderate interface	3.25 MPa	0.65	5 MPa
Weak interface	0	0	0

Details of the model set-up, including 1) element size and boundary location and 2) error assessment are presented in Cooke and Underwood (2001). The report focuses on the results of the modeling presented below.

### Model Results

To investigate the potential for fracture propagation through, termination at or step-over at sliding and opening interfaces, we examine the maximum principal tensile stress along the top of the interface (the intact side of the interface). Along a bonded interface, two locations of greatest

principal tension exist to either side of the fracture (Figures 35a and 35b). These peaks are most pronounced when the fracture is within 1 cm of the interface and the greatest principal tension occurs along the interface within 1 cm of  $x=0$  (Figure 35b). However, if the interface slips and/or opens the magnitude and position of greatest principal tension will differ. To determine whether the fracture will propagate through slipping/opening interfaces, we compare the patterns of greatest maximum tensions in those cases to that produced along bonded interfaces. Because fractures are observed to propagate straight through bonded interfaces (through  $x=0$ ), we assume that if the greatest value of maximum tension along sliding/opening interface develops within  $\sim 1$  cm of  $x=0$ , and the magnitude of the greatest maximum tension meets or exceeds that along the bonded interface, the fracture will propagate through the interface at  $x=0$ . If the greatest value of maximum principal tension is less than that along the bonded interface, the fracture may terminate at the interface. If the greatest maximum principal tension along sliding/opening interfaces occurs at  $|x| > 1$  cm, a new fracture may develop along the top of the interface that steps-over from the parent fracture.

Once the interface slips, the maximum tensile stress along the bottom of the interface differs from that along the top of the interface due to the anti-symmetry of stresses around a sliding fracture (e.g. Lawn, 1993). The greatest maximum tension along the bottom of the interface could exceed the greatest maximum tension above the interface to either side of the parent fracture. Under such conditions, flaws along the bottom of the interface would initiate fractures that propagate downwards from the interface. Because these new fractures would propagate into the stress shadow of the parent fracture, their propagation may be arrested due to lack of driving stress so that they do not extend far into the layer (Nemat-Nasser and others, 1978; Pollard and

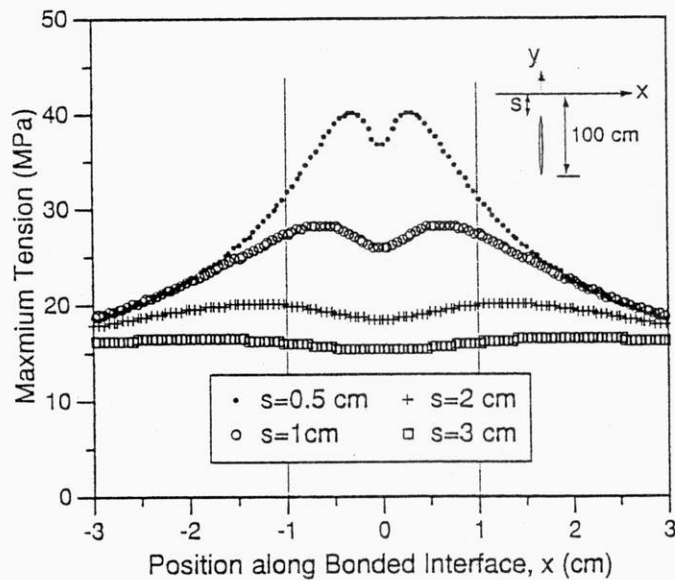
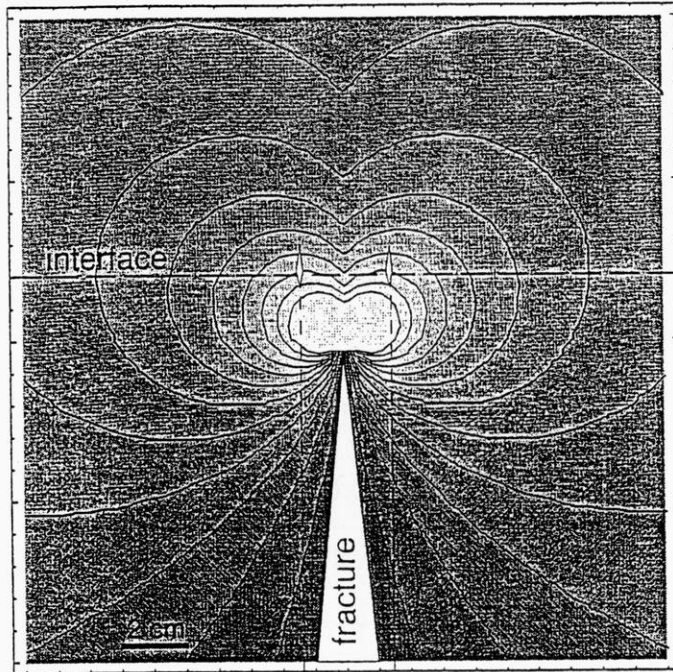


**Figure 35. A)** Maximum tension (principal stress) around the tip of a 1m vertical fracture under 5 MPa remote isotropic tension. Contours range from 2 to 24 MPa (tension is positive). Along a bonded interface 2 cm ahead of the fracture, the greatest value of maximum tension occurs about 1.5 cm to either side of the parent fracture. Two hypothetical daughter fractures are sketched perpendicular to the maximum tension in these locations ahead of the parent fracture tip. **B)** Maximum tensile stress along a bonded interface. Maximum tension increases as the fracture approaches the interface. The greatest tension occurs to either side of the parent fracture and moves closer to  $x=0$  as the fracture approaches the interface.

Aydin, 1988; Gross and others, 1995). Alternatively, the fractures growing from the bottom of the interface might propagate to link up with the parent fracture. Although these scenarios warrant further investigation, we are interested in the development of new fractures above the interface and correspondingly limit our analysis to fracture development there.

### *Sliding-only Interface Models*

Along both infinitely weak and moderate-strength sliding interfaces, the maximum tensile stress exceeds that for the bonded interface and occurs in front of the fracture at  $x=0$  along interface (Figures 36 and 37). These results suggest that interface sliding alone enhances the likelihood that fractures propagate through bedding contacts. This result, however, is not consistent with our observations that fractures often terminate at non-bonded bedding contacts. Therefore, another mechanism must be responsible for the termination of fractures in rock strata and our original supposition that slip alone along bedding could act to blunt the crack tip (e.g. Figure 32b) is not substantiated.

### *Opening-only Interface Models*

To isolate the influence of interface opening on fracture propagation or termination, we disallow sliding along the modeled interfaces. The greatest values of maximum tension develop <sup>+</sup>no<sub>^</sub> in front of the fracture ( $x=0$ ) but to either side (Figure 38). The maximum tension occurs near the ends of the open segments producing a stepped fracture pattern across the interface.

Opening along bedding contacts provides a compelling mechanism for the development of step-over fractures at bedding contacts (Figure 38). If the stresses are not great enough to initiate new

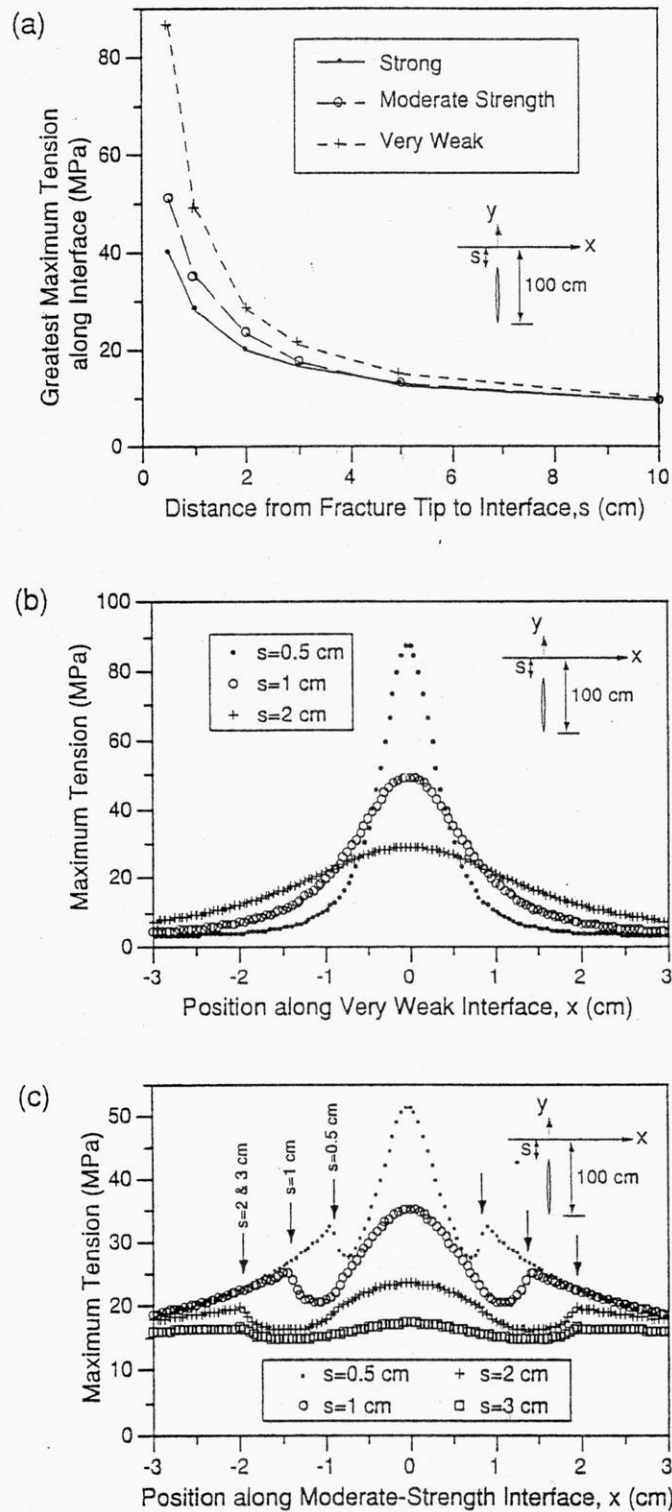


**Figure 36.** (a) Greatest values of maximum tensile stress along the bonded and sliding-only interface models. Distribution of maximum tension along the (b) very weak ( $m=0$ ;  $c=0$  MPa) and (c) moderate-strength ( $m=0.65$ ;  $c=3.25$  MPa) interfaces. The ends of slipped segments of the moderate-strength interface are marked with arrows.

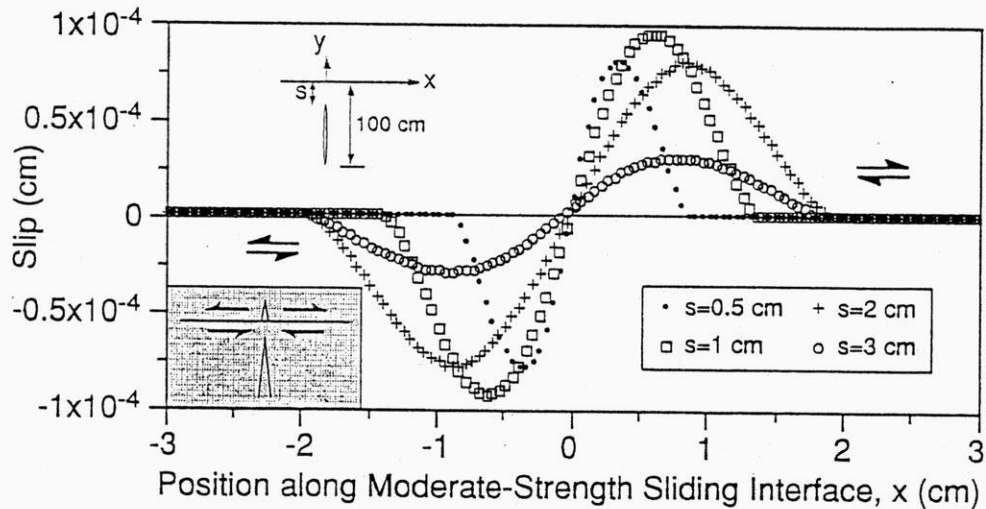


**Figure 37.** Slip distribution along the moderate-strength ( $m=0.65$ ;  $c=3.25$  MPa) sliding-only interface. Right-handed slip is positive and left-handed is negative. The inset on the lower left shows the slip-sense reversal at  $x=0$  producing high tensile stresses above the interface at  $x=0$  that promote fracture propagation straight through the interface.

step-over fractures, the parent fracture may terminate at the bedding contact. Within a small range of conditions, when stresses are not great enough to create new step-over fractures but are great enough for through propagation when the fracture is close to a bedding contact, fractures might propagate through the contact.

### *Sliding and Opening Interface Models*

Along the very weak interface, the maximum tensile strength occurs at  $x=0$  ahead of the fracture and has limited magnitude (Figure 39). In contrast, along the moderate strength interface, the greatest value of maximum principal tension occurs farther than 2.5 cm away from the parent fracture and may exceed the rock's tensile strength (Figure 39). These results suggest that the combination of slip and opening along an interface may either terminate fractures at bedding contacts if the contacts are very weak or produce step-over fractures to the left and/or right of the parent fracture if the contacts are moderately strong (Figure 39). If the stresses are not great

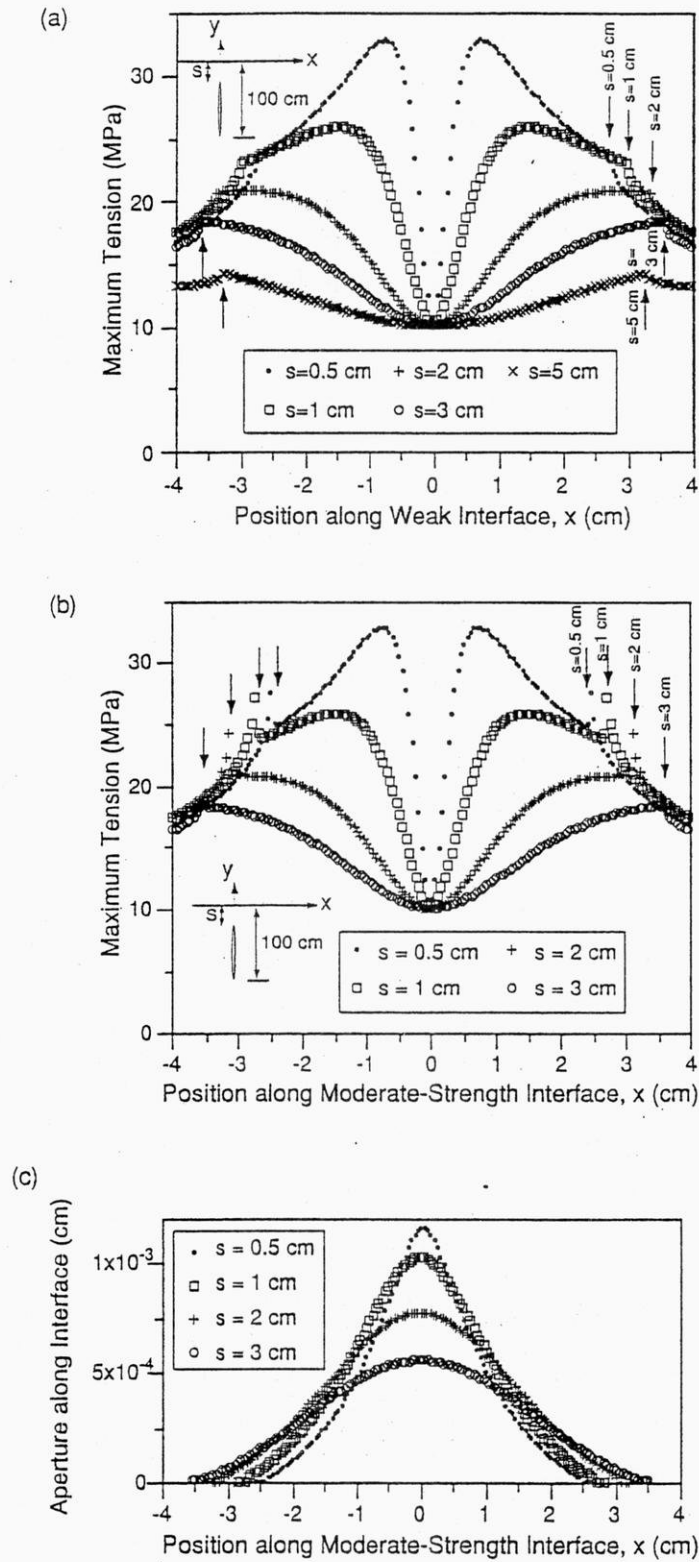


**Figure 38.** Distribution of maximum tension along (a) very weak ( $T=0$  MPa) and (b) moderate-strength ( $T=5$  MPa) opening-only interfaces. The locations of the ends of the open interface segments are indicated with arrows. (c) The distribution of aperture along the moderate-strength opening-only interface.

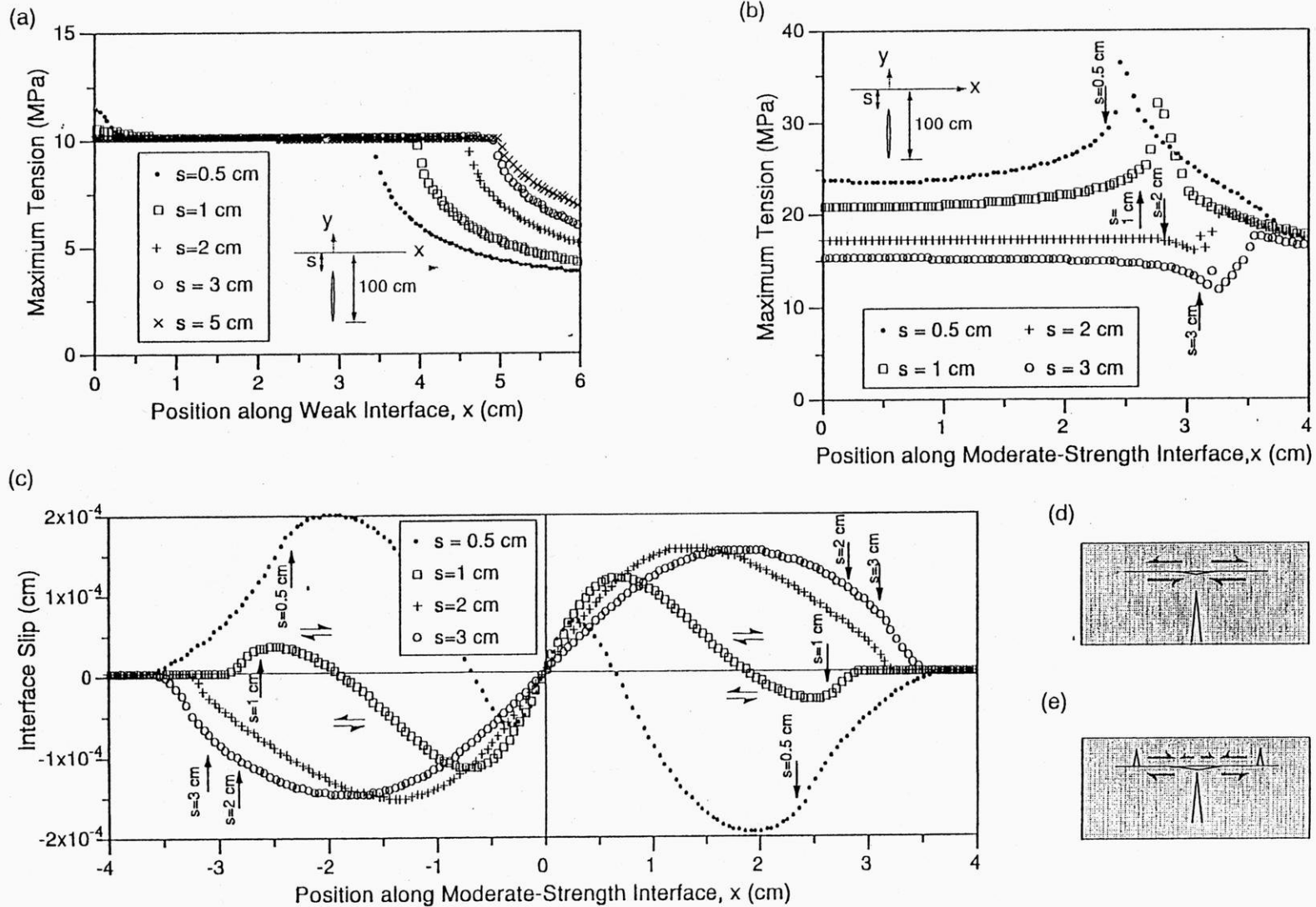


**Figure 39.** Distribution of maximum tension along (a) very weak ( $m=0$ ;  $c=0$  MPa;  $T=0$  MPa) and (b) moderate-strength ( $m=0.65$ ;  $c=3.25$  MPa;  $T=5$  MPa) interfaces that deform under combination of sliding and opening. To improve clarity of data presentation only deformation along the right half of the moderate-strength interface is presented. Arrows indicate position of the tips of open segments along the interfaces. (c) The slip sense and magnitude along the moderate-strength interface change as the fracture approaches the interface. (d) Cartoon showing slip sense along an interface when the fracture is farther from the interface ( $2\text{ cm} = s = 3\text{ cm}$ ). (e) Cartoon showing slip sense along the interface when the fracture tip is close ( $s = 2\text{ cm}$ ) to the interface.

enough to initiate new step-over fractures across the moderate-strength interface, the parent fracture may terminate at the bedding contact (Figure 39).

## **Discussion**

The numerical models within this study assume that the host rock around the fractures deforms as a linear and elastic material. However, this assumption is not valid near fracture tips where high stresses produce local inelastic yielding of the host material (Lawn, 1993). The zone of inelastic yielding (process zone) scales with fracture size so that a 1 m long fracture has a process zone of ~1 cm (e.g. Broek, 1991). As the fracture tip approaches within 1 cm of the interface, local failure via microcracking and other mechanisms reduce stresses along the interface. Thus, the stresses reported here for distance less than 1 cm from the interface are likely to be greater than those experienced along natural bedding contacts. Interestingly, for the case of a 1 m long fracture at 200 m depth, the maximum tensile stress along the interface is great enough to produce new step-over fractures when the fracture tip is still 5 or 10 cm from the interface (and neither opening or slip has yet occurred). Although in thinner beds the fracture would need to be closer to the interface before new fractures develop, the fracture may not necessarily need to be as close as the length of the process zone.

### ***Expected types of fracture intersection with bed contacts***

Using numerical models, we explored the influence of several end-member mechanisms and interface strengths on fracture intersection with sliding and opening interfaces. The model results can be used to infer fracture termination at, propagation through and step-over at different types of bedding contacts (Figure 40). Bedding contacts that are strongly welded or well-

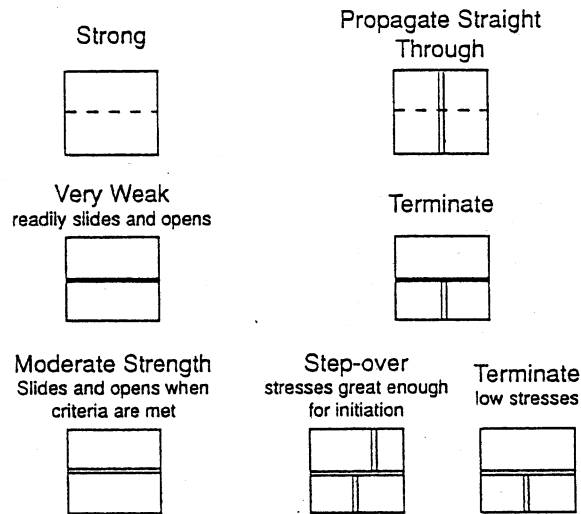


**Figure 40.** Inferred variations in geometry of fracture-bed contact intersection for bedding contacts with different strengths.

cemented, such as gradual contacts and reworked (e.g. bioturbated) contacts may be approximated by bonded interfaces. The model results suggest that most fractures would propagate through such contacts (Figure 40). Fracture propagation has been observed through bedding contacts that became silicified during diagenesis and appear well-cemented within the Silurian dolomite of Door County, Wisconsin (Underwood, 1999). In contrast to strongly cemented contacts, some bedding planes within the Silurian dolomite, such as laminated organic partings, have very little cementation and may be approximated by interfaces that are very weak in both shear and opening. The model results suggest that such contacts would terminate propagating fractures (Figure 40). Fracture termination has been observed at weak contacts such as unmineralized pre-existing joints (Dyer, 1988; Gross, 1993), thin organic layers in the Silurian dolomite (Underwood, 1999) and uncemented bedding contacts (Narr and Suppe, 1991; Becker and Gross, 1996).

Most sedimentary bed contacts are neither strongly bonded nor infinitely weak. The numerical experiments simulate such contacts with moderate-strength interfaces that are permitted to both open and slide when the debonding and sliding criteria are met. The model results suggest that fractures approaching moderate-strength contacts may either produce step-over fractures across the contact or terminate at the contact if the stresses are insufficient to initiate new fractures (Figure 40). Step-over fractures have been observed in laboratory experiments (Renshaw and Pollard, 1995) and recognized in the field (Helgeson and Aydin, 1991) as part of composite joints. The development of right- or left-stepping fractures depends on the distribution of flaws within the regions of elevated maximum tension.

Some important factors, such as depth of burial, driving stress and fracture length control fracture intersections with bedding contacts. The results of our modeling work suggest that localized interface opening rather than sliding is responsible for fracture termination. Because contact slip and opening are both inhibited at greater burial depths, the influence of greater depth is comparable to increasing the strength of the contacts. Deep burial could suppress the small and localized contact opening that acts to terminate fractures and promote either step-over fractures or fracture propagation through weak and moderate-strength interfaces.

The length of fractures also controls the nature of fracture-bed contact intersection. Increases in fracture length are associated with increases in stress concentration (e.g. Lawn, 1993). The longer fractures in thicker beds, would produce greater stress concentrations and greater levels of local slip and opening along contacts with adjacent beds than fractures in thinner beds. An increase in the length of opening and sliding segments along the contacts increases the distance

from parent crack to the peaks in maximum tension that may produce new step-over fractures. Thus, thicker layers may be associated with greater amounts of fracture step-over.

Increased stress concentrations are also associated with fractures under greater driving stress (e.g. Lawn, 1993). Greater layer-parallel effective tension increases both the stress concentration associated with the parent crack as well as the overall tension within the adjacent intact beds. This combined influence produces localized regions of tension within the adjacent beds and encourages propagation of fractures from existing flaws in these regions. Increased driving stress either in the form of increased remote tension or elevated fluid pressures would promote the development of step-over fractures and through fracture propagation. Additionally, increased levels of opening and sliding along the interface due to increased driving stress would increase the step-over distance of fractures.

Our modeling did not examine deformation once the fracture intersects the interface. Since the stresses along the interface far exceeded the tensile strength of average rock prior to fracture intersection with the interface, the new fracture would initiate prior to this intersection. However, a qualitative consideration of this intersection in the case of fluid-driven growth may be illustrative. If the fracture growth is driven by fluid pressures, we might expect this fluid to enter the bed contact upon fracture propagation to the interface. Once the fluids have entered the contact, the volume available to the fluid greatly increases. Unless there is additional influx of fluids, the fluid pressure would drop, preventing further propagation. Thus, in the case of relatively rapid propagation of a fluid-filled fracture, some new fractures may develop within the intact rock prior to the fracture intersecting the bedding contact. Yet after intersection and

dispersion of fluid pressure, these small fractures might arrest. Fluid pressures may therefore encourage fracture termination by facilitating interface opening. Thus, fractures driven by fluid pressure may be more likely to terminate against bedding contacts than fractures driven by equivalent remote layer-parallel tension.

In summary, fracture termination is more likely under conditions of shallower depth, lower effective layer-parallel tension (i.e. greater effective layer-parallel compression) and fluid-driven fracture propagation. Furthermore, thicker beds and greater layer-parallel tension may produce greater amounts of step-over than thinner beds and more compressive layers.

### **Conclusions**

The numerical experiments of this study explore the influence of deformation along bedding contacts, in the form of local sliding and/or debonding and subsequent opening, on fracture intersection with bed contacts. Fractures propagating toward a bedding contact may either 1) terminate at the contact, 2) propagate straight through the contact or 3) step-over to the left or right at the bedding contact. The model results suggest that local interface opening, rather than sliding, is primarily responsible for the termination and step over of fractures. Furthermore, the model results suggest that the strength of bedding contacts controls the type of resulting fracture intersection. Fracture termination is favored at very weak bedding contacts, where as fractures propagate straight through strong contacts. Most sedimentary contacts will fall between these two end-members. Such moderate-strength contacts may develop step-over fractures due to local opening along the interface or, if the stresses are not great enough to produce new fractures, the parent fracture will terminate at the moderate-strength contact. Fracture termination is more

likely under conditions of shallower burial depth, lower effective layer-parallel tension, and fluid-driven propagation, rather than equivalent remote layer-parallel tension. Thicker beds and greater effective layer-parallel tension may produce greater amounts of step-over than thinner beds and more compressive layers. Fractures aligned within several centimeters across a bed contact may be coincidentally aligned or the result of fracture step-over. Careful characterization of the fractures and analysis of the pattern may distinguish between whether the fractures are the result of coincidental alignment or fracture step-over.

# SIMULATION OF FLUID FLOW

## Introduction

In fractured rocks, typically only a small number of fractures are hydrologically active (Committee of Fracture Characterization and Fluid Flow, 1996, p. 337). This appears to be true of the fractured-carbonate aquifer in Door County. In boreholes, caliper logs typically indicate numerous open bedding-plane partings, however, flow logs indicate that only a few of these contribute water to the borehole (Muldoon and others, in review). Similarly, weathered fractured pavements, suggest that only a small percent of the exposed fractures have been significantly widened by dissolution. Characterization of the interconnected, hydrologically important fractures is time-consuming and expensive even at small sites (Muldoon, 1999) and probably unrealistic at regional scales.

Numerical modeling provides a tool to explore the development of the interconnected fracture network over larger areas and to assess the role of fractures in the development of the regional flow system. One of our original objectives was to assess whether the carbonate flow system that evolves from the integrated mechanical-hydrologic models resembles the observed flow system in Door County. The fracture networks generated from the mechanical models were to serve as input for numerical flow models that couple discrete fracture flow with reactive transport.

## Summary of existing codes

At the time we wrote the proposal, both of the codes that we proposed to use were under development. The FRAC3DVS code, originally developed by Therrien and Sudicky (1996) is a 3-D, finite element, discrete fracture flow code that was being modified to include carbonate dissolution (Annable and Sudicky, 1997). The work on this code modification is being completed by a PhD and it was completed in time for us to use the code as part of this project. The CAVE (Carbonate Aquifer Void Evolution) model developed by Clemens and others (1996) is a hybrid model that incorporates both porous media flow (matrix) and pipe flow (fractures). It has been linked with a reactive transport model to simulate the development of karst conduits in two dimensions and model-simulated results compare favorably with field-mapped conduit systems. The code was being modified to handle 3-D analyses but this work has not yet been completed.

After looking at the 2-D CAVE code in more detail, and comparing its results to the results of some more recently developed karst genesis codes, we decided that the code was unsuitable for our analyses and began to evaluate some additional codes. One model, developed by Groves and Howard (1994a and b, 1995) was rather limited in terms of the geometry of the fracture network that it could simulate -- it solved for flow through a 2-D pipe network consisting of circular conduits. This is not really the type of karst we see in Door County and since the flow solution utilized the equation for flow through pipes, it could not be easily modified to solve for flow through planar fractures. A more recent code developed by Kaufmann and Braun (1999) is more flexible in terms of how it simulates the conduit geometry and we have some hope that this code may be capable of handling the complex fracture geometry that results from our mechanical

stratigraphy analyses. In the future, we hope to acquire this code and modify it to 1) accept input of the fracture network and 2) to simulate dolomite dissolution (these codes include the kinetics for limestone dissolution). Given that this will require extensive coding on our part, we were not able to complete the flow simulations that we had proposed.

## References Cited

- Annabelle, W.K. and E.A. Sudicky, 1997. Simulation of karst genesis: Hydrodynamic and geochemical rock-water interactions in partially-filled conduits. In *Proceedings of 6th Conference on Limestone Hydrology and Fissured Aquifers: Modelling in Karst Systems*, LeChaux de Fonds, Switzerland, August, 1997.
- Baer, G., 1991. Mechanisms of dike propagation in layered rocks and in massive porous sedimentary rocks. *Journal of Geophysical Research* 96, 11, 911-11, 929.
- Bai, T. and Pollard, D.D., 2000. Fracture spacing in layered rocks: a new explanation. *Journal of Structural Geology*, v. 22, no. 1, p. 43.
- Becker, A. and Gross, M.R., 1996. Mechanisms for joint saturation in mechanically layered rocks: An example from southern Israel: *Tectonophysics*, v. 257, p. 223.
- Birch, F., 1966. Compressibility; elastic constants. In: Sydney P. Clark, J. (Eds.), *Handbook of Physical Constants Memoir 97*. Geological Society of America, 97-173.
- Bradbury, K.R., 1989. In: *Conference Proceedings, Door County and the Niagara Escarpment: Foundations for the future*, K. Hershbell, ed., Wisconsin Academy of Sciences, Arts, and Letters, Madison. p. 36-44.
- Bradbury, K.R., M.A. Muldoon, A. Zaporozec, and J. Levy, 1991. *Delineation of wellhead protection areas in fractured rocks*. Technical Guidance Document, U.S. Environmental Protection Agency, EPA 570/9-91-009. 144 p.
- Bradbury, K. R. and Muldoon, M.A., 1992. Hydrogeology and groundwater monitoring of fractured dolomite in the Upper Door Priority Watershed, Door County, Wisconsin: Wisconsin Geological and Natural History Survey Open File Report 92-2.
- Bradbury, K. R. and Muldoon, M.A., 1993. Preliminary comparison of a discrete fracture model with a continuum model for groundwater movement in fractured dolomite: Wisconsin Geological and Natural History Survey Open File Report 93-6, 44 p. plus 1 computer diskette.
- Bradbury, K. R., T. W. Rayne, M. A. Muldoon, and P. D. Roffers, 1998. *Application of a discrete fracture flow model for wellhead protection at Sturgeon Bay, Wisconsin*. Wisconsin Geological and Natural History Survey Open File Report, WOFR 1998-04, 62 p.

- Bradbury, K.R., T.W. Rayne, and M.A. Muldoon, 2000. Field Verification of Capture Zones for Municipal Wells at Sturgeon Bay, Wisconsin: Wisconsin Geological Survey Open File Report, WOFR 2001-1, 29 p.
- Chamberlain, T. C., 1877. Geology of Wisconsin: Geological Survey of Wisconsin, Survey of 1873-1877.
- Broek, D., 1991. Elementary Engineering Fracture Mechanics. Kluwer Academic Publishers, Boston.
- Cooke, M. 1996. Frictional slip and fractures associated with faults and folds. Unpublished PhD thesis, Stanford University.
- Cook, T. S. and Erdogan, F., 1972. Stresses in bonded materials with a crack perpendicular to the interface: *International Journal of Engineering Science*, v. 10, p. 677.
- Cooke, M., and Pollard, D., 1997. Bedding plane slip in initial stages of fault-related folding. *Journal of Structural Geology* 19, 567-581.
- Cooke and Underwood, 2001. Fracture termination and offset at bedding interfaces due to frictional slip and interface debonding: *Journal of Structural Geology*, vol 23, p. 223-238.
- Corbett, K., Friedman, M., and Spang, J., 1987. Fracture development and mechanical stratigraphy of Austin Chalk, Texas.: *The American Association of Petroleum Geologists Bulletin*, v. 71, no. 1.
- Craddock, J.P. and van der Pluijm, B.A., 1989. Late Paleozoic deformation of the cratonic carbonate cover of eastern North America. *Geology*, v. 17, p. 416.
- Crouch, S. L., Starfield, A. M. 1990. *Boundary Element Methods in Solid Mechanics*. Unwin Hyman, Boston.
- Dunham, R. J., 1962. Classification of carbonate rocks according to depositional texture. In: W.E. Ham, ed., *Classification of Carbonate Rocks*, American Association of Petroleum Geologists, Memoir 1, p. 108-121.
- Dyer, R., 1988. Using joint interactions to estimate paleostress ratios. *Journal of Structural Geology*, v. 10, no. 7, p. 685.
- Ellefson, B. R., K. S. Rury, and J. T. Krohelski, 1987. *Water use in Wisconsin, 1985*. U.S. Geological Survey Open-file Report 87-699, One atlas sheet.
- Engelder, T., 1985. Loading paths to joint propagation during a tectonic cycle: an example from the Appalachian Plateau, USA. *Journal of Structural Geology*, v. 7, p. 459.
- Erdogan, F. and Biricikoglu, V., 1973. Two bonded half planes with a crack going through the interface. *International Journal of Engineering Science*, v. 11, p. 745.
- Goodman, R. E. 1989. *Introduction to Rock Mechanics*. John Wiley & Sons, New York.

- Gross, M. R., 1993. The origin and spacing of cross joints: Example from the Monterey Formation, Santa Barbara Coastline, California: *Journal of Structural Geology*, v. 15, no. 6, p. 737.
- Gross, M. R., Fischer, M.P., Engelder, T., and Greenfield, R.J., 1995. Factors controlling joint spacing in interbedded sedimentary rocks: Interpreting numerical models with field observations from the Monterey Formation, USA, in Ameen, M. S., ed., *Fractography: fracture topography as a tool in fracture mechanics and stress analysis.*, Geological Society of America Special Publication, p. 215.
- Groves and Howard, 1994a. Minimum hydrochemical conditions allowing limestone cave development. *Water Resources Research*, vol. 30, p. 607-615
- Groves and Howard, 1994b. Early development of karst systems 1. Preferential flow path enlargement under laminar flow. *Water Resources Research* vol. 30, p. 2837-2846
- Haimson, B.C., 1978. Crustal stress in the Michigan Basin. *Journal of Geophysical Research*, v. 83, no. B12, p. 5857.
- Hanks, C. L., Lorenz, J., Lawrence, T., and Krumhardt, A. P., 1997. Lithologic and structural controls on natural fracture distribution and behavior within the Lisburne Group, northeastern Brooks Range and North Slope subsurface, Alaska: *American Association of Petroleum Geologists Bulletin*, v. 81, no. 10, p. 1700.
- Harbaugh, J.W., Doveton, J.H., and Davis, J.C., 1977. *Probability Methods in Oil Exploration*. John Wiley and Sons, 269 p.
- Harris, M. T. and Waldhuetter, K.R., 1996. Silurian of the Great Lakes Region, Part 3: Llandoverly Strata: *Milwaukee Public Museum Contributions in Biology and Geology*, 90.
- Hegrenes, D. P., 1996. A core study of the sedimentology, stratigraphy, porosity, and hydrogeology of the Silurian aquifer in Door County, Wisconsin. [Masters thesis]: University of Wisconsin - Milwaukee, 156 p.
- Helgeson, D.E. and Aydin, A., 1991. Characteristics of joint propagation across layer interfaces in sedimentary rocks. *Journal of Structural Geology*, v. 13, no. 8, p. 897.
- Hobbs, D. W., 1967. The formation of tension joints in sedimentary rocks: An explanation: *Geological Magazine*, v. 014, no. 6, p. 551.
- Holst, T. B., 1982. Regional jointing in the northern Michigan Basin: *Geology*, v. 10, no. 273.
- Holst, T. B. and Foote, G.R., 1981. Joint orientation in the Devonian rocks in the northern portion of the lower peninsula of Michigan: *Geological Society of America Bulletin*, v. 92, p. 85.

- Howard and Groves, 1995. Early development of karst systems 2. Turbulent flow. *Water Resources Research*, vol. 31, no. 1, p. 19-26
- Howell, P.D., and van der Pluijm, B.A., 1999. Structural sequences and styles of subsidence in the Michigan basin. *Geological Society of America Bulletin*, v. 111, no. 7, p. 974.
- Howell, P.D., and van der Pluijm, B.A., 1990. Early history of the Michigan Basin: Subsidence and Appalachian Tectonics. *Geology*, v. 18, p. 1195.
- Huang, Q. and Angelier, J., 1989. Fracture spacing and its relation to bed thickness: *Geological Magazine*, v. 126, no. 4, p. 355.
- Ji, S., Saruwatari, K., 1998. A revised model for the relationship between joint spacing and layer thickness. *Journal of Structural Geology* 20, 1495-1508.
- Kaufmann, G. and Braun, J. 1999. Karst aquifer evolution in fractured rocks, *Water Resources Research*, Vol. 35, No. 11, p. 3223-3238
- La Pointe, P. R. and Hudson, J.A., 1985. Characterization and interpretation of rock mass joint patterns: *Geological Society of America Special Paper* 199.
- Lachenbruch, A. H., 1961. Depth and spacing of tension cracks: *Journal of Geophysical Research*, v. 66, p. 4273.
- Ladeira, F. L. and Price, N.J., 1981. Relationship between fracture spacing and bed thickness: *Journal of Structural Geology*, v. 3, no. 2, p. 179.
- Lajtai, E.Z., 1977. A mechanistic view of some aspects of jointing in rocks. *Tectonophysics*, v. 38, no. 3-4, p. 327.
- Laslett, G. M., 1982. Censoring and edge effects in areal and line transect sampling of rock joint traces. *Mathematical Geology*, 14(2), 125-140.
- Lawn, B. 1993. *Fracture of Brittle Solids – Second Edition*. Cambridge University Press, New York.
- Lorenz, J., Lawrence, T., and Warpinski, N.R., 1991. Regional Fractures I: A mechanism for the formation of regional fractures at depth in flat-lying reservoirs. *American Association of Petroleum Geologists Bulletin*, v. 75, no. 11, p. 1714.
- Magara, K., 1981. Mechanisms of natural fracturing in a sedimentary basin. *American Association of Petroleum Geologists Bulletin*, v. 65, no. 1, p. 123.
- McQuillan, H., 1973. Small-scale fracture density in Asmani Formation of Southwest Iran and its relation to bed thickness and structural setting: 57, p. 2367.
- Muldoon, M. A., and K. R. Bradbury, 1998. *Tracer study for characterization of groundwater movement and contaminant transport in fractured dolomite*. Wisconsin Geological and Natural History Survey Open File Report, WOFR 1998-2, 85 p.

- Muldoon, M.A., 1999. Hydrogeologic Characterization of the Silurian Dolomite in Door County, Wisconsin, at Regional and Site-Specific Scales: Comparison of Continuum and Discrete-fracture Approaches, Unpublished PhD, UW-Madison, 231 p.
- Muldoon, M.A., J.A. Simo, and K.R. Bradbury, in review. Correlation of high-permeability zones with stratigraphy in a fractured-dolomite aquifer, Door County, Wisconsin. Submitted to *Hydrogeology Journal*
- Narr, W. and Currie, J.B., 1982. Origin of fracture porosity B example from Altamont field, Utah. *American Association of Petroleum Geologists Bulletin*, v. 66, p. 1231.
- Narr, W. and Lerche, I., 1984. A method for estimating subsurface fracture density in core. *AAPG Bulletin*, v. 66, p. 637.
- Narr, W. and Suppe, J., 1991. Joint spacing in sedimentary rocks: *Journal of Structural Geology*, v. 13, no. 9, p. 1037.
- National Research Council (Committee on Fracture Characterization and Fluid Flow), 1996. *Rock Fractures and Fluid Flow: Contemporary Understanding and Applications*. National Academy Press, Washington D.C., 551 p.
- Nauta, R., 1987. *A three-dimensional groundwater flow model of the Silurian dolomite aquifer of Door County, Wisconsin*: M.S. Thesis - Geology, UW-Madison, 105 p.
- Nemat-Nasser, S., Keer, L. M., Parihar, K. S., 1978. Unstable growth of thermally induced interacting cracks in brittle solids. *International Journal of Solids and Structures* 14, 49-430.
- Nur, A., 1982. The origin of tensile fracture lineaments: *Journal of Structural Geology*, v. 4, p. 31.
- Pollard, D. D., Aydin, A., 1988. Progress in understanding jointing over the past century. *Geological Society of America Bulletin* 100, 1181-1204.
- Pollard, D. D. and Segall, P., 1987, Theoretical displacements and stresses near fractures in rock: With applications to faults, joints, veins, dikes, and solution surfaces, in Atkinson, B. K., ed., *Fracture Mechanics of Rock*: London, Academic Press, p. 277-349.
- Poole, R. W. and Farmer, I. N., 1980. Consistency and repeatability of Schmidt Hammer rebound data during field testing. *International Journal of Rock Mechanics and Mining Sciences*, v. 17, no. 3, p. 167.
- Price, N. J., 1966. *Fault and Joint Development in brittle and semi-brittle rock*: Oxford, England, Pergamon Press, 176 p.

- Renshaw, C.E. and Pollard, D.D., 1995. An experimentally verified criterion for propagation across unbounded interfaces in brittle linear elastic materials. *International Journal of Rock Mechanics Mining Sciences and Geomechanics Abstracts*, v. 32, no. 3, p. 237.
- Rijken, P. and Cooke, M.L., in review. Role of shale on vertical connectivity of fractures in the Austin Chalk, Texas: Application of crack-bridging theory.
- Roffers, P. D., 1996, Multiscale analysis of vertical bedrock fractures in Door County, Wisconsin [Masters thesis]: University of Wisconsin - Madison, 118 p.
- Secor, D.T., 1967. Role of fluid pressure in jointing. *American Journal of Science*, v. 263, p. 633.
- Shaver, R. H., C. H. Ault, W. I. Ausich, J.B. Droste, A. S. Horowitz, W. C. James, S. M. Okla, C. B. Rexroad, D. M. Suchomel, and J. R. Welch, 1978. *The search for a Silurian Reef Model, Great Lakes Area*: Indiana Department of Natural Resources Geological Survey Special Report 15, 36 p.
- Sherrill, M. G., 1978. Geology and groundwater in Door County, Wisconsin with emphasis on contamination potential in the Silurian Dolomite: United States Geological Survey Water Supply Paper 2047.
- Simo, J. A., Harris, M.T., and Muldoon, M.A., 1998. Stratigraphy and sedimentology of the Silurian dolostones, Door County, Wisconsin, in SEPM Research Conference, Fluid Flow in Carbonates, Door County, Wisconsin, p. 3-15.
- Sleep, N. H. and Sloss, L.L., 1978. A deep borehole in the Michigan Basin: *Journal of Geophysical Research*, v. 83, no. B12, p. 5815.
- Stieglitz, R.D., and S.B. Johnson, 1986. Mapping and Inventorying of Geologic Features in the Upper Door Priority Watershed-Technical Report. University of Wisconsin-Green Bay, 44 pp.
- Stieglitz, R.D., and T.J. Dueppen, 1994. Mapping and Inventorying of Geologic Features in the Sturgeon Bay-Red River Priority Watershed-Technical Report. University of Wisconsin-Green Bay, 85 pp.
- Suppe, J. 1985. *Principles of Structural Geology*. Prentice-Hall, Inc., Englewood Cliffs, NJ.
- Teufel, L.W. and Clark, J.A., 1984. Hydraulic fracture propagation in layered rocks: Experimental studies of fracture containment. *Society of Petroleum Engineers Journal*, v. 24, p. 19.
- Therrien, R. and E.A. Sudicky, 1996. Three-dimensional analysis of variably-saturated flow and transport in discretely-fractured porous media: Model development and illustrative examples. *Journal of Contaminant Hydrology* 23 (1-2): 1-44.

- Underwood, 1999. Stratigraphic controls on vertical fracture patterns within the Silurian dolomite of Door County, Wisconsin and implications for groundwater flow. Unpublished Master's thesis, University of Wisconsin, Madison, WI.
- Voight, B. and St. Pierre, B.H.P., 1974. Stress history and rock stress. Proceedings of the 3<sup>rd</sup> Congress of the International Society of Rock Mechanics, 2A, p. 580.
- Watkins, R. and Kuglitsch, J. J., 1997. Lower Silurian (Aeronian) megafaunal and conodont biofacies of the northwestern Michigan Basin. Canadian Journal of Earth Sciences, v. 34, no. 6, p. 753.
- Waldhuetter, K. R., 1994. Stratigraphy, sedimentology, and porosity distribution of the Silurian Aquifer, the Door Peninsula, Wisconsin [Masters thesis]: University of Wisconsin - Milwaukee, 210 p.
- Wu, H. and Pollard, D.D., 1995. An experimental study of the relationship between joint spacing and layer thickness: Journal of Structural Geology, v. 17, p. 887.

APPENDIX A  
Data from scanline surveys across fracture pavements

SITE: Big Quarry  
 MAPPING PROJECT: 1st level  
 LITHOLOGY: Byron  
 SCANLINE DESCRIPTION: 72 degrees

DATE MAPPED: 6/9/99  
 COMPASS DECLINATION: 1 degree  
 MAPPED BY: Anne Ebenreiter

Location (m)	Strike (deg)	Length (m)	Aperture	Termination	Censoring
0.395	341	0.815	V	R/FP	N
0.502	344	1.1	V	R/FP	N
0.616	342	1.935	V	FP/FP	N
0.69	41	0.68	V	S/FP	N
0.81	51	1.685	O	R/FP	N
1.25	340	3.85	O	FP/R	N
1.352	335	1.135	V	R/R	N
1.524	342	0.86	F	R/R	N
1.775	340	0.79	V	FP/R	N
1.91	336	1.2	V	B?/FP	N
2.06	341	1.182	V	R/FP	N
2.12	340	9.5	V	R/R	N
2.19	343	1.48	O	FP/FP	N
2.206	341	0.42	V	R/FL	N
2.428	343	0.28	V	R/FP	N
2.498	344	1.11	V	FP/S	N
2.665	343	3.18	O	S.FL	N
2.73	341	0.9	F	R.FL	N
3.06	342	3.24	O	FP/FP	N
3.212	345	0.9	V	FP/R	N
3.418	346	0.33	F	FP/FP	N
3.47	345	1.55	O	FP/S	N
3.685	328	0.225	V	FP/FP	N
3.8	336	0.25	F	FP/FP	N
3.91	343	2.215	V	FP/R	N
4.05	338	0.91	V	R/FP	N
4.26	343	2.915	V	FP/R	N
4.33	342	2.995	O	FP/R	N
4.5	340	1.9	V	FP/R	N
4.78	337	2.89	V	R/FL	N
4.93	342	0.31	V	FP/FP	N
5.12	346	1.07	V	R/FP	N
5.204	340	0.36	V	R/R	N
5.29	341	1.44	V	FP/FP	N
5.385	340	1.5	V	FP/S	N
5.43	341	0.25	F	R/FL	N
5.49	346	0.98	V	R./R	N
5.615	344	2.24	V	FP/R	N
5.65	336	0.405	F	FL/FL	N
5.68	344	0.565	V	FP/FP	N
5.848	344	1.99	O	FP/B	N
5.91	341	1.52	V	FP/B	N
5.98	343	0.335	F	R/FP	N
6	343	0.315	F	FP/S	N
6.045	336	1.1	F	R/S	N
6.095	341	3.6	O	FP/FP	N
6.13	342	0.94	V	R/FL	N
6.46	344	0.47	F	FP/R	N
6.5	341	0.66	V	FP/FP	N
6.62	343	0.39	F	FP/S	N

END TOTAL LENGTH 6.62 METERS

SITE: Big Quarry  
 MAPPING PROJECT: 1st level  
 LITHOLOGY: Byron  
 SCANLINE DESCRIPTION: 339 degrees

DATE MAPPED: 6/9/99  
 COMPASS DECLINATION: 1 degree  
 MAPPED BY: Anne Ebenreiter

Location (m)	Strike (deg)	Length (m)	Aperture	Termination	Censoring
0.32	79	0.418	F	FP/R	N
0.516	42	2.05	V	FP/B	N
0.828	58	2.62	O	B/R	N
1.37	72	2.71	V	FP/FP	N
1.455	88	1.172	V	FP/FP	N
1.56	63	0.24	F	R/FP	N
1.65	61	0.65	O	FP/FP	N
1.795	58	1.452	V	FP/FP	N
1.892	52	0.345	F	FP/FP	N
2.208	63	2.39	O	FP/FL	N
2.36	54	2.12	O	FP/R	N
2.62	68	0.73	F	FP/R	N
2.76	64	1.07	V	FP/FP	N
2.862	62	1.03	V	R/FP	N
2.99	74	0.53	F	FP/R	N
3.002	70	0.98	V	R/FP	N
3.25	94	2.276	V	R/FP	N
3.318	105	0.54	F	R/FP	N
3.455	83	0.962	V	FP/FL	N
3.585	45	1.38	O	FP/FP	N
3.72	61	0.09	V	FP/FP	N
3.77	74	0.47	V	FP/FP	N
3.965	35	0.172	V	FP/FP	N
4.025	39	0.142	V	FP/FP	N
4.092	97	1.432	F	FP/B	N
4.186	76	1.14	V	S/FP	N
4.42	50	0.18	V	FP/FP	N
4.592	121	0.63	V	FP/FP	N
4.615	76	0.326	V	FL/FP	N
4.86	70	0.938	O	FP/FP	N
5.21	66	2.39	V	FP/S	N
5.725	83	1.99	O	FL/FL	N
5.92	48	2.18	O	B/R	Y-1
6.49	62	2.18	O	B/R	Y-1
6.995	51	0.92	V	FP/B	Y-1
7.23	93	0.57	V	FL/B	Y-1
7.312	59	1.39	V	R/R	N
7.385	98	0.31	V	FL/S	N
7.66	64	1.145	F	FP/FP	N
7.765	29	0.34	F	R/FP	N
SKIP 7.8 M TO 13 M DUE TO LARGE BLAST AREA					
13.02	70	1.224	V	FP/FL	N
13.53	64	1.57	V	FP/FL	N
13.73	52	0.73	V	FL/S	N
13.775	297	1.18	V	FP/FL	N
14.165	47	0.79	O	FP/FP	N
14.332	49	0.67	V	FP/R	N
14.45	63	1.895	V	FP/FL	N
14.54	54	1.35	O	B/FP	Y-1
14.652	68	1.11	V	FL/R	N
14.695	83	0.63	V	FL/FL	N

END - TOTAL LENGTH = 14.7 METERS

SITE: Big Quarry  
 MAPPING PROJECT: Second level from the road  
 LITHOLOGY: Byron; Mudcrack surface  
 SCANLINE DESCRIPTION: 52 degrees

DATE MAPPED: 6/5/99  
 COMPASS DECLINATION: 1 degree  
 MAPPED BY: Anne Ebenreiter

Location (m)	Strike (deg)	Length (m)	Aperture	Termination	Censoring
0.472	306	0.45	F	FP/FP	N
0.639	346	0.99	F	C/FP	Y-1
0.675	352	1.162	O	FP/FP	N
1.24	341	4.16	O	C/C	Y-2
1.504	11	0.272	F	FP/FP	N
2.79	248	0.922	F	FL/FP	N
3.4	174	1.658	V	C/FP	Y-1
3.56	342	1.08	V	R/C	Y-1
4.5	344	0.71	F	R/R	N
4.6	339	1.16	V	R/FP	N
5.396	340	3.31	O	FP/C	Y-1
6.13	338	1.945	O	FP/FP	N
8.425	346	1.96	V-O	R/R	N
9.54	343	2	V	R/FP	N
12.38	337	2.68	F	R/R	N
12.795	294	2.52	F	FP/FL	N
13.52	335	0.6	F	R/R	N
14.79	337	0.615	F	FP/R	N
15.08	341	1.95	F	R/R	N
15.124	343	4.48	F	FL/R	N
15.9	348	1.34	F	FP/R	N
16.502	344	0.67	F	R/FP	N
17.642	346	1.34	F	R/R	N
17.835	345	1.544	F	R/R	N
17.96	345	2.74	V	R/FP	N
20.49	340	0.55	F	FP/R	N
21.19	344	1	F	R/R	N
21.58	285	0.22	F	FL/FL	N
21.63	283	1.41	F	FL/FP	N
22.06	348	1.78	V	FP/R	N
22.415	340	1.4	F	R/R	N
23.75	337	0.445	F	FP/R	N
24.58	348	2.95	V	FP/R	N
25.83	276	1.49	F	FP/FP	N
28.41	353	3.35	V	FL/R	N
26.63	338	0.45	F	FP/FP	N
27.12	14	1.245	F	R/R	N
29.14	66	1.2	O	C/C	Y-2
31.29	278	1.32	V	C/C	Y-2
31.39	285	0.84	V	C/C	Y-2
32.36	357	1	F	R/FP	N
32.69	278	0.733	F	FP/FP	N
34.99	46	7	V	C/C	Y-2
35.052	342	1.77	V	R/C	Y-1
35.46	44	3.4	V	R/C	Y-1

TOTAL LENGTH = 39.3 METERS

SITE: Big Quarry  
MAPPING PROJECT: 2nd level Scanline #2  
LITHOLOGY: Byron; Mudcracks  
SCANLINE DESCRIPTION: 52 degrees

DATE MAPPED: 6/5/99  
COMPASS DECLINATION: 1 degree  
MAPPED BY: Anne Ebenreiter

Location (m)	Strike (deg)	Length (m)	Aperture	Termination	Censoring	THIS LINE IS
3.21	15	1.456	F	S/FP	N	
4.15	343	0.715	F	C/FL	Y-1	
4.398	337	1.04	V	R/R	N	
6.15	331	0.43	F	R/R	N	
7.546	342	4.41	F	FL/R	N	
9.82	342	2.35	O	C/C	Y-2	

TOTAL LENGTH = 10 METERS

SITE: Big Quarry  
 MAPPING PROJECT: 2nd level from the road  
 LITHOLOGY: Byron  
 SCANLINE DESCRIPTION: 340 degrees

DATE MAPPED: 6/5/99  
 COMPASS DECLINATION: 1 degree  
 MAPPED BY: Anne Ebenreiter

Location (m)	Strike (deg)	Length (m)	Aperture	Termination	Censoring
0.28	59	0.38	F	FP/C	Y-1
0.49	57	1.69	O	R/FP	N
0.545	51	3.21	O	FP/R	N
2.182	60	4.7	V	R/FL	N
3.158	61	1.59	F	R/R	N
4.09	63	0.74	V	R/FL	N
4.222	81	0.378	F	R/FL	N
4.438	78	1.15	V	R/FL	N
5.493	49	0.78	F	FP/R	N
6.48	45	3.38	O	FL/C	Y-1
6.66	44	0.6	V	FL/R	N
6.848	43	11.79	V	C/C	Y-2
7.968	52	0.144	F	R/R	N
8.044	50	0.374	F	R/FL	N
8.22	48	1.89	V	R/C	Y-1
8.744	90	0.25	F	FP/FL	N
9.09	9	2.23	V	FP/C	Y-1
9.26	282	1.08	V	FP/C	Y-1
11.848	48	0.49	F	R/R	N
12.96	53	0.45	F	FP/R	N
13.19	55	4.16	V-0	R/R	N
13.23	79	2.84	O	FL/FL	N
13.63	63	0.812	F	R/FP	N
14.06	70	0.658	V	R/FP	N
15.37	110	0.812	F	R/FP	N
16.81	63	3.11	V	FP/R	N
17.355	90	1.535	V	S/FL	N
17.9	3	0.423	F	R/R	N
18.62	43	4.74	V	S/FP	N
19.042	46	1.2	F	FP/R	N
20.39	46	11.7	O	C/C	Y-2
21.64	56	1.74	V	S/C	Y-1

END - TOTAL LENGTH IS 22 METERS

SITE: Big Quarry  
MAPPING PROJECT: 2nd level from the road  
LITHOLOGY: Byron  
SCANLINE DESCRIPTION: 340 degrees, #2

DATE MAPPED: 6/5/99  
COMPASS DECLINATION: 1 degree  
MAPPED BY: Anne Ebenreiter

Location (m)	Strike (deg)	Length (m)	Aperture	Termination	Censoring
0.28	101	0.91	V	FP/C	Y-1
0.788	59	1.68	V	R/S	N
1.35	49	0.71	F	R/S	N
2.236	47	5.82	O	FL/R	N
3.63	51	1.44	V	C/R	Y-1
7.75	57	0.43	F	R/R	N
8.88	56	0.72	F	R/R	N

END - TOTAL LENGTH 10 METERS

SITE: Big Quarry  
MAPPING PROJECT: 2nd level from the road  
LITHOLOGY: Byron  
SCANLINE DESCRIPTION: 340 degrees, #3

DATE MAPPED: 6/6/99  
COMPASS DECLINATION: 1 degree  
MAPPED BY: Anne Ebenreiter

Location (m)	Strike (deg)	Length (m)	Aperture	Termination	Censoring
0.748	46	4.09	O	FP/R	N
1.566	42	0.79	V	FP/FP	N
1.9	52	0.34	F	FP/R	N
2.61	352	5.45	O	R/R	N
3.85	74	0.51	F	R/FP	N
3.902	59	0.534	F	S/FP	N
4.096	51	0.625	F	FL/FP	N
4.556	61	0.318	F	S/R	N
4.94	72	0.282	F	R/R	N
4.978	75	1.65	O	FL/FP	N
5.06	64	0.43	F	FL/FP	N

END TOTAL LENGTH = 5.1 METERS

SITE: Big Quarry  
 MAPPING PROJECT: 3rd level  
 LITHOLOGY: Byron  
 SCANLINE DESCRIPTION: 44 degrees  
 NOTE: Measured from the quarry wall

DATE MAPPED: 6/8/99  
 COMPASS DECLINATION: 1 degree  
 MAPPED BY: Anne Ebenreiter

Location (m)	Strike (deg)	Length (m)	Aperture	Termination	Censoring
0.54	283	0.48	V	FP/S	N
0.62	352	0.93	V	FP/FP	N
0.966	344	0.24	F	R/FP	N
1.27	324	0.59	F	FP/FP	N
1.634	340	2.1	O	FP/A	Y-1
1.85	345	0.84	V	FP/FP	N
2.265	318	0.8	O	C/FP	Y-1
2.315	344	0.63	O	FP/FL	N
2.67	346	1.4	O	FP/A	Y-1
3.004	342	0.54	F	FL/S	N
3.18	311	1.158	O	FP/FP	N
3.715	280	0.66	V	FP/FP	N
3.945	348	1.47	O	FP/S	N
4.598	346	1.23	V	FP/FP	N
5.33	345	3.63	O	R/C	Y-1

END - TOTAL LENGTH = 6.3 METERS

SITE: Big Quarry  
 MAPPING PROJECT: 3rd level from the road  
 LITHOLOGY: Byron  
 SCANLINE DESCRIPTION: 49 degrees

DATE MAPPED: 6/8/99  
 COMPASS DECLINATION: 1 degree  
 MAPPED BY: Anne Ebenreiter

NOTE: Scanline from the edge of the quarry wall running from east to west

Location (m)	Strike (deg)	Length (m)	Aperture	Termination	Censoring
0.5	343	0.53	O	FP/FP	N
1.09	348	1.118	V-O	FP/FP	N
1.22	357	0.51	O	FP/FL	N
1.57	330	0.41	F	FP/FP	N
2.21	338	0.24	F	FP/FP	N
2.76	342	4.72	O	S/S	N
3.238	335	0.77	V	FP/FP	N
3.76	342	3	V	C/C	Y-2
4.66	339	0.94	V	C/C	Y-2
4.91	342	0.465	V	FP/R	N

END - TOTAL LENGTH = 5.5 METERS

SITE: Big Quarry  
MAPPING PROJECT: 3rd level  
LITHOLOGY: Byron  
SCANLINE DESCRIPTION: 51 degrees  
NOTE: Not measured from the quarry wall

DATE MAPPED: 6/9/99  
COMPASS DECLINATION: 1 degree  
MAPPED BY: Anne Ebenreiter

Location (m)	Strike (deg)	Length (m)	Aperture	Termination	Censoring
0.44	351	1.375	V	FP/FP	N
1.278	294	1.13	V	S/C	Y-1
1.765	354	0.57	F	S/C	Y-1
1.855	346	0.95	V	R/C	Y-1
2.05	345	0.775	F	FP/R	N
2.18	4	1.26	O	FP/C	Y-1
2.524	11	1.14	F	S/FP	N
2.675	339	2.1	V	FP/R	N
4.22	280	1.29	V	FP/FP	N
4.355	266	0.69	F	FL/FL	N
4.59	334	1.57	F	FP/R	N
5.046	339	5.74	V	FP/R	N
5.295	344	0.76	F	FP/R	N
5.652	341	0.455	F	FP/R	N
5.712	343	0.43	F	FP/FP	N
5.83	337	0.822	F	FP/FP	N
6.24	334	1.16	F	R/FP	N
6.68	320	0.808	F	S/FL	N
7.055	333	2.09	V	S/FP	N
8.44	338	3.82	V-O	FP/S	N
10.2	334	0.42	F	FP/R	N
10.622	340	1.72	V	FP/FP	N
11.688	319	0.35	V	FP/FP	N
11.735	272	1.33	O	FP/FL	N
12.01	341	0.765	F	R/FP	N

END - TOTAL LENGTH = 12.1 METERS

SITE: Big Quarry  
 MAPPING PROJECT: 3rd level  
 LITHOLOGY: Byron  
 SCANLINE DESCRIPTION: 311 degrees

DATE MAPPED: 6/6/99  
 COMPASS DECLINATION: 1 degree  
 MAPPED BY: Anne Ebenreiter

Location (m)	Strike (deg)	Length (m)	Aperture	Termination	Censoring
1.59	43	1.845	O	FP/FP	N
2.45	346	4.79	O	FP/C	Y-1
2.64	346	0.75	F	FP/FP	N
3.177	46	0.635	V	FP/R	N
3.238	44	1.635	V	FP/FP	N
3.334	44	1.735	F	FP/FP	N
4.652	46	0.88	F	R/R	N
5.178	45	1.25	V	R/C	Y-1

END - TOTAL LENGTH = 5.2 METERS

SITE: Big Quarry  
 MAPPING PROJECT: 3rd level from the road  
 LITHOLOGY: Byron  
 SCANLINE DESCRIPTION: 340 degrees

DATE MAPPED: 6/6/99  
 COMPASS DECLINATION: 1 degree  
 MAPPED BY: Anne Ebenreiter

NOTE: Overall, the third level is much more weathered; therefore it is hard to see some of the faint f

Location (m)	Strike (deg)	Length (m)	Aperture	Termination	Censoring
0.554	63	0.36	F	C/FP	Y-1
1.288	45	0.86	F	C/FP	Y-1
2.07	102	1.03	V	B/FP	Y-1
2.202	69	0.484	F	FP/FL	N
2.795	47	0.668	V	B/FP	Y-1
2.82	43	1.24	V	B/C	Y-2
3.035	52	1.095	F	C/FP	Y-1
3.615	81	0.735	V	C/C	Y-2
4.28	46	3.57	V	R/C	Y-1
4.396	43	1.444	F	FL/FP	N
6.352	304	0.71	F	FP/C	Y-1
6.702	48	3.54	O	C/C	Y-2
6.996	59	0.59	F	R/R	N
7.016	54	0.35	F	R/R	N
7.64	44	2.236	V	C/FP	Y-1
7.782	67	0.693	F	R/FP	N
8.068	62	0.755	F	R/FP	N
8.79	44	1.58	O	C/C	Y-2
9.86	53	0.27	F	FP/C	Y-1
10.04	47	0.34	F	R/R	N
10.876	49	2.61	V	C/FP	Y-1
12.274	48	2.68	V	FP/R	N
12.358	46	1.93	F-V	R/C	Y-1
12.432	47	0.64	F	R/FP	N
12.525	78	3.325	V	FP/FP	N
13.565	73	1.89	O	FP/C	Y-1
13.665	109	0.74	V	FP/FL	N
13.684	65	0.525	V	FL/FL	N
14.165	43	3.26	V	R/FP	N
17.925	43	1.04	F	C/FP	Y-1
19.128	44	2.36	F	FP/R	N
19.445	44	3.75	V	C/R	Y-1
19.565	37	1.71	F	FL/R	N

END - TOTAL LENGTH = 22.2 METERS

SITE: Big Quarry  
MAPPING PROJECT: 3rd level  
Byron  
SCANLINE DESCRIPTION: 340 degrees

DATE MAPPED: 6/6/99  
COMPASS DECLINATION:  
MAPPED BY: Anne Ebenre

Location (m)	Strike (deg)	Length (m)	Aperture	Termination	Censoring
0.1	22	1.18	O	C/FP	Y-1
0.35	14	0.48	F	FP/S	N
1.745	90	0.28	F	C/C	Y-2
2.12	71	1.02	V	FP/FP	N
2.532	48	2.25	V	R/R	N
3.312	43	0.98	F	C/C	Y-2
3.86	48	1.55	O	FP/FP	N
4.55	63	2.32	F	FP/S	N
5.29	52	0.29	V	S/B	N

END - TOTAL LENGTH = 5.3 METERS

SITE: Big Quarry

DATE MAPPED: 6/9/99

MAPPING PROJECT: 2nd level - Horizontal core simula

COMPASS DECLINATION: 1 degree

LITHOLOGY: Byron; Mudcracks

MAPPED BY: Anne Ebenreiter

SCANLINE DESCRIPTION: 55 degrees

Wall is trending 340 degrees

Location (m)	Strike (deg)	Length (m)	Aperture	Termination	Censoring
0.33	322	0.24	F	R/R	N
0.404	308	0.16	F	R/FP	N
0.554	349	1.26	V	FP/R	N
1.2	319	0.42	V	R/FP	N
1.228	311	0.512	V	FP/FL	N
2.278	301	1.62	V	FP/R	N
3.052	344	1.16	F	R/R	N
3.276	346	4.1	V	C/R	Y-1
3.41	341	3.3	O	C/R	Y-1
3.49	343	3.6	O	C/C	Y-2
3.9	343	0.77	F	R/R	N
4.4	346	2.32	V	FP/R	N
4.61	345	2.645	V	FP/FP	N
5.835	261	0.48	O	FP/S	N
6.08	340	10.3	O	FP/FL	N
6.715	271	2.765	O	FL/FP	N
6.835	282	2.49	O	FL/FP	N
7.312	345	0.53	F	R/FP	N
8.13	341	2.63	O	FP/FP	N
8.355	347	1.27	V	FP/FP	N
9.302	345	0.98	O	S/C	Y-1
9.41	346	3.46	V	R/C	Y-1
9.66	352	0.74	F	FL/FP	N
9.835	345	4.96	O	R/FP	N

TOTAL LENGTH = 10 METERS

SITE: Big Quarry

DATE MAPPED: 6/9/99

MAPPING PROJECT: 2nd level, 2nd horz. Core simulati

COMPASS DECLINATION: 1 degree

LITHOLOGY: Byron, Mudcrack Facies

MAPPED BY: Anne Ebenreiter

SCANLINE DESCRIPTION: 59 degrees

Location (m)	Strike (deg)	Length (m)	Aperture	Termination	Censoring
0.565	336	2.245	O	FL/FP	N
0.95	331	4	V	FP/B	N
1.96	333	2.94	O	FL/C	Y-1
2.44	336	1.8	O	C/S	Y-1
2.932	345	0.22	F	R/R	N
3.734	316	1.81	O	S/FP	N
4.165	272	0.95	V	FP/FL	N
4.4	343	4.24	O	FP/R	N
5.15	298	1.12	F	R/FL	N
5.57	339	1.85	O	FP/FP	N
6.27	282	2.12	V	FL/C	Y-1
6.59	299	3.6	O	FP/C	Y-1
7.582	304	1.98	V	FP/FL	N
7.64	339	2.6	O	FP/C	Y-1
8.756	338	6.5	O	S/C	Y-1

END - TOTAL LENGTH IS 10 METERS

SITE: Cave Point Road Quarry  
MAPPING PROJECT: Western pavement  
LITHOLOGY: Engadine  
SCANLINE DESCRIPTION: 62 degrees

DATE MAPPED: 6/10/99  
COMPASS DECLINATION: 1 degree  
MAPPED BY: Anne Ebenreiter

Location (m)	Strike (deg)	Length (m)	Aperture	Termination	Censoring
0.5	286	0.95	F	R/R	N
1.325	347	0.945	F	R/FP	N
2.18	337	8.82	O	C/S	Y-1
2.67	339	2.49	V	C/R	Y-1
3.18	4	0.91	F	R/R	N

END - TOTAL LENGTH 3.5 METERS

SITE: Cave Point Road quarry  
MAPPING PROJECT: Northern pavement  
LITHOLOGY: Engadine???  
SCANLINE DESCRIPTION: 76 degrees

DATE MAPPED: 6/10/99  
COMPASS DECLINATION: 1 degree  
MAPPED BY: Anne Ebenreiter

Location (m)	Strike (deg)	Length (m)	Aperture	Termination	Censoring
1.09	340	3.19	O	C/S	Y-1
1.27	332	2.46	V	C/SL	Y-2
4.46	337	5.23	V	FP/R	N
5.05	342	6.49	V	C/R	Y-1
5.21	346	0.515	F	S/FL	N
5.955	2	0.55	F	B?/R	Y-1
7.732	334	3.53	V	C/R	Y-1
10.55	341	3.59	O	FP/S	N
11.882	346	2.41	V	FP/FP	N
13.465	319	0.58	V	FP/R	N
14.49	342	3.89	O	C/S	Y-1
14.61	338	3.1	V	FL/C	Y-1

END - TOTAL LENGTH 15.56 METERS

SITE: Cave Point Road Quarry  
MAPPING PROJECT: Southern pavement  
LITHOLOGY: Engadine  
SCANLINE DESCRIPTION: 76 degrees

DATE MAPPED: 6/10/99  
COMPASS DECLINATION: 1 degree  
MAPPED BY: Anne Ebenreiter

NOTE: poor pavement and rather grown over. Mapped fractures by vegetation patterns. Also, very lichen covered, so many faint fractures are probably missed.

Location (m)	Strike (deg)	Length (m)	Aperture	Termination	Censoring
0.1	343	5.05	O	A/C	Y-2
1.69	349	0.45	V	FP/FP	N
1.81	345	1.47	V	C/C	Y-2
5.1	337	4.35	O	A/C	Y-2
7.85	344	6.9	O	A/C	Y-2
8.885	354	0.32	V	R/R	N

END - TOTAL LENGTH 10 METERS

SITE: Cave Point Road Quarry  
 MAPPING PROJECT: Southern Pavement  
 LITHOLOGY: Engadine  
 SCANLINE DESCRIPTION: ~345 degrees (forgot to measure. Sorry.)  
 NOTE: see note on other Southern pavement sheet

DATE MAPPED: 6/10/99  
 COMPASS DECLINATION: 1 degree  
 MAPPED BY: Anne Ebenreiter

Location (m)	Strike (deg)	Length (m)	Aperture	Termination	Censoring
0.25	68	9.4	O	C/C	Y-2
0.64	59	1.2	V	FP/FP	N
0.83	66	3.7	O	C/C	Y-2
1.17	71	0.57	V	FP/FP	N
2.05	84	2.53	V	FP/C	Y-1
2.48	73	0.75	F	FP/R	N
3.45	76	6.5	O	FP/FL	N

END - TOTAL LENGTH 5.1 METERS

SITE: Cave Point Road Quarry  
 MAPPING PROJECT: Northern Pavement  
 LITHOLOGY: Engadine?  
 SCANLINE DESCRIPTION: 355 degrees

DATE MAPPED: 6/10/99  
 COMPASS DECLINATION: 1 degree  
 MAPPED BY: Anne Ebenreiter

Location (m)	Strike (deg)	Length (m)	Aperture	Termination	Censoring
1.68	88	13.4	O	C/C	Y-2
1.75	90	1.45	V	FL/FL	N
2.62	235	1.16	V	FP/R	N
2.95	338	0.75	V	R/R	N
3.31	94	0.22	V	FP/FP	N
3.69	342	5.32	V	FP/R	N
4.92	70	1.7	O	FP/S	N
5.75	75	3.58	V	S/S	N
7.9	340	2.74	V	R/R	N
8.1	79	12.4	O	C/C	Y-2
8.5	78	1.52	V	FP/R	N
8.755	83	1.31	V	FP/FP	N

END - TOTAL LENGTH 9.5 METERS

SITE: Cave Point Road Quarry  
 MAPPING PROJECT: Western pavement  
 LITHOLOGY: Engadine?  
 SCANLINE DESCRIPTION: 358 degrees

DATE MAPPED: 6/10/99  
 COMPASS DECLINATION: 1 degree  
 MAPPED BY: Anne Ebenreiter

Location (m)	Strike (deg)	Length (m)	Aperture	Termination	Censoring
0.83	71	0.74	V	R/C	Y-1
3.74	82	9.8	O	C/A	Y-2
4.09	85	2.12	V	R/R	N
6.35	81	7.4	O	C/A	Y-2

END - TOTAL LENGTH 6.8 METERS

SITE: Cave Point County park  
MAPPING PROJECT: Rocky Shoreline  
LITHOLOGY:

SCANLINE DESCRIPTION: 330degrees

\* No other fractures of any other orientation seen

DATE MAPPED: 6//99

COMPASS DECLINATION: 1 degree

MAPPED BY: Anne Ebenreiter

Location (m)	Strike (deg)	Length (m)	Aperture	Termination	Censoring
2.6	65	>20 meters	v	C/W	Y-2
8.9	43	>20	v	C/W	Y-2
13	72	>20	v	C/W	Y-2

End - total length ~15 meters (ended in the water)

SITE: First Ln/ Hwy 57  
MAPPING PROJECT: massive dolomite/ small paveme  
LITHOLOGY:  
SCANLINE DESCRIPTION: 74 degrees

DATE MAPPED: 6/12/99  
COMPASS DECLINATION: 1 degree  
MAPPED BY: Anne Ebenreiter

Location (m)	Strike (deg)	Length (m)	Aperture	Termination	Censoring
3.86	342	1.63	F	R/R	N
8.7	344	9.6	O	C/FP	Y-1
13.29	342	0.71	F	R/R	N

END - TOTAL LENGTH IS 17.5 METERS

SITE: First Ln/ hwy 57  
MAPPING PROJECT: small pavement  
LITHOLOGY: massive dolomite  
SCANLINE DESCRIPTION: 338 degrees

DATE MAPPED: 6/12/99  
COMPASS DECLINATION: 1 degree  
MAPPED BY: Anne Ebenreiter

Location (m)	Strike (deg)	Length (m)	Aperture	Termination	Censoring
2.34	66	5.43	V	R/R	N
4.69	61	2	V	C/R	Y-1
5.95	74	4.56	V	FP/R	N
8.29	76	0.42	F	R/R	N
9.95	70	7.4	O	C/C	Y-2

END - TOTAL LENGTH 10 METERS

SITE: Garrett Bay Rd Quarry  
MAPPING PROJECT: mossy pavement in the woods  
LITHOLOGY: mud cracks?  
SCANLINE DESCRIPTION: 73 degrees

DATE MAPPED: 6/16/99  
COMPASS DECLINATION: 1 degree  
MAPPED BY: Anne Ebenreiter

Location (m)	Strike (deg)	Length (m)	Aperture	Termination	Censoring
0.46	342	2.1	F	FP/FP	N
0.77	349	0.25	F	R/R	N
1.8	6	2.9	V	FP/C	Y-1
2.95	301	4.2	V	FP/S	N
3.1	336	0.8	F	FP/FP	N
3.27	329	1.1	V	C/FP	Y-1
5.265	343	1.1	F	S/FP	N
5.81	347	4.1	V	C/C	Y-2
7.93	328	1.8	V	R/FP	N

END TOTAL LENGTH IS 9 METERS

SITE: Garrett Bay Rd  
MAPPING PROJECT: Mossy pavement  
LITHOLOGY: mud cracks  
SCANLINE DESCRIPTION: 325 degrees

DATE MAPPED: 6//99  
COMPASS DECLINATION: 1 degree  
MAPPED BY: Anne Ebenreiter

NOTE: Moss covers much of the pavement, so some fractures may be missed.  
Some fractures are mapped by vegetation

Location (m)	Strike (deg)	Length (m)	Aperture	Termination	Censoring
1.6	59	14.9	O	C/C	Y-2
2.85	69	2.6	F	C/S	Y-1
4.85	91	4.7	F	C/C	Y-2
5.75	67	7.9	V	C/C	Y-2
6	76	12.9	V	FL/C	Y-1

END TOTAL LENGTH IS 7 METERS

SITE: Gibson Lane/ Beautiful Lake  
MAPPING PROJECT: In back of house  
LITHOLOGY:

DATE MAPPED: 6/12/99  
COMPASS DECLINATION: 1 degree  
MAPPED BY: Anne Ebenreiter

SCANLINE DESCRIPTION: 69 degrees  
Note: virtually all fractures were mapped by vegetation patterns

Location (m)	Strike (deg)	Length (m)	Aperture	Termination	Censoring
1.1	346		10 V	FP/A	Y-1
14.8	331	20.1	O	A/R	Y-1

End - TOTAL LENGTH IS 24 METERS

SITE: Gibson Lane/Beautiful Lake  
MAPPING PROJECT: Playground  
LITHOLOGY:

DATE MAPPED: 6/12/99  
COMPASS DECLINATION: 1 degree  
MAPPED BY: Anne Ebenreiter

SCANLINE DESCRIPTION: 80 degrees

Location (m)	Strike (deg)	Length (m)	Aperture	Termination	Censoring
5.3	353		4.3 O	FP/FP	N
8.13	355		5 O	FP/FP	N

END - TOTAL LENGTH 10 METERS

SITE: Gibson Lane/Beautiful Lake  
MAPPING PROJECT: W side of quarry  
LITHOLOGY:

DATE MAPPED: 6/12/99  
COMPASS DECLINATION: 1 degree  
MAPPED BY: Anne Ebenreiter

SCANLINE DESCRIPTION: 85 degrees

Location (m)	Strike (deg)	Length (m)	Aperture	Termination	Censoring
2.39	310		1.75 F	R/R	N
6.27	17		6.2 F	FP/C	Y-1
7.6	12		10.2 O	C/C	Y-2
14.93			4.7 V	C/C	Y-1

End - TOTAL LENGTH 17 METERS

SITE: Gibson Ln/Beautiful Lake  
MAPPING PROJECT: in front of house  
LITHOLOGY:

DATE MAPPED: 6/12/99  
COMPASS DECLINATION: 1 degree  
MAPPED BY: Anne Ebenreiter

SCANLINE DESCRIPTION: 339 degrees

Note: All fractures are mapped by vegetation patterns

Location (m)	Strike (deg)	Length (m)	Aperture	Termination	Censoring
2.92	68		2.34 V	R/FP	N
4.5	76		30 O	A/C	Y-2
15.65	74		21.9 O	C/C	Y-2
18.5	100		28.3 O	A/C	Y-2
22	95		18.4 O	C/C	Y-2

END TOTAL LENGTH = 22.4 METERS

SITE: Gibson Lane/ Beautiful Lake  
MAPPING PROJECT: Playground  
LITHOLOGY:

DATE MAPPED: 6/12/99  
COMPASS DECLINATION: 1 degree  
MAPPED BY: Anne Ebenreiter

SCANLINE DESCRIPTION: 348 degrees

NOTE: All O fractures are mapped by vegetation patterns

Location (m)	Strike (deg)	Length (m)	Aperture	Termination	Censoring
3.5	89		18.5 O	A/FL	Y-1
8.7	86		21.3 O	A/C	Y-2

END TOTAL LENGTH 12 METERS

SITE: Gibson Lane/ Beautiful Lake  
MAPPING PROJECT: West end of quarry  
LITHOLOGY:  
SCANLINE DESCRIPTION: 358 degrees

DATE MAPPED: 6/12/99  
COMPASS DECLINATION: 1 degree  
MAPPED BY: Anne Ebenreiter

Location (m)	Strike (deg)	Length (m)	Aperture	Termination	Censoring
4.81	105	7.58	V	A/FL	Y-1
10.17	91	7.1	V	FP/C	Y-1
11.58	91	9.7	O	A/C	Y-2
12.74	90	6.4	O	S/C	Y-1
14.57	315	3.38	O	R/FP	N

END - TOTAL LENGTH IS 16 METERS

SITE: HWY 42/ N of Carlsville  
 MAPPING PROJECT:  
 LITHOLOGY: Near Hendrix  
 SCANLINE DESCRIPTION: degrees

DATE MAPPED: 6/16/99  
 COMPASS DECLINATION: 1 degree  
 MAPPED BY: Anne Ebenreiter

Location (m)	Strike (deg)	Length (m)	Aperture	Termination	Censoring
0.7	71	1.95	O	FP/FP	N
1.05	51	1.4	O	FP/FL	N
1.63	46	1.05	V	FL/R	N
2.15	48	1.1	V	FP/S	N
2.8	291	5.3	V	FP/FP	N
3.73	60	3.95	V	FP/FL	N
4.12	42	7.4	V	FP/R	N
4.69	66	1.55	V	R/FL	N
4.84	78	2.35	V	R/FP	N
5.71	43	0.95	F	R/R	N
5.9	74	14.2	O	FP/C	Y-1
6.8	39	2.4	F	R/S	N
8.05	45	7.1	P	FP/R	N
9.18	13	1.4	F	R/FP	N
9.66	62	6.65	V	FP/FL	N

END - TOTAL LENGTH IS 10 METERS

SITE: HWY 42/ N of Carlsville  
 MAPPING PROJECT: Landscaping quarry  
 LITHOLOGY: near hendrix  
 SCANLINE DESCRIPTION: 66 degrees

DATE MAPPED: 6/16/99  
 COMPASS DECLINATION: 1 degree  
 MAPPED BY: Anne Ebenreiter

Location (m)	Strike (deg)	Length (m)	Aperture	Termination	Censoring
0.48	349	0.85	V	FP/FP	N
0.55	346	2.2	V	FP/FP	N
1	52	0.6	F	FP/R	N
1.82	302	1.35	V	R/FL	N
3.4	343	3.25	F	FP/FP	N
4.23	340	2.23	F	FP/FP	N
4.63	33	2.05	V	FL/FL	N
4.7	341	2.31	V	FP/FP	N
7.9	356	11.5	O	FP/C	Y-1
9.01	275	3.6	O	FL/FL	N
9.79	283	1.55	V	FP/FP	N
10.55	298	5.2	O	FP/C	Y-1
11.35	38	0.85	V	FP/FP	N

END - TOTAL LENGTH 11.5 METERS

SITE: Kisser South  
 MAPPING PROJECT:  
 LITHOLOGY: Coral bed above laminites  
 SCANLINE DESCRIPTION: 70 degrees

DATE MAPPED: 6/17/99  
 COMPASS DECLINATION: 1 degree  
 MAPPED BY: Anne Ebenreiter + Toni

Location (m)	Strike (deg)	Length (m)	Aperture	Termination	Censoring
1.64	337	2.3	O	S/R	N
2.83	341	8.3	O	R/R	N
3.04	6	2.5	O	R/FP	N
4.95	16	5.04	O	R/FP	N
5.1	329	0.45	V-F	R/FL	N
5.18	326	0.23	V-F	R/FL	N
5.48	332	0.44	F	R/R	N
5.58	322	0.25	F	R/R	N
5.72	323	0.12	F	R/R	N
5.78	322	0.23	F	R/R	N
6.02	334	1.3	V	S/R	N
6.09	335	0.63	V	R/R	N
6.12	341	0.26	F	R/R	N
6.9	56	1.63	V	R/R	N
7.1	340	0.11	F	FP/R	N
7.19	338	0.13	F	R/R	N
7.44	334	2.67	O	FP/FL	N
9.44	336	3.85	O	R/FP	N
9.62	338	1.65	O	S/FL	N
10.84	337	0.43	F	R/R	N
11.45	332	0.18	F	R/R	N
11.9	339	9.7	O	C/FP	Y-1
12	358	2.6	O	FL/R	N
12.5	324	0.16	F	R/R	N
12.5	224	0.3	F	R/R	N

END - TOTAL LENGTH IS 13 METERS

SITE: Kisser South  
 MAPPING PROJECT: coral bed above laminites  
 LITHOLOGY:  
 SCANLINE DESCRIPTION: 337 degrees

DATE MAPPED: 6/17/99  
 COMPASS DECLINATION: 1 degree  
 MAPPED BY: Anne Ebenreiter

Location (m)	Strike (deg)	Length (m)	Aperture	Termination	Censoring
0.27	58	2.8	O	FP/FP	N
0.35	104	0.58	V	FP/FL	N
0.71	100	2.25	V	FP/FP	N
2.23	250	1.8	O	FL/FP	N
2.6	250	3.9	O	FP/FP	N
5.6	249	8.6	O	C/FP	Y-1
6.34	243	1.4	V	FP/R	N
6.37	239	2.13	V	S/S	N
8.7	67	1.05	O	FP/R	N
9.22	116	1.85	V	S/R	N
10.5	227	8.1	O	R/C	Y-1
12.09	290	2.05	V	FP/FP	N
12.59	241	3.7	O	R/C	Y-1
13.7	240	7.3	O	C/FP	Y-1

END TOTAL LENGTH 13.9 METERS

SITE: Lily Bay Rd Quarry  
 MAPPING PROJECT: pavement above Quarry  
 LITHOLOGY: Coral facies  
 SCANLINE DESCRIPTION: 64 degrees

DATE MAPPED: 6/12/99  
 COMPASS DECLINATION: 1 degree  
 MAPPED BY: Anne Ebenreiter

Location (m)	Strike (deg)	Length (m)	Aperture	Termination	Censoring
2.035	334	3.45	V	R/FP	N
3.76	330	0.51	F	R/FP	N
4.69	342	0.66	V	FP/FP	N
7.01	82	0.73	O	R/R	N
7.38	337	0.77	F	R/R	N
7.53	340	1.35	F	FP/FP	N
10.015	358	0.79	V	R/S	N

END - TOTAL LENGTH 11 METERS

NOTE: I scouted the rest of the pavement for more N-S fractures, but none were found. The upper surface (the southern half) is completely void of them. There were more E-W fractures to be measured, but many were probably ones that I had already measured

SITE: Lily Bay Road Quarry  
 MAPPING PROJECT: Pavement above quarry (E)  
 LITHOLOGY: Coral facies  
 SCANLINE DESCRIPTION: 338 degrees

DATE MAPPED: 6/12/99  
 COMPASS DECLINATION: 1 degree  
 MAPPED BY: Anne Ebenreiter

NOTE: More E-W fractures, BUT...no N-S, se note on Lily Bay 64 degrees

Location (m)	Strike (deg)	Length (m)	Aperture	Termination	Censoring
1.13	67	9.56	V	C/C	Y-2
2.14	74	1.36	V	S/R	N
2.5	66	1.77	O	R/R	N
2.81	76	2.07	V	R/R	N
3.43	71	9.17	O	R/C	Y-1
3.92	70	6.5	O	C/R	Y-1
4.33	74	2.66	V	FL/R	N
4.59	68	1.61	V	R/FL	N
4.79	45	3.31	V	S/FL	N
4.85	59	0.63	F	R/FL	N
6.15	76	6.2	O	C/R	Y-1
6.84	68	31.2	O	C/C	Y-2
7.57	76	0.92	V	FL/FL	N
7.63	72	3.76	V	C/FL	Y-1
7.77	76	1.3	V	FP/C	Y-1

END - TOTAL LENGTH 8 METERS

SITE: Little Quarry  
 MAPPING PROJECT: pavement on North half  
 LITHOLOGY:  
 SCANLINE DESCRIPTION: 62degrees

DATE MAPPED: 6/10/99  
 COMPASS DECLINATION: 1 degree  
 MAPPED BY: Anne Ebenreiter

Location (m)	Strike (deg)	Length (m)	Aperture	Termination	Censoring
0.615	341	1.24	V	FP/R	N
0.86	268	1.03	V	FL/FP	N
1.94	279	0.5	V	R/FL	N
1.96	45	1.74	V	FL/FP	N
2.67	377	2.42	V	FP/C	Y-1
2.82	11	1.87	V	C/R	Y-1
3.05	333	0.44	F	R/FP	N
3.1	340	0.385	F	FP/FP	N
3.16	335	0.47	F	FL/R	N
3.2	333	1.89	V	FP/FP	N
3.25	335	0.25	F	FP/FL	N
3.28	311	0.18	F	FL/FL	N
3.33	331	0.15	F	R/FP	N
3.45	326	0.35	F	FP/FP	N
3.485	331	0.27	F	FP/FP	N
3.55	11	0.34	F	FL/R	N
3.595	336	1.025	V	FP/FP	N
3.64	330	0.44	F	FP/FL	N
3.75	334	0.21	F	FP/R	N
3.8	337	0.795	O	FP/FP	N
4.41	342	0.54	F	FP/R	N
4.52	328	1.37	V	R/C	Y-1
4.6	353	2.97	V	FP/C	Y-1
4.62	349	4.78	O	FP/C	Y-1
4.77	291	2.44	V	FP/FP	N
5.1	333	1.15	V	FP/FP	N
5.14	335	3.45	V	FP/FL	N
5.65	335	2.91	V	FP/FP	N
6.82	283	1.46	V	FP/FP	N
7.09	336	0.57	F	FP/R	N
7.45	347	0.6	F	R/FP	N
7.73	337	2.05	O	B/FP	Y-1
7.88	333	0.6	F	FP/R	N
8.18	346	2.34	O	FP/FP	N
8.6	337	0.55	V	FP/R	N
9.15	340	0.94	V	FP/FP	N
9.49	334	1.2	V	FP/FP	N
9.97	350	3.96	O	C/R	Y-1
10.1	26	5.02	O	R/R	N
10.8	341	0.52	F	R/FP	N
11.2	341	2.1	V	FP/R	N
11.63	336	1.48	F	R/FL	N
11.74	331	3.68	V	R/FP	N
12.305	41	0.915	F	R/FL	N
12.475	339	3.12	O	R/B	N
13.01	325	0.57	F	FP/FP	N
13.26	323	0.84	F	FP/FL	N
13.4	82	1.77	V	R/R	N
13.53	83	0.51	F	R/FL	N
13.835	338	1.77	V	R/R	N

SITE: Little Quarry  
 MAPPING PROJECT: pavement on N. half  
 LITHOLOGY:  
 SCANLINE DESCRIPTION: 342 degrees

DATE MAPPED: 6/10/99  
 COMPASS DECLINATION: 1 degree  
 MAPPED BY: Anne Ebenreiter

Location (m)	Strike (deg)	Length (m)	Aperture	Termination	Censoring
0.325	71	0.53	V	FP/FP	N
0.47	63	4.16	O	S/S	N
0.495	330	0.735	V	FP/FP	N
0.65	74	0.15	F	FP/FP	N
1.06	66	5.2	V-O	R/FP	N
1.444	93	2.08	V	S/FL	N
1.632	70	0.145	F	FP/R	N
1.7	329	1.64	V	FP/S	N
1.932	327	0.72	F	B/FL	N
1.95	287	0.46	F	B/FP	N
2.425	50	0.8	V	R/C	Y-1
2.455	282	0.27	V	FL/FL	N
2.554	76	1.606	O	FL/FP	N
2.592	78	0.7	V	R/C	Y-1
2.896	77	1.1	V	S/C	Y-1
3.28	332	1.53	V	FP/R	N
3.96	68	3.64	V	C/R	Y-1
4.335	81	2.8	O	C/C	Y-2
4.95	55	1.82	V	C/FP	Y-1
SKIP TO 6 METERS, DUE TO BLAST ZONE					
6.035	56	0.47	F	FL/FP	N
6.07	53	0.64	F	FP/FP	N
6.135	286	0.53	V	FP/S	N
6.315	42	0.88	V	B/S	N
7.81	67	0.45	F	R/FL	N
7.91	74	1.64	O	S/R	N
7.97	73	0.6	F	R/R	N
7.98	71	0.34	F	R/R	N
8.06	93	0.195	F	FP/FL	N
8.09	74	0.39	F	FP/FL	N
8.355	312	1.56	O	R/FP	N
8.454	77	0.76	F	R/FL	N
8.58	63	3.22	V	FP/C	Y-1
8.76	85	0.24	F	FP/FP	N
8.88	89	0.22	F	FP/FP	N
9.102	278	5.9	V	FP/R	N
9.992	285	3.24	V	FP/FP	N
9.992	55	2.62	V	R/R	N
10.57	56	0.77	F	R/FL	N
10.83	275	1.49	F	FL/FL	N
11.11	48	0.65	F	R/R	N
11.17	56	0.9	V	R/R	N
11.39	46	1.07	V	S/FP	N
11.53	49	1.75	O	FL/FP	N
11.75	322	0.41	F	R/FP	N
11.91	326	1.24	V	FP/R	N
12.29	93	0.34	F	R/FL	N
12.4	86	1.1	F	R/FL	N
12.445	94	3.59	V	FP/C	Y-1
12.485	80	1.37	V	FP/FL	N
12.74	74	1.84	V	FP/R	N

SITE: Lower Mathehy Road pavement  
 MAPPING PROJECT: Pavement on W side of road  
 LITHOLOGY: coral facies???  
 SCANLINE DESCRIPTION: 75 degrees  
 NOTE: Most fractures are mapped by vegetation patterns

DATE MAPPED: 6/16/99  
 COMPASS DECLINATION: 1 degree  
 MAPPED BY: Anne Ebenreiter

Location (m)	Strike (deg)	Length (m)	Aperture	Termination	Censoring
1	348	17.2	O	FP/C	Y-1

End total length is 11 meters

SITE: Lower Mathehy Road pavement  
 MAPPING PROJECT: Pavement on W side of road  
 LITHOLOGY: coral facies???  
 SCANLINE DESCRIPTION: 75 degrees  
 NOTE: Most fractures are mapped by vegetation patterns

DATE MAPPED: 6/16/99  
 COMPASS DECLINATION: 1 degree  
 MAPPED BY: Anne Ebenreiter

Location (m)	Strike (deg)	Length (m)	Aperture	Termination	Censoring
6.2	337	15.6	O	R/FP	N
15.05	346	3.9	V	R/FP	N
20.2	343	4.3	F	R/FP	N
23.2	342	0.9	F	R/R	N
25.9	339	22.1	O	R/C	Y-1

END TOTAL LENGTH = 27.5 METERS

SITE: Lower Mathey Rd Surface  
 MAPPING PROJECT: Coral facies???  
 LITHOLOGY:  
 SCANLINE DESCRIPTION: 335 degrees  
 NOTE: Most fractures are mapped by vegetation patterns

DATE MAPPED: 6/16/99  
 COMPASS DECLINATION: 1 degree  
 MAPPED BY: Anne Ebenreiter

Location (m)	Strike (deg)	Length (m)	Aperture	Termination	Censoring
5.85	71	18.4	O	FP/C	Y-1
9.25	74	8.8	O	FL/R	N
11.2	70	4.5	O	FL/FL	N
12.1	68	13.1	O	R/C	Y-1
15.3	66	3.65	O	R/R	N
16.15	58	3.8	O	R/R	N
18.15	69	1.65	V	R/FL	N
21.55	41	0.6	F	R/R	N
24.2	57	12.6	O	R/C	Y-1
28.3	63	7.8	O	R/C	Y-1
31.95	74	6.8	O	R/C	Y-1

END - TOTAL LENGTH 33 METERS

SITE: Newport State Park  
 MAPPING PROJECT: N Shore  
 LITHOLOGY:  
 SCANLINE DESCRIPTION: 77 degrees

DATE MAPPED: 6/17/99  
 COMPASS DECLINATION: 1 degree  
 MAPPED BY: Anne Ebenreiter

Location (m)	Strike (deg)	Length (m)	Aperture	Termination	Censoring
3.19	336	5.1	V	R/A	Y-1
4.32	284	7.3	O	FL/FP	N
4.39	284	7.3	O	FL/FP	N
5.32	332	6.9	O	FP/FP	N
8.47	34	0.24	V	A/FL	Y-1
8.52	33	1.44	V	A/FP	Y-1
9.77	329	4.7	O	S/A	Y-1
10	344	5.15	O	FP/FL	N
10.39	333	0.3	F	R/FP	N
14.9	41	5.75	O	C/FP	Y-1
15.15	338	2.5	O	C/FP	Y-1
15.3	332	4.1	O	C/A	Y-2
15.6	337	0.65	V	FP/C	Y-1
16.7	65	0.6	V	R/R	N
21.71	338	6.45	O	A/C	Y-2
21.77	334	6.45	O	A/C	Y-2
22.4	331	5.05	O	R/C	Y-1

END TOTAL LENGTH 23 METERS

SITE: Newport State Park  
 MAPPING PROJECT: North Shore  
 LITHOLOGY:  
 SCANLINE DESCRIPTION: 331 degrees

DATE MAPPED: 6/17/99  
 COMPASS DECLINATION: 1 degree  
 MAPPED BY: Anne Ebenreiter

Location (m)	Strike (deg)	Length (m)	Aperture	Termination	Censoring
1	61	23	O	FP/C	Y-1
2.44	46	2.5	F	R/FP	N
5.75	95	1.8	O	FL/C	Y-1
5.85	98	1.5	O	FL/C	Y-1
7.15	74	1.25	F-O	FL/FP	N
7.2	44	1.25	O	FP/C	Y-1
7.41	54	5.38	V	FL/C	Y-1
7.47	48	0.6	O	FL/FP	N
7.61	47	2.3	O	FL/A	Y-1
8.33	63	1.2	O	C/C	Y-2
8.9	66	1.6	O	C/R	Y-1
10.05	56	4.9	V	C/FL	Y-1

END TOTAL LENGTH IS 10.5 METERS

SITE: Newport State Park  
 MAPPING PROJECT: North Shore  
 LITHOLOGY:  
 SCANLINE DESCRIPTION: 343 degrees

DATE MAPPED: 6/17/99  
 COMPASS DECLINATION: 1 degree  
 MAPPED BY: Anne Ebenreiter + Toni Simo

Location (m)	Strike (deg)	Length (m)	Aperture	Termination	Censoring
0.11	78	0.6	F	A/A	Y-2
1.26	75	12.2	O	A/FP	Y-1
1.36	73	4.6	O	A/C	Y-2
2.03	80	0.45	V	FL/FL	N
2.13	76	10.6	V	FP/C	Y-1
2.2	51	0.3	F	FL/R	N
2.66	84	8.3	O	C/R	Y-1
2.79	75	1.3	V	FL/FL	N
3.39	72	1.35	V	A/R	Y-1

END TOTAL LENGTH IS 6.2 METERS

SITE: Penninsula Players Rd. Quarry  
 MAPPING PROJECT: Pavement on West half of quarr  
 LITHOLOGY:  
 SCANLINE DESCRIPTION: 74degrees  
 \*See note on Penn. Players Rd. 347 degrees

DATE MAPPED: 6/11/99  
 COMPASS DECLINATION: 1 degree  
 MAPPED BY: Anne Ebenreiter

Location (m)	Strike (deg)	Length (m)	Aperture	Termination	Censoring
2.04	335	1.06	V	FP/R	N
2.49	338	0.57	V	FP/R	N
5.355	346	5.75	V	B/R	Y-1
6.625	341	0.66	F	FP/FL	N
6.945	322	0.55	F	FP/FP	N
7.185	339	7.37	V	FP/R	N
7.23	342	1.1	V	FL/FP	N
12.34	337	5.19	V	FP/FP	N
14.08	341	5.33	F	FP/R	N
14.465	338	0.53	F	FP/FP	N

END - TOTAL LENGTH 15 METERS

SITE: Penninsula Players Rd Quarry  
 MAPPING PROJECT: Pavement on W half of quarry  
 LITHOLOGY:  
 SCANLINE DESCRIPTION: 75 degrees  
 \*See note on Penn. Players 347

DATE MAPPED: 6/75/99  
 COMPASS DECLINATION: 1 degree  
 MAPPED BY: Anne Ebenreiter

Location (m)	Strike (deg)	Length (m)	Aperture	Termination	Censoring
0.36	350	1.85	F	FP/FP	N
1.28	329	0.44	F	R/R	N
1.5	336	1.78	O	FP/FP	N
2.04	343	5.98	V	S/B	Y-1
2.405	341	0.76	V	FP/FP	N
3.355	343	0.565	F	FP/FP	N
3.745	342	5.75	V	FP/FP	N
4.77	340	3.82	V	FP/FP	N

End - TOTAL LENGTH 5 METERS

SITE: Penninsula Players Rd. Quarry  
MAPPING PROJECT: Pavement on W. half of Quarry  
LITHOLOGY:

DATE MAPPED: 6/11/99  
COMPASS DECLINATION: 1 degree  
MAPPED BY: Anne Ebenreiter

SCANLINE DESCRIPTION: 347 degrees

NOTE: This is an extremely poor pavement. There are a ton of blast holes (~every 2 m).  
I tried to map only the original fractures

Location (m)	Strike (deg)	Length (m)	Aperture	Termination	Censoring
0.88	81	1.435	V	C/FP	Y-1
1.74	44	5.72	V	FP/C	Y-1
2.15	75	7.3	O	C/FL	Y-1
2.655	78	1.875	V	C/FP	Y-1
3.33	79	4.9	O	C/B	Y-2
3.89	62	5.55	O	C/FL	Y-1
4.515	75	8.5	V	C/B	Y-2
5.575	75	23.2	O	C/B	Y-2
6.732	78	2.04	V	FL/FL	N
7.15	76	1.27	F	FP/R	N
9.36	84	12.55	O	FP/FL	N
9.52	81	5.29	V	FP/R	N
11.218	61	4.93	V	FL/R	N
11.455	72	4.21	V-O	FP/C	Y-1
11.74	95	2.68	F	FP/FP	N
12.19	89	0.74	F	R/FP	N
12.66	71	0.7	F	R/FP	N
14.95	79	10.43	V	B/R	Y-1
15.704	82	14.91	V	C/FL	Y-1
16.88	76	3.2	O	FP/C	Y-1
17.65	40	12.8	V	C/FP	Y-1

END - TOTAL LENGTH 18.4 METERS

SITE: Button Marsh/ Spring Rd.  
 MAPPING PROJECT: Blue Beds  
 LITHOLOGY:  
 SCANLINE DESCRIPTION: 65 degrees

DATE MAPPED: 6/18/99  
 COMPASS DECLINATION: 1 degree  
 MAPPED BY: Anne Ebenreiter

Location (m)	Strike (deg)	Length (m)	Aperture	Termination	Censoring
0.55	12	1.9	O	FP/FP	N
0.93	341	0.7	O	FP/FP	N
0.98	342	0.43	F	FP/R	N
1.09	268	0.75	V	FP/FP	N
1.35	333	0.4	F	FP/FP	N
1.43	350	2.65	O	FP/A	Y-1
1.34	11	0.8	O	FP/FP	N
1.72	354	0.61	F	FP/FP	N
1.92	340	5.2	O	FP/FP	N
2.03	23	0.25	F	FP/FP	N
2.15	336	6.1	O	C/A	Y-2
2.15	337	0.75	F	R/FL	N
2.45	332	0.27	V	FP/FP	N
2.77	339	0.2	V	FP/FP	N
2.89	332	0.84	O	FP/R	N
3.16	338	9.25	O	FP/FP	N
3.35	334	1.2	O	FP/FP	N
3.49	82	0.95	O	FP/FP	N
3.73	335	0.27	V	FP/FP	N
3.78	34	0.21	V	R/FP	N
4.25	339	0.18	F	FP/FP	N
4.67	342	0.5	V	C/C	Y-2

END TOTAL LENGTH IS 5 METERS

SITE: Spring Road/button Marsh  
 MAPPING PROJECT: Blue Beds  
 LITHOLOGY:  
 SCANLINE DESCRIPTION: 334 degrees

DATE MAPPED: 6/18/99  
 COMPASS DECLINATION: 1 degree  
 MAPPED BY: Anne Ebenreiter

Location (m)	Strike (deg)	Length (m)	Aperture	Termination	Censoring
0.31	65	1.22	V	FP/FP	N
0.39	23	0.6	F	R/FP	N
0.57	59	0.85	V	FP/FP	N
0.6	37	0.85	V	FP/FP	N
0.78	289	1.15	V	FP/FP	N
0.98	70	0.38	V	FP/FP	N
1.11	68	0.95	V	C/FP	Y-1
1.18	73	0.75	V	C/FP	Y-1
1.31	66	0.75	O	FP/C	Y-1
1.45	52	1.15	O	FL/C	Y-1
1.7	58	0.35	F	R/FL	N
1.735	56	0.39	F	R/FL	N
1.76	59	0.35	F	R/FL	N
1.85	32	0.4	O	R/FP	N
1.98	295	0.19	O	FP/FP	N
2.03	64	0.49	O	FP/FL	N
2.11	57	1.61	V	FP/FP	N
2.17	54	2.6	V	FP/C	Y-1
2.38	59	1.18	V	FP/FP	N
2.87	52	1.45	F	FP/R	N
2.89	43	1.05	V	FP/R	N
2.91	50	1.1	V	R/R	N

END TOTAL LENGTH IS 3 METERS

SITE: Toff's Point  
 MAPPING PROJECT: Pavement N. of parking  
 LITHOLOGY:  
 SCANLINE DESCRIPTION: 82 degrees

DATE MAPPED: 6/11/99  
 COMPASS DECLINATION: 1 degree  
 MAPPED BY: Anne Ebenreiter

Location (m)	Strike (deg)	Length (m)	Aperture	Termination	Censoring
2.7	357	2.6	O	C/C	Y-2
3.6	346	4.6	V-O	R/FP	N
4.35	6	0.55	F	FP/FP	N
5.85	339	2.8	O	C/FP	Y-1
6.6	342	1.1	F	FP/FP	N
6.85	347	1.5	V	C/FP	Y-1
9.9	328	3.2	V	FP/R	N
11.45	332	2.7	V	R/FP	N
12.3	340	2.4	V	FP/FP	N
13.25	342	1.1	O	C/FP	Y-1
13.65	332	1.2	V	C/FP	Y-1

END - TOTAL LENGTH IS 15 METERS

SITE: Toff's Point  
 MAPPING PROJECT: Pavement N. of parking area  
 LITHOLOGY:  
 SCANLINE DESCRIPTION: 82 degrees

DATE MAPPED: 6/11/99  
 COMPASS DECLINATION: 1 degree  
 MAPPED BY: Anne Ebenreiter

NOTE: see Note on Toff's Point 338 degrees

Location (m)	Strike (deg)	Length (m)	Aperture	Termination	Censoring
0.4	346	0.95	F	FP/FP	N
3.9	351	3.3	O	FP/R	N
5.5	345	5.8	O	A/FP	Y-1
6.4	332	0.87	F	FP/FP	N
6.85	334	0.81	V	FP/FP	N
9.25	351	4.1	O	FP/FP	N
10.5	337	2.4	O	C/FP	Y-1
14.2	353	2.75	O	FP/C	Y-1
15.05	331	2.65	O	R/FP	N

END TOTAL LENGTH = 16 METERS

SITE: Toff's Point  
 MAPPING PROJECT: Pavement N of parking area  
 LITHOLOGY:  
 SCANLINE DESCRIPTION: 83degrees

DATE MAPPED: 6/11/99  
 COMPASS DECLINATION: 1 degree  
 MAPPED BY: Anne Ebenreiter

\* See note on Toff's point 338 degrees

Location (m)	Strike (deg)	Length (m)	Aperture	Termination	Censoring
1.6	344	0.65	V	R/FP	N
1.85	341	0.8	V	FP/FP	N
5.2	350	8.3	O	A/FP	Y-1
6.05	341	6.2	O	FP/FP	N
7.6	334	4.9	O	FP/FP	N
9.35	334	4.1	V	FP/C	Y-1
9.9	340	3.5	O	A/FP	Y-1
10.5	335	1.15	O	FP/FP	N

END - TOTAL LENGTH = 11.7 METERS

SITE: Toff's Point  
 MAPPING PROJECT: Pavement N of parking circle  
 LITHOLOGY:  
 SCANLINE DESCRIPTION: 338 degrees

DATE MAPPED: 6/11/99  
 COMPASS DECLINATION: 1 degree  
 MAPPED BY: Anne Ebenreiter

Location (m) Strike (deg) Length (m) Aperture Termination Censoring

\*\*\*NOTE: This is a shoreline pavement. Due to wave weathering, the aperture is over-exaggerated. (i.e.. No faint or visible apertures, all are open, for the most part) Therefore, these measurements are mostly good for orientation. Termination is also very difficult to determine (i.e.. Shoreline or cover) Additionally, scanline length measurements are not completely precise due to the unevenness of the pavement surface. Length of fractures is also exaggerated (due to weathering)

1.41	70	4.2	O	R/A	Y-1
2.35	73	6.35	O	FP/A	Y-1
3.13	73	5.6	O	FL/A	Y-1
3.89	72	4.55	O	FP/FP	N
4.32	74	0.98	V	FP/FP	N
4.98	64	1.6	O	R/FP	N
6.18	85	14.95	O	R/A	Y-1
7.3	84	16.5	O	R/A	Y-1
7.75	69	2.1	O	R/FP	N
8.4	68	1.2	V	R/FP	N
8.7	66	13.7	O	FP/FP	N
9.35	87	0.9	F	R/A	Y-1
9.95	83	4.1	V	R/C	Y-1
13.1	78	6.5	V	FP/C	Y-1

END - TOTAL LENGTH IS 13.8 METERS

SITE: Toff's Point  
 MAPPING PROJECT: North of parking - West of previo  
 LITHOLOGY:  
 SCANLINE DESCRIPTION: 356 degrees  
 NOTE: \*see note on toff' Point 338 degree

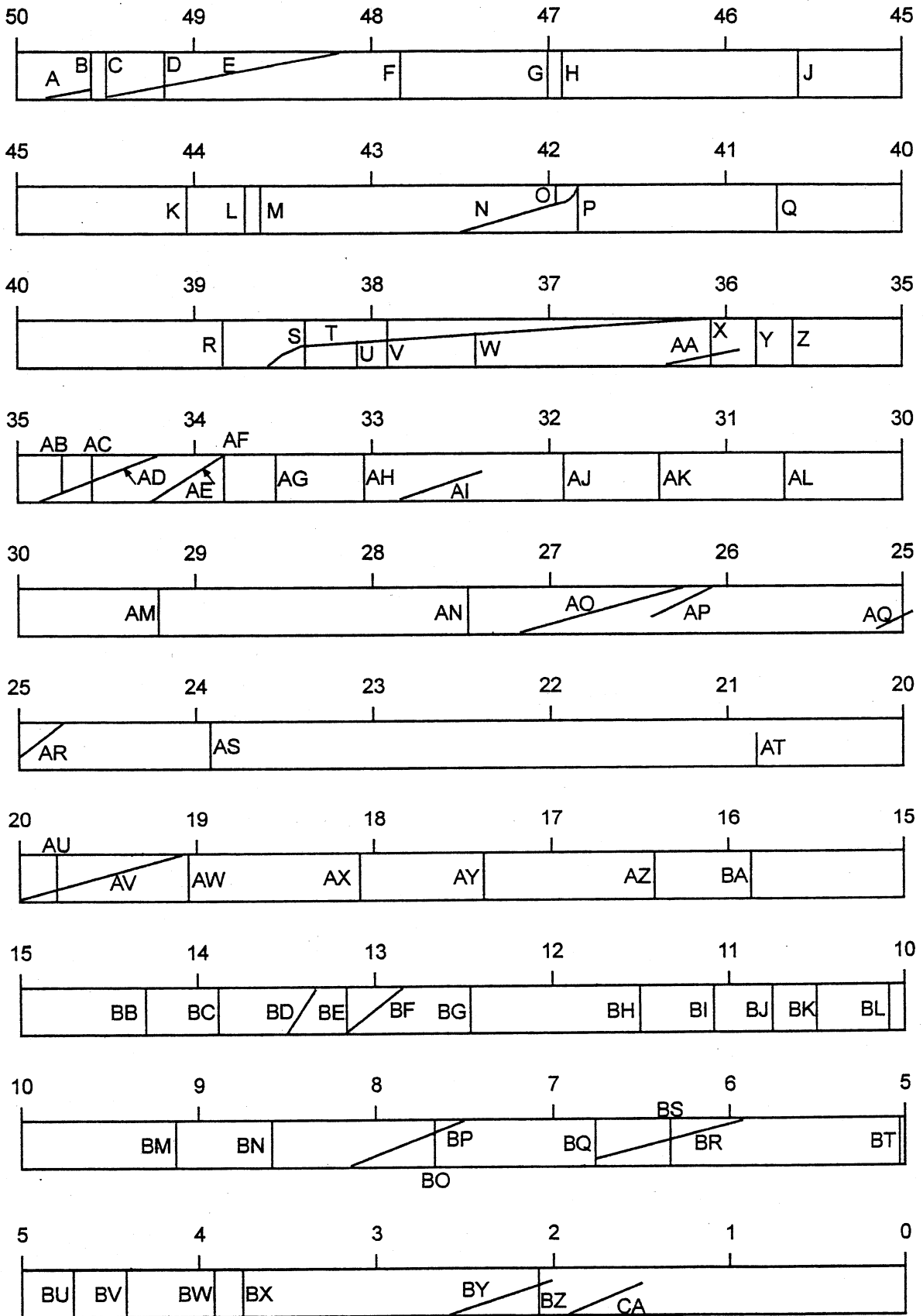
DATE MAPPED: 6/11/99  
 COMPASS DECLINATION: 1 degree  
 MAPPED BY: Anne Ebenreiter

Location (m)	Strike (deg)	Length (m)	Aperture	Termination	Censoring
0.7	82	1.6	O	R/FP	N
1.55	83	6.7	O	FP/R	N
2.8	84	10.5	O	FP/FP	N
3.25	85	5.2	O	C/A	Y-2
5.3	78	21.2	O	FP/C	Y-1
6.45	86	8.9	O	C/C	Y-2
6.9	80	11.1	O	C/C	Y-2
7.2	82	1.9	V	FP/FP	N
7.45	86	19.5	O	C/C	Y-2
8.15	71	4.6	V	R/R	N
8.8	72	7.4	O	R/R	N
9.2	78	1.45	V	FL/FP	N

END - TOTAL LENGTH 10 METERS

APPENDIX B  
Log of horizontal core showing fracture locations

The scale of the log is 0.1 inch on the log = 1 inch of core.  
The origin of the core (quarry face) = 50 ft



89075141713



B89075141713A



89075141713



b89075141713a